INTERACTIONS AND ELECTRON TRANSFER INVOLVED IN PYRUVATE FORMATE-LYASE ACTIVATION

by

Adam Vernon Crain

A dissertation submitted in partial fulfillment
of the requirements for the degree

of

Doctor of Philosophy

in

Biochemistry

MONTANA STATE UNIVERSITY
Bozeman, Montana

May 2013

APPROVAL

of a dissertation submitted by

Adam Vernon Crain

This dissertation has been read by each member of the dissertation committee and has been found to be satisfactory regarding content, English usage, format, citation, bibliographic style, and consistency and is ready for submission to The Graduate School.

Dr. Joan B. Broderick

Approved for the Department of Chemistry and Biochemistry

Dr. Mary J. Cloninger

Approved for The Graduate School

Dr. Ronald W. Larsen

STATEMENT OF PERMISSION TO USE

In presenting this dissertation in partial fulfillment of the requirements for a doctoral degree at Montana State University, I agree that the Library shall make it available to borrowers under rules of the Library. I further agree that copying of this dissertation is allowable only for scholarly purposes, consistent with "fair use" as prescribed in the U.S. Copyright Law. Requests for extensive copying or reproduction of this dissertation should be referred to ProQuest Information and Learning, 300 North Zeeb Road, Ann Arbor, Michigan 48106, to whom I have granted "the exclusive right to reproduce and distribute my dissertation in and from microform along with the non-exclusive right to reproduce and distribute my abstract in any format in whole or in part."

Adam Vernon Crain

May 2013

DEDICATION

To my mother, Shelley, and my father, Max

ACKNOWLEDGEMENTS

To my advisor, Dr. Joan B. Broderick, I am extremely grateful for all of your guidance and help through out my graduate career. Thank you for allowing me to design my own project based on my interests in biochemical protein-protein interactions. I would like to thank my committee members Dr. John Peters, Dr. Valérie Copié, Dr. Robert Szilagyi, Dr. Martin Teinze and Dr. Bill Hoch for guiding and supporting me in graduate school at Montana State University. A special thanks goes out committee members Dr. Martin Lawrence and Dr. Eric Shepard who stepped in for Dr. Valérie Copié and Dr. Robert Szilagyi while they were on sabbaticals. I would also like to thank Jason Schuman for SPR training and Biacore for the Biacore X-100 Inspiration Contest. To Dr. Michele McGuirl, thank you for all your help with circular dichroism and isothermal titration calorimetry. To members of the Broderick lab, thank you for all of your discussions and everything I have learned from each of you over the course of my training.

TABLE OF CONTENTS

TABLE OF CONTENTS - CONTINUED

TABLE OF CONTENTS - CONTINUED

TABLE OF CONTENTS - CONTINUED

TABLE OF CONTENTS - CONTINUED

LIST OF TABLES

LIST OF FIGURES

Figure Page

LIST OF FIGURES - CONTINUED

Figure Page

LIST OF FIGURES - CONTINUED

Figure Page

LIST OF FIGURES - CONTINUED

Figure Page

KEY TO SYMBOLS AND ABBREVIATIONS

Flavodoxin (Fld)

Pyruvate Formate-Lyase Activating Enzyme (PFL-AE)

Pyruvate Formate-Lyase (PFL)

Pyruvate:Flavodoxin Oxidoreductase (PFOR)

$NADP^+$ Flavodoxin Oxidoreductase (FNR)

S-adenosylmethionine (SAM)

Thiamine Pyrophosphate (TPP)

Flavin Mononucleotide (FMN)

ABSTRACT

Pyruvate formate-lyase activating enzyme (PFL-AE) is one of the best-characterized members of the radical S-adenosyl-L-methionine (SAM) superfamily. The radical SAM enzymes utilize an iron-sulfur cluster and SAM to catalyze a diverse set of reactions such as vitamin synthesis, enzyme activation, DNA repair, and sulfur insertion to name a few. PFL-AE contains one [4Fe-4S] cluster coordinated by cysteine residues from a canonical CX3CX2C radical SAM motif. Iron-sulfur cluster-initiated reductive cleavage of S-adenosylmethionine results in a highly reactive 5'-deoxyadenosyl radical that abstracts a pro-S hydrogen from glycine 734 on PFL creating a stable glycyl radical. PFL utilizes this glycyl radical to catalyze the reaction pyruvate + CoA formate + acetyl-CoA, thereby providing the main source of acetyl-CoA for the citric acid cycle under anaerobic conditions. We have undertaken experiments using circular dichroism and isothermal titration calorimetry to characterize interactions between flavodoxin (Fld) and its cofactor (FMN). These experiments show that cofactor binding significantly increases flavodoxin stability and structure, which is required for protein-protein interactions. Anaerobic surface plasmon resonance experiments were used to provide insight into protein-protein interactions between the enzymes involved in PFL activation and in all cases, the proteins interact with low micromolar affinity. SAM binding experiments with PFL-AE were performed in the presence and absence of PFL, which demonstrate that PFL binding to PFL-AE does not alter SAM binding affinity for PFL-AE. PFL activation studies using PFL-AE in the presence of PFL substrates/analogues show that they are not required for PFL activation, however they do play a large role in activation and their inclusion resulted in 3.7 fold higher glycyl radical concentrations. In vivo concentrations were calculated for proteins and small molecules involved in PFL activation and activity in E. coli to provide a context for our measured equilibrium constants and to determine the amount of bound protein in vivo. Activity assays and UV-vis electron transfer assays show that pyruvate:flavodoxin oxidoreductase (PFOR) is capable of activating the PFL system. The aggregate data suggests that electron transfer from Fld to PFL-AE only occurs when SAM and PFL are bound to PFL-AE.

CHAPTER 1

IRON SULFUR CLUSTERS, *S*-ADENOSYLMETIONINE ENZYMES, AND THEIR ROLE IN HYDROGENASE MATURATION

Contribution of Authors and Co-Authors

Manuscripts in Chapters 1, 3, 4, 5, 6

Author Adam V. Crain

Contributions: Conceived and wrote the review article

Co-Author: Kaitlin, S. Duschene

Contributions: Provided the figures for the manuscript

Co-Author: Dr. Joan B. Broderick

Contributions: Provided oversight and guidance in experimental design and interpretation. Provided all funding and resources for the projects. Advised on manuscript preparation and edited manuscript drafts.

Co-Author: John W. Peters

Contributions: Provided revisions for the manuscript

CHAPTER 1

Introduction

IRON SULFUR CLUSTERS, *S*-ADENOSYLMETIONINE ENZYMES, AND THEIR ROLE IN HYDROGENASE MATURATION

Adam V. Crain, Kaitlin S. Duschene, John W. Peters, and Joan B. Broderick
Department of Chemistry and Biochemistry, Montana State University, Bozeman, Montana 59718
Email addresses: Adam Crain: acrain@chemistry.montana.edu, Kaitlin Duschene: kduschene@gmail.com, John Peters: john.peters@chemistry.montana.edu, Joan Broderick: jbroderick@chemistry.montana.edu

Keywords
Metalloenzymes, Radical Reactions, Metal Cluster Biosynthesis, Enzyme Activation

Iron Sulfur Clusters in Biology

Iron sulfur clusters are ubiquitous in biology and take on many forms in nature (1,2). The simplest clusters in enzymes are the [2Fe-2S] clusters, [3Fe-4S] clusters, and [4Fe-4S] clusters; these are most often coordinated to the protein by cysteinal ligation of all irons of the cluster, however arginine, histidine, glutamic acid and aspartic acid have all been observed coordinating to biological iron-sulfur clusters. Iron-sulfur clusters span a remarkable range of reduction potentials from <-400 to > +400 mV, giving them unusual versatility in functions in biology (3-5). Biological iron-sulfur clusters exhibit intriguing similarities to abundant iron-sulfur minerals; this similarity has led to the hypothesis that iron-sulfur minerals played a central role in the emergence of life by catalyzing the formation of the basic building blocks of biological molecules, and that these mineral clusters were incorporated into early proteins as essential components of

catalysis (6). In modern biology, iron-sulfur clusters have such diverse and essential functions as electron transfer in photosynthesis and respiration, catalysis in central metabolic pathways, gene regulation in response to environmental signals, and protein structure stabilization (7). Further, these clusters exhibit structural diversity; in addition to the simple [2Fe-2S], [3Fe-4S], and [4Fe-4S] clusters mentioned above, more complex clusters containing heterometals, nonprotein ligands, and alternate structures are found in a number of enzymes, including those involved in metabolism of one carbon compounds, hydrogen, and nitrogen (1,8).

Radical SAM Enzymes: Historical Perspective

Radical SAM enzymes are a superfamily of enzymes that use a [4Fe-4S] cluster and *S*-adenosylmethionine (SAM) to initiate diverse radical reactions (Figure 1.1). Although the superfamily was first identified in 2001, the earliest studies on radical SAM enzymes preceded this date by approximately 30 years, originating in the laboratories of Knappe and Barker in the late 60's and early 70's. The Knappe laboratory identified a novel anaerobic enzymatic reaction requiring SAM, Fe^{2+}, and flavodoxin, and two protein components to convert pyruvate to formate and acetyl-CoA (9,10). The first protein component, pyruvate formate-lyase (PFL), was later found to contain a catalytically essential glycyl radical in its active state; the second protein component (pyruvate formate-lyase activating enzyme, PFL-AE) was found to catalyze the formation of this glycyl radical (11). PFL-AE was ultimately shown to require an iron-sulfur cluster, rather than simply Fe^{2+} (12). A similar system involved in anaerobic ribonucleotide reduction that also utilized an iron-sulfur cluster and SAM to generate a

catalytically essential glycyl radical was also described prior to the identification of the superfamily (13,14). The activating enzymes for PFL and the anaerobic ribonucleotide reductase are part of a sub-class of radical SAM enzymes referred to as glycyl radical enzyme-activating enzymes (GRE-AE, Figure 1.1). Like PFL/PFL-AE, lysine 2,3-aminomutase (LAM) was discovered in the late 1960s, in *Clostridium subterminale* during the anaerobic fermentation of lysine to acetate, butyrate, and ammonia (15). LAM enzyme activity was initially reported to be dependent on Fe^{2+}, SAM, PLP, and reducing equivalents, however later work showed the requirement for iron-sulfur clusters rather than Fe^{2+} (16). The final two early "iron-sulfur cluster – SAM" enzymes were lipoate synthase and biotin synthase, both of which were shown to catalyze the insertion of sulfur into C-H bonds (17,18).

Therefore, prior to the identification of the radical SAM superfamily, five different enzyme systems had been identified in which iron-sulfur clusters and *S*-adenosylmethionine were required for catalysis. The bioinformatics study of Heidi Sofia published in 2001 showed that these five enzymes were part of a much larger superfamily of enzymes that spanned the phylogenetic kingdom. Although the superfamily members showed little overall sequence homology, most contained a conserved cysteine motif, CX_3CX_2C, to coordinate an iron sulfur cluster. Other limited sequence conservation appears to be associated with the binding of SAM (19). The discovery of the radical SAM superfamily and the identification of hundreds of additional members generated an increase in research on superfamily members, with numerous discoveries of new enzymatic reactions catalyzed through the use of iron-sulfur clusters and SAM. It is now

clear that radical SAM enzymes are capable of mediating numerous and diverse reactions, and the superfamily may in fact represent the most common method in biology for initiating radical reactions (20).

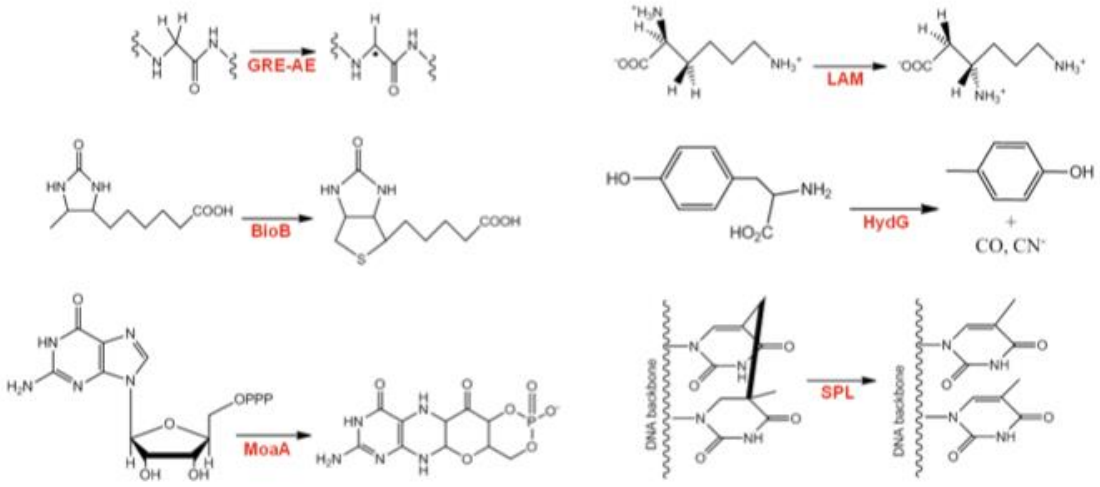

Figure 1.1: Representative radical SAM reactions. Shown are the reactions catalyzed by the glycyl radical enzyme-activating enzymes (GRE-AE), lysine 2,3-aminomutase (LAM), biotin synthase (BioB), a hydrogenase maturation protein (HydG), an enzyme involved in the synthesis of the molybdopterin cofactor (MoaA), and the spore photoproduct lyase (SPL)

Mechanism and Structure in Radical SAM Enzymes

The diverse reactions catalyzed by radical SAM enzymes are thought to utilize a common mechanism, the details of which have been deconvoluted based primarily on the studies of PFL-AE and LAM (21,22). A novel aspect of this chemistry is the direct coordination of SAM, via the amino and carboxylate moieties, to the unique site of a site-differentiated [4Fe-4S] cluster (Figure 1.2). The coordination of SAM to the unique iron of the site-differentiated [4Fe-4S] cluster is a novel feature of radical SAM enzymes that was first identified by spectroscopic studies of PFL-AE. Mössbauer studies provided the

first direct evidence for a unique iron site, while electron-nuclear double resonance (ENDOR) spectroscopy confirmed direct coordination of the cluster by amino and carboxylate moieties of SAM (23,24). Orbital overlap of the iron-sulfur cluster and the sulfonium sulfur of SAM was also indicated by these ENDOR studies, suggesting an inner sphere electron transfer between these moieties.

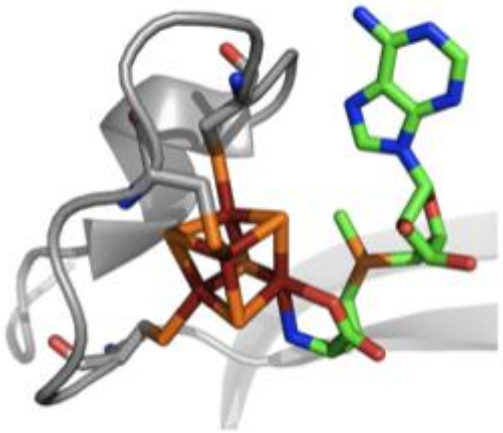

Figure 1.2: Site differentiated [4Fe-4S] cluster chelated at the unique iron site by amino and carboxylate moieties of S-adenosylmethionine in PFL-AE (3CB8)

The catalytically active state of the iron sulfur cluster is the $[4Fe\text{-}4S]^{+}$ state, which transfers an electron to the bound *S*-adenosylmethionine via inner sphere electron transfer to the sulfonium sulfur (Figure 1.3). The reduction of SAM results in homolytic cleavage of the S-C5' bond to produce a 5'-deoxyadenosyl radical intermediate and methionine. The highly reactive 5'-deoxyadenosyl radical then abstracts a hydrogen from the substrate to initiate catalysis (21). In most of the radical SAM enzymes characterized to date, SAM is a co-substrate, and the SAM cleavage products (methionine and 5'-

deoxyadenosine) must dissociate from the enzyme and be replaced by another SAM molecule before a second round of catalysis can occur. LAM and some other radical SAM enzymes use SAM as a cofactor that is not consumed during turnover, but rather reversibly generates the 5'-deoxyadenosyl radical in much the same way as coenzyme B12 (25,26). Further, there is emerging evidence that a subcategory of radical SAM enzymes may catalyze reductive cleavage of SAM in which an alternative S-C bond is cleaved and thus an alternate radical intermediate (other than the 5'-deoxyadenosyl radical) is generated. Once the 5'-dAdo (or alternative) radical is generated, the reaction diverges depending on the substrate involved leading a variety of chemically distinct reactions (20).

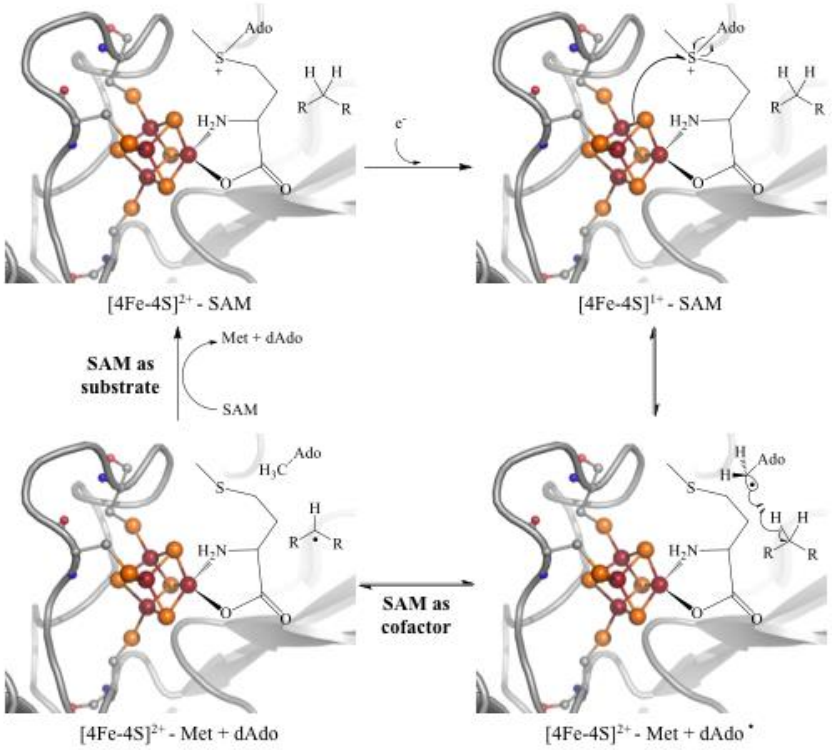

Figure 1.3: Proposed mechanism for radical SAM enzymes. SAM is shown bound to the unique iron of the oxidized $[4Fe\text{-}4S]^{2+}$ cluster (upper left). Reduction of this cluster generates the catalytically active $[4Fe\text{-}4S]^{+}$ state, which undergoes inner-sphere electron transfer to the sulfonium of SAM, thereby promoting the cleavage of the S-C(5') bond of SAM (upper right). The homolytic cleavage of SAM produces the 5-deoxyadenosyl radical intermediate, which directly abstracts a hydrogen atom from substrate (lower right). The substrate radical generally undergoes further radical-SAM mediated chemical transformations. In most radical SAM enzymes characterized to date, the methionine and 5-deoxyadenosine (lower left) are released as products of the reaction; in these cases, SAM is acting as a substrate of the reaction. In a few examples of radical SAM enzymes, however, a rearranged product radical re-abstracts a hydrogen atom from 5–deoxyadenosine to regenerate the 5-deoxyadenosyl radical intermediate, which recombines with the methionine to regenerate SAM; in these cases, SAM acts as a cofactor rather than a substrate.

Significant insights into the energetics of radical SAM reactions have been revealed by studies of LAM. The reduction potentials of the [4Fe-4S] clusters in radical SAM enzymes are in the range of ~ - 400 to - 550 mV, however best estimates for the

reduction potential of SAM are ~ -1.7 V; this > 1 V gap helps to explain the prohibitive nature of electron transfer from the catalytic cluster to an isolated SAM to promote reductive cleavage. However, the potential of the cluster in LAM in the presence of SAM, PLP, and lysine decreases to - 600 mV, while that of SAM increases to - 990 mV, decreasing the energy barrier from ~ 32 kcal/mole to 9 kcal/mole, making reductive SAM cleavage more feasible. It has also been proposed that electron transfer from the pentacoordinate $[4Fe\text{-}4S]^{+}$ cluster (with SAM coordinated as a bidentate ligand to the unique site) to the sulfonium in SAM results in a more favorable hexacoordinate $[4Fe\text{-}4S]^{2+}$ (with methionine coordinated in a tridentate fashion to the unique iron) and may facilitate inner-sphere electron transfer (27). LAM remains one of the best-characterized examples of a radical SAM enzyme and putative characteristics of other members of the superfamily have been extrapolated using LAM as a model system. Radical SAM enzymes also exhibit common structural features, as elucidated by spectroscopic and structural studies of a number of superfamily members. All of the radical SAM crystal structures reported to date show the presence of a partial or complete TIM (triose phosphate isomerase) barrel, with the degree of completeness of the barrel correlating with the size of the substrate. For example, when the substrate is a large macromolecule, as in the case of PFL-AE, whose substrate is the 170 kDa PFL, the barrel is less complete, leaving a wide opening for binding the large substrate (Figure 1.4); radical SAM enzymes that act on smaller substrates have more complete barrels, thereby limiting active site accessibility to small molecules. Regardless of the completeness of the TIM barrel, the [4Fe-4S] cluster binding site is at one end of the barrel. Three of the four irons

of the [4Fe-4S] cluster are coordinated by cysteine residues from a conserved motif (usually CX_3CX_2C but variations exist in the superfamily), while the fourth iron is chelated by SAM. Substrate binds in close proximity to SAM, thereby allowing for direct H-atom abstraction from substrate by the 5'-deoxyadenosyl radical intermediate.

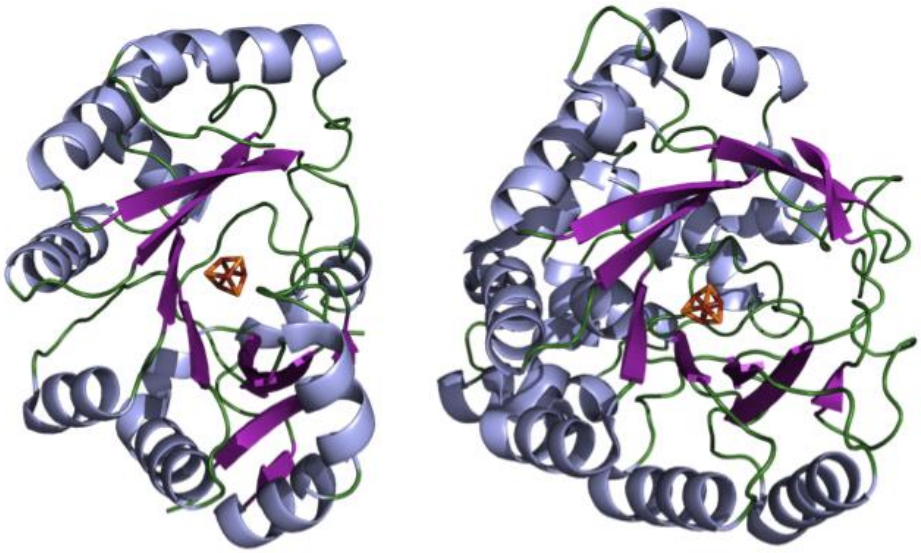

Figure 1.4: Structures of the radical SAM enzymes PFL- AE (3CB8, left) and LAM (2A5H, right). The completeness of the TIM barrel structure correlates with the size of the substrate: PFL- AE acts on a very large protein substrate and has an incomplete and thus quite open barrel, while LAM acts on a small-molecule substrate and its barrel is more complete

Diverse Reactions Catalyzed by Radical SAM Enzymes

Radical SAM reactions are involved in diverse reactions in all kingdoms of life, including anaerobic glycolysis and nucleotide metabolism, DNA repair, vitamin and cofactor biosynthesis, and synthesis of complex metal clusters, as well as many more unmentioned and yet to be discovered reactions (Figure 1.1). These reactions range from simple ones whereby H-atom abstraction is the initial and only step required to convert substrate to product, to reactions in which H-atom abstraction initiates complex and

sometimes perplexing transformations. Several examples of radical SAM enzymes are described in the following paragraphs, while more complete discussions of superfamily members can be found in recent reviews (6,20,28).

PFL-AE is a radical SAM enzyme that activates PFL, a central enzyme in anaerobic glycolysis, by generating a catalytically essential radical at G734 of PFL; PFL-AE is therefore a GRE-AE (11). Active PFL catalyzes the reaction of pyruvate and CoA to formate and acetyl-CoA and provides the sole source of acetyl-CoA for the citric acid cycle under anaerobic conditions. The catalytically active $[4Fe\text{-}4S]^{+}$ cluster of PFL-AE is oxidizied to the $[4Fe\text{-}4S]^{2+}$ in a 1:1 stoichiometric ratio with glycyl radical formation, indicating that the reduced cluster provides the electron necessary for the reductive cleavage of SAM to generate the deoxyadenosyl radical intermediate, which in turn abstracts a hydrogen atom from G734 of PFL (29). 5'-Deoxyadenosine and methionine are products of the PFL-AE reaction, and direct label transfer from G734 to the 5'-dAdo product demonstrates this direct H-atom abstraction. Further biochemical experiments demonstrated that this H-atom abstraction was stereospecific for the pro-*S* hydrogen of G734 (21). Recent biophysical studies of PFL suggest that major structural rearrangement of PFL must occur in order for the normally buried G734 to bind in the active site of PFL-AE such that direct H-atom abstraction can occur (30).

Lysine 2,3-aminomutase (LAM) is part of group of radical SAM enzymes that catalyze isomerization reactions. In the presence of reducing equivalents, SAM, PLP, and a [4Fe-4S] cluster, LAM catalyzes the conversion of L-α-lysine to L-β-lysine (16). Evidence for a 5'-deoxyadeosyl radical intermediate in the LAM mechanism was

demonstrated using the SAM analog 3', 4' – anhydroadenosylmethinine (anSAM) in conjunction with EPR measurements that assigned a new signal to the allylically stabilized 3', 4' – anhydroadenosyl radical intermediate (25). Subsequent ENDOR experiments demonstrated that anSAM, PLP, and the [4Fe-4S] cluster were within van der Waals distance of each other, making direct hydrogen abstraction feasible (31).

Biotin synthase or BioB is an example of a radical SAM enzyme that catalyzes a sulfur insertion reaction. BioB contains a [4Fe-4S] cluster chelated at the unique iron by SAM and also contains a labile [2Fe-2S] cluster that is used as sulfur source for the synthesis of biotin from dethiobiotin (32). Two SAM molecules are required to carry out two sequential H-atom abstraction reactions from positions C6 and C8 of dethiobiotin; these react with a bridging sulfide of the [2Fe-2S] cluster to generate the thiophane ring of biotin (33). The [2Fe-2S] cluster of biotin synthase is thus proposed to act as a substrate in the reaction, and must therefore be re-built after each turnover; this need to rebuild the substrate cluster is thought to be at least partly responsible for the limited amount of turnover observed for BioB *in vitro.*

Spore photoproduct (SP) lyase is a radical SAM enzyme that repairs the thymine dimer 5-thyminyl-5,6-dihydrothymine (SP), a major UV photoproduct in spore DNA. This repair reaction is initiated by direct H-atom abstraction from the C-6 position of SP by the 5'-dAdo radical intermediate (26). Enzymatic assays carried out with synthetic, stereochemically-defined SP dinucleosides and dinucleotides have demonstrated that the repair reaction is stereospecific for the 5R diastereomer of SP (34).

The molybdenum cofactor biosynthesis enzyme MoaA catalyzes the remarkably complex rearrangement of 5'-GTP to form precursor Z in molybdenum cofactor biosynthesis. Subsequent enzymatic reactions generate the dithiolene group of molybdopterin, which coordinates molybdenum (28). The formation of precursor Z also requires the presence of an additional enzyme known as MoaC, although the precise roles of each enzyme remain to be elucidated (35). MoaA contains an N-terminal radical SAM [4Fe-4S] cluster and an additional C-terminal cluster that has been shown to bind GTP (36).

Two radical SAM enzymes (HydE and HydG) have also been identified as essential in maturation of the [FeFe]-hydrogenase. These two enzymes, together with the GTPase HydF, are in fact the only proteins required for heterologous expression of an active [FeFe]-hydrogenase (HydA) (37). The reactions catalyzed by these radical SAM enzymes, and their roles in [FeFe]-hydrogenase maturation, will be discussed below.

The [FeFe]-Hydrogenase and its Maturation

Hydrogenases catalyze the reversible interconversion of protons and molecular hydrogen, $2H^+ + 2e^- \quad H_2$. Two types of hydrogenases catalyze this reaction, the [NiFe]-hydrogenase and the [FeFe]-hydrogenase. These enzymes are evolutionarily unrelated and yet contain some unusual active site features in common, including the presence of biologically unusual CO and CN^- ligands to the active site metals. The metal content is correlated with the catalytic bias, with hydrogen oxidation the favored direction of catalysis in the [NiFe]-enzymes (38). In [FeFe]-hydrogenases, hydrogen production is greatly favored over hydrogen oxidation, making it an ideal catalyst for alternative

energy especially when coupled to photosynthesis. Unfortunately several barriers exist to photosynthetic commercial hydrogen production such as competition between hydrogenase and NADPH-dependent carbon dioxide fixation and the strict requirement of anaerobic conditions (39).

[FeFe]-hydrogenases from *Clostridium pasteurianum* (CpI) and *Desulfovibrio desulfuricans* have been structurally characterized (40,41). These X-ray structures, together with detailed spectroscopic studies, have provided a picture of the remarkable active site H-cluster. The H-cluster is composed of a [4Fe-4S] cluster coordinated to the protein by four cysteinate ligands, with one of these cysteinates bridging to a 2Fe cluster whose remaining ligands consist of three CO and two CN^-, as well as a bridging dithiolate. The identity of the central atom in the dithiolate linker is an area of controversy and has been proposed to be carbon, nitrogen, or oxygen (6). However, dithiomethylamine is favored based on a recent spectroscopic study, as well as for mechanistic reasons, because a nitrogen would have the ability to act as a proton donor and acceptor for proton reduction or hydrogen oxidation (42,43). The distal iron of the H-cluster has been proposed to be the site of hydrogen oxidation and proton reduction. The structures of both of the above mentioned hydrogenase enzymes also show accessory clusters or F clusters made up of two ferredoxin like [4Fe-4S] clusters, one histidine ligated [4Fe-4S] cluster and one [2Fe-2S] cluster. The F clusters have been proposed to be involved in shuttling electrons to and from the H-cluster via donor and acceptor proteins which bind acidic and basic patches on either side of the domain (40).

Biosynthesis of the H-cluster and maturation of an active [FeFe]-hydrogenase requires three maturase proteins known as HydE, HydF, and HydG; HydE and HydG were proposed from sequence annotations to be radical SAM enzymes, while HydF was suggested to be a GTPase (37). Recent biochemical and spectroscopic studies have begun to reveal the specific roles for each of these accessory proteins in hydrogenase maturation (20). It was shown that when HydE, HydF, and HydG were expressed together in *E. coli*, they generated an activating component associated with HydF, that could be transferred to the inactive [FeFe]-hydrogenase (HydA) to generate the active enzyme (44). EPR and FTIR spectroscopic studies have provided evidence that this activating component is a CO and CN^- ligated 2Fe H-cluster precursor, and that this activating component is generated by the actions of the radical SAM enzymes HydE and HydG (45). Consistent with these results, HydA expressed in *E. coli* in the absence of the accessory proteins contains not the entire H-cluster, but rather a simple [4Fe-4S] cluster that is essential for subsequent maturation. This [4Fe-4S] cluster lies at the end of a cationic channel that presumably functions in transfer of the 2Fe H-cluster precursor into the active site of HydA (46). Together, these results point to a model in which the radical SAM enzymes HydE and HydG build a 2Fe H-cluster precursor on HydF, and this precursor is then delivered to HydA to assemble the full H-cluster.

What are the specific functions of the radical SAM enzymes in H-cluster maturation? It seemed likely that these enzymes would be involved in synthesizing the unique ligands of the H-cluster, however identifying specific functions first required that the substrates for these enzymes be identified. HydG has significant sequence similarity

to ThiH, another radical SAM enzyme that catalyzes the cleavage of tyrosine to form *p*-cresol. This sequence homology inspired exploration of the possibility that tyrosine could be cleaved by HydG, and indeed HydG was shown to cleave tyrosine to produce p-cresol under anaerobic reducing conditions in the presence of SAM (47). Subsequent studies designed to detect any CN^- and CO produced in this reaction demonstrated that the HydG-catalyzed cleavage of tyrosine was accompanied by production of these two diatomic ligands. These experiments utilized isotopically labeled tyrosine in order to unequivocally demonstrate that the CO and CN^- were derived from tyrosine (48,49). A recent study using cell free extracts and isotopic labeling demonstrated that all five CO and CN^- diatomic ligands of the H-cluster originate from the amino and carboxylate moieties on tyrosine (50). This data supports a model for H-cluster assembly in which HydG synthesizes the diatomic ligands and delivers them to HydF, where the 2Fe H-cluster precursor is assembled.

If HydG synthesizes the diatomic ligands to the H-cluster, then it is likely that HydE should synthesize the other unique feature of this cluster, the nonprotein dithiolate. Synthesis of such a ligand could proceed by radical-SAM mediated insertion of sulfur into a C-H bond in a manner analogous to BioB (Figure 1.1). However identification of a substrate for HydE, and thus any further details of its function, remain elusive. The crystal structure of HydE from *Thermotoga maritima* has been solved and *in silico* efforts have identified three anion binding sites and a binding site for thiocyanate (51). HydE has a very similar fold to BioB, and both contain a [4Fe-4S] cluster that binds SAM and an additional labile [2Fe-2S] cluster (Figure 1.5). It is possible that the [2Fe-2S] cluster in

HydE could be used for sulfur insertion reactions similar to BioB, in synthesis of the dithiolate linker. *In vitro* studies have shown that hydrogenase activity is increased in the presence of SAM, tyrosine, and cysteine; indicating that cysteine may act as a substrate in the formation of the dithiolate bridge of the H-cluster (52).

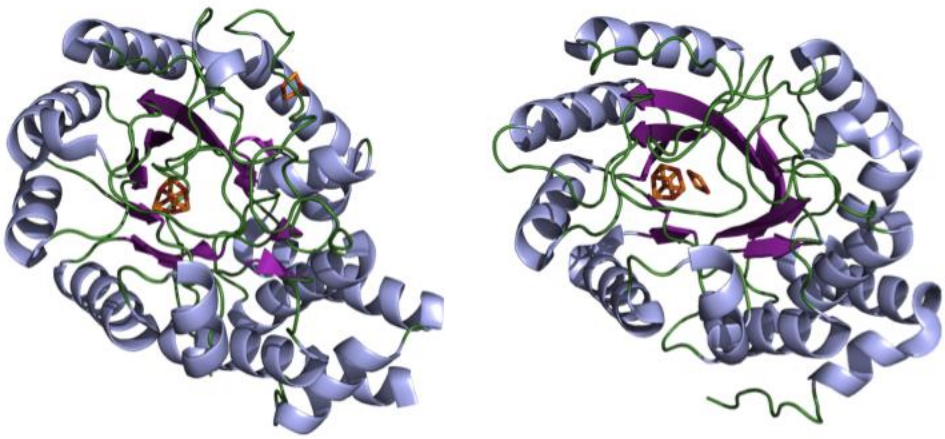

Figure 1.5: Structural similarity between BioB (1R30, left), which catalyzes a radical SAM sulfur insertion reaction, and HydE (3CIX, right), whose specific reaction is currently unknown.

Overall, the model for biosynthesis of the H-cluster and maturation of the active [FeFe]-hydrogenase is one in which radical SAM chemistry plays a central role (Figure 1.6). HydE is proposed to catalyze a BioB type reaction to insert the bridging sulfides from a [2Fe-2S] cluster on HydF into C-H bonds of an unknown substrate to generate the bridging dithiolate of the H-cluster. HydG then catalyzes the cleavage of tyrosine, generating one equivalent each of CO and CN^-, which are delivered to the modified 2Fe

cluster on HydF. Two additional turnovers of tyrosine catalyzed by HydG would be required to generate the remaining CO ligands for the H-cluster. However, since the H-cluster has three CO ligands but only two CN- ligands, this scenario leaves one cyanide leftover after assembling the H-cluster precursor. The fate of this "extra" cyanide is unknown at this time.

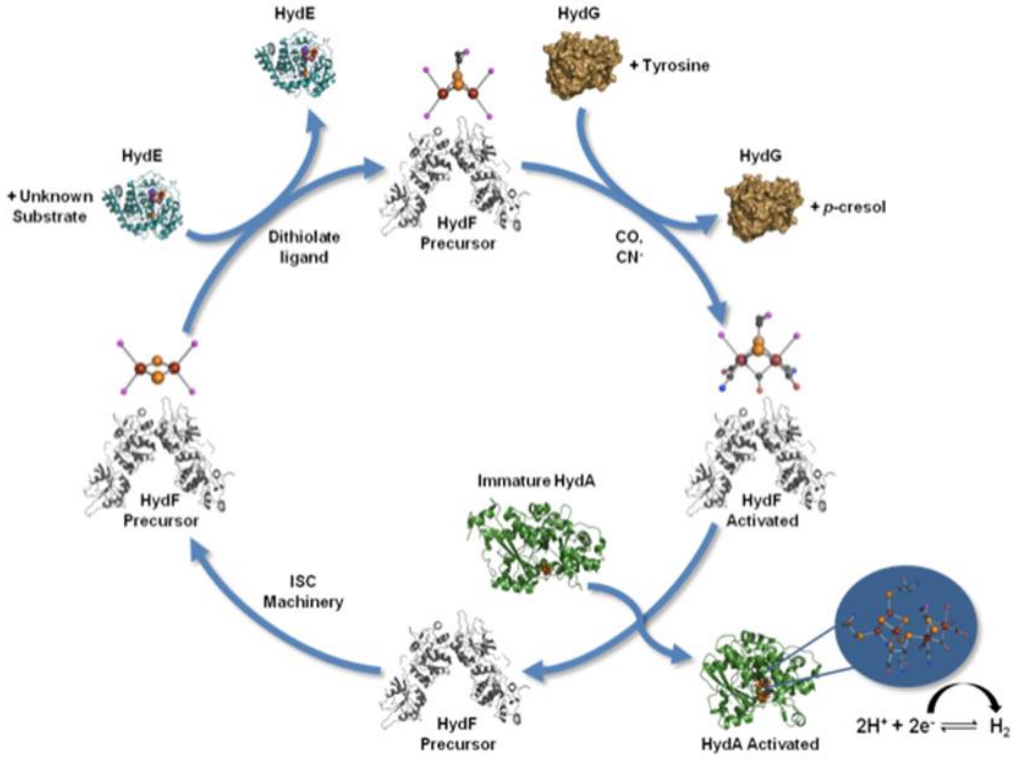

Figure 1.6: Schematic representation of our current model for the maturation of the [FeFe]-hydrogenase. The HydF protein contains a [2Fe-2S] cluster (left) that serves as a substrate/precursor for synthesis of the 2Fe subcluster of the H-cluster. This cluster is acted on by HydE, utilizing an unknown substrate, to synthesize the bridging dithiolate of the H-cluster (top). HydG then catalyzes the decomposition of tyrosine to produce the diatomic ligands to the cluster. The resulting "activated" form of HydF (right) then transfers the 2Fe H-cluster precursor to HydA to generate the active hydrogenase. The individual proteins in the scheme are represented by their crystal structures where available (HydA, 3LX4; HydF, 3QQ5; HydE, 3IIZ). No crystal structure is available for HydG, and so it is represented using a surface rendering of the HydE structure

Conclusion

Radical SAM enzymes catalyze an incredibly diverse array of reactions in biochemistry using a novel radical initiation mechanism and many additional features to control radical chemistry. The common intermediate in radical SAM reactions, the SAM derived 5'-deoxyadenosyl radical intermediate, is an extremely reactive primary carbon radical that could in principle abstract a hydrogen atom from nearly any organic species; therefore substrate binding in proximity to SAM, and orientation of the substrate for abstraction of the *correct* H atom, are presumably critical features of catalysis. Characterized radical SAM reactions include DNA and RNA modifications, vitamin synthesis, sulfur insertion reactions, cofactor synthesis, and complex substrate catalysis to name a few. These enzymes are also seminal in hydrogenase maturation in eucarya, archaea, and bacteria, underlining their important role in emerging biotechnology and alternative energy. Newly characterized motifs and mechanisms are emerging rapidly and will require many years of additional research before the full potential of radical SAM enzymes are realized.

References

1. Beinert, H. (2000) *J. Biol. Inorg. Chem.* 5, 2-15

2. Johnson, D., C., Dean, D., R., Smith, A., D. , and Johnson, M., K. (2005) *Annu. Rev. Biochem.* 74, 247-281

3. Zu, Y., Couture, M., M.-J., Kolling, D., R. J., Crofts, A., R., Eltis, L., D., Fee, J., A., and Hirst, J. (2003) *Biochemistry* 42, 12400-12408

4. Broach, R., B., and Jarrett, J., T. (2006) *Biochemistry* 45, 14166-14174

5. Subramanian, P., Rodrigues, A., V., Ghimire-Rijal, S., and Stemmler, T., L. (2011) *Curr. Opin. Chem. Biol.* 15, 312-318

6. Shepard, E., M., and Broderick, J., B. . (2010) S-adenosylmethionine and iron-sulfur clusters in biological radical reactions: the radical SAM superfamily. in *Comprehensive natural products II chemistry and biology* (Mander, L., Lui, H.-W. ed.), Elsevier, Oxford. pp

7. Ayala-Castro, C., Saini, A., and Outten, F. W. (2008) *Microbiol. Mol. Biol. Rev.* 72, 110-125

8. Drennan, C., L., and Peters, J., W. (2003) *Curr. Opin. Struct. Biol.* 13, 220-226

9. Knappe, J., Bohnert, E., and Brummer, W. (1965) *Biochim. Biophys. Acta* 107, 603-605

10. Knappe, J., and Blaschkowski, H., P. (1975) *Methods Enzymol.* 41, 508-518

11. Knappe, J., Neugebauer, F., A., Blaschkowski, H., P. , and Gänzler, M. (1984) *Proc. Natl. Acad. Sci. USA* 81, 1332-1335

12. Broderick, J., B., Duderstadt, R., E., Fernandez, D., C., Wojtuszewski, K., Henshaw, T., F. , and Johnson, M. K. (1997) *J. AM. CHEM. SOC.* 119, 7396-7397

13. Eliasson, R., Fontecave, M., Jörnvall, H., Krook, M., and Pontis, E. (1990) *Proc. Natl. Acad. Sci. USA* 87, 3314-3318

14. Mulliez, E., Fontecave, M., Gaillard, J., and Reichard, P. (1993) *J. Biol. Chem.* 268, 2296-2299

15. Chirpich, T. P., Zappia, V., Costilow, R. N., and Barker, H. A. (1970) *J. Biol. Chem.* 245, 1778-1789

16. Petrovich, R., M., Ruzicka, F., J., Reed, G., H. , and Frey, P., A. (1991) *J. Biol. Chem.* 266, 7656-7660

17. Busby, R., W., Schelvis, J., P., Yu, D., S., Babcock, G., T., and Marletta, M., A. (1999) *J. AM. CHEM. SOC.* 121, 4706-4707

18. Sanyal, I., Cohen, G., and Flint, D., H. (1994) *Biochemistry* 33, 3625-3631

19. Sofia, H., J., Chen, G., Hetzler, B., G., Reyes-Spindola, J., F. , and Miller, N., E. (2001) *Nucleic Acids Res.* 29, 1097-1106

20. Challand, M., R., Driesener, R., C. , and Roach, P. (2011) *Nat. Prod. Rep.* 28, 1696-1721

21. Frey, M., Rothe, M., Wagner, V., A. , and Knappe, J. (1994) *J. Biol. Chem.* 269, 12432-12437

22. Moss, M., L., and Frey, P., A. . (1990) *J. Biol. Chem.* 265, 18112-18115

23. Krebs, C., Broderick, W., E., Henshaw, T., F., Broderick, J., B. , and Huynh, B. H. H. (2002) *J. Am. Chem. Soc.* 124, 912-913

24. Walsby, C., J., Ortillo, D., Broderick, W., E., Broderick, J., B., and Hoffman, B., M. (2002) *J. Am. Chem. Soc.* 124, 11270-11271

25. Magnusson, O., T., Reed, G., H. , and Frey, P., A. (1999) *J. Am. Chem. Soc.* 121, 9764-9765

26. Cheek, J., and Broderick, J. (2002) *J. Am. Chem. Soc.* 124, 2860-2861

27. Wang, S., C., and Frey, P. (2007) *Biochemistry* 46, 12889-12895

28. Vey, J., L., and Drennan, C., L. (2011) *Chem. Rev.* 111, 2487-2506

29. Henshaw, T., F., Cheek, J., and Broderick, J., B. (2000) *J. Am. Chem. Soc.* 122, 8331-8332

30. Peng, Y., Veneziano, S., E., Gillispie, G., D. , and Broderick, J. (2010) *J. Biol. Chem.* 285, 27224-27231

31. Lees, N., S., Chen, D., Walsby, C., J., Behshad, E., Frey, P., A. , and Hoffman, B., M. (2006) *J. Am. Chem. Soc.* 128, 10145-10154

32. Tse Sum Bui, B., Benda, R., Schünemann, V., Florentin, D., Trautwein, A., X. , and Marquet, A. (2003) *Biochemistry* 42, 8791-8798

33. Taylor, A., M., Farrar, C., E. , and Jarrett, J., T. (2008) *Biochemistry* 47, 9309-9317

34. Tilak Chandra, S. C. S., Egidijus Zilinskas, Eric M. Shepard, William E. Broderick, and Joan B. Broderick. (2009) *J. Am. Chem. Soc.* 131, 2420-2421

35. Wuebbens, M., M., Liu, M., T., Rajagopalan, K., V. , and Schindelin, H. (2000) *Structure* 8, 709-718

36. Hänzelmann, P., and Schindelin, H. (2006) *Proc. Natl. Acad. Sci. USA* 103, 6829-6834

37. Posewitz, M., C., King, P., W., Smolinski, S., L., Zhang, L., Seibert, M., and Ghirardi, M., L. (2004) *J. Biol. Chem.* 279, 25711-25720

38. Vignais, P., M., and Billoud, B. (2007) *Chem. Rev.* 107, 4206-4272

39. Yacoby, I., Pochekailov, S., Toporik, H., Ghirardi, M., L., King, P., W. , and Zhang, S. (2011) *Proc. Natl. Acad. Sci. USA* 108, 9396-9401

40. Peters, J., W., Lanzilotta, W., N., Lemon, B., J., and Seefeldt, L., C. (1998) *Science* 282, 1853-1858

41. Nicolet, Y., Piras, C., Legrand, P., Hatchikian, C., E. , and Fontecilla-Camps, J., C. (1999) *Structure* 7, 13-23

42. Silakov, A., Wenk, B., Reijerse, E., and Lubitz, W. (2009) *Phys. Chem. Chem. Phys.* 11, 6592-6599

43. Nicolet, Y., De Lacey, A., L., Vernède, X., Fernandez, V., M., Hatchikian, E. C., and Fontecilla-Camps, J., C. (2001) *J. Am. Chem. Soc.* 123, 1596-1601

44. McGlynn, S., E., Ruebush, S., S., Naumov, A., Nagy, L., E., Dubini, A., King, P., W., Broderick, J., B., Posewitz, M., C. , and Peters, J., W. (2007) *J. Biol. Inorg. Chem.* 12, 443-447

45. Shepard, E., M., McGlynn, S., E., Bueling, A., L., Grady-Smith, C., S., George, S., J., Winslow, M., A., Cramer, S., P., Peters, J., W. , and Broderick, J., B. (2010) *Proc. Natl. Acad. Sci. USA* **107**, 10448-10453

46. Mulder, D., W., Boyd, E., S., Sarma, R., Lange, R., K., Endrizzi, J., A., Broderick, J., B. , and Peters, J., W. (2010) *nature* **465**, 248-251

47. Pilet, E., Nicolet, Y., Mathevon, C., Douki, T., Fontecilla-Camps, J., C. , and Fontecave, M. (2009) *FEBS Lett.* **583**, 506-511

48. Driesener, R., C., Challand, M., R., McGlynn, S., E., Shepard, E., M., Boyd, E., S., Broderick, J., B., Peters, J., W. , and Roach, P., L. (2010) *Angew. Chem., Int. Ed. Engl.* **49**, 1687-1690

49. Shepard, E., M., Duffus, B., R., George, S., J., McGlynn, S., E., Challand, M., R., Swanson, K., D., Roach, P., L., Cramer, S., P., Peters, J., W., and Broderick, J., B. (2010) *J. AM. CHEM. SOC.* **132**, 9247-9249

50. Kuchenreuther, J., M., George, S., J., Grady-Smith, C., S., Cramer, S., P., and Swartz, J., R. (2011) *PLoS ONE* **6**, e20346

51. Nicolet, Y., Rubach, J., K., Posewitz, M., C., Amara, P., Mathevon, C., Atta, M., Fontecave, M., and Fontecilla-Camps, J., C. (2008) *J. Biol. Chem.* **283**, 18861-18872

52. Kuchenreuther, J., M., Stapleton, J., A., and Swartz, J., R. (2009) *PLoS ONE* **4**, e7565

CHAPTER 2

EXPRESSION, PURIFICATION, AND CHARACTERIZATION OF PYRUVATE FORMATE-LYASE ACTIVATING ENZYME, PYRUVATE FORMATE-LYASE, FLAVODOXIN, NADPH AND PYRUVATE DEPENDENT FLAVODOXIN OXIDOREDUCTASES

Introduction

During the late 1960's and early 1970's novel anaerobic enzymatic reactions involved in the dissimilation of pyruvate into acetyl-CoA were discovered in the laboratory of Joachim Knappe (1,2). It was shown that a novel enzyme named pyruvate formate-lyase (PFL) could carry out the reaction of pyruvate + CoA ⇆ acetyl-CoA + formate, thereby providing the sole source of acetyl-CoA for anaerobic metabolism in *E. coli* (3). PFL could be isolated in an inactive form and subsequently activated by another enzyme named pyruvate formate-lyase activating enzyme (PFL-AE) via a post-translational modification step (4). PFL activation by PFL-AE was shown to be dependent on the presence of iron, *S*-adenosylmethionine (SAM), oxamate or pyruvate, and flavodoxin (5). Active PFL was later shown to contain a stable glycyl radical on the C-2 carbon backbone of G734 that could undergo many rounds of catalysis before inactivation under anaerobic conditions (6).

When PFL-AE was purified it contained a chromophore that was assigned to a [4Fe-4S] cluster that was necessary for enzyme activity (7). The cluster is ligated by the canonical CX_3CX_2C radical SAM motif that was later described by Sofia et al. in a bioinformatics study that identified the radical SAM superfamily (8). Mössbauer studies

indicated that three irons in the [4Fe-4S] cluster were coordinated by cysteines, while the fourth unique iron appeared to be coordinated by SAM when it was present (9). This interaction between SAM and the cluster was confirmed by ENDOR studies which demonstrate orbital overlap between the cluster and the sulfonium sulfur of SAM, in addition to coordination of the amino and carboxylate moieties to the unique iron (10). The catalytically active oxidation state of PFL-AE was determined to be the $[4Fe\text{-}4S]^{1+}$, which is stoichiometrically converted to the $[4Fe\text{-}4S]^{2+}$ cluster with the activation of PFL (11). The electron transferred from the $[4Fe\text{-}4S]^{1+}$ goes into the sulfonium of center of SAM, thereby initiating homolytic cleavage of the S-C(5') bond to produce methionine and a 5'-deoxyadenosyl radical intermediate. This radical intermediate is the species that abstracts the pro-*S* hydrogen atom from glycine 734 on PFL to generate the active, glycyl radical containing form of PFL (4,6). Several studies have shown that flavodoxin can serve as an electron donor for the PFL system and presumably reduces PFL-AE in the presence of PFL and substrates (2,12-15).

The catalytically active oxidation state of PFL-AE was determined to be the $[4Fe\text{-}4S]^{1+}$, which is stoichiometrically converted to the $[4Fe\text{-}4S]^{2+}$ cluster with the activation of PFL (11). Although PFL is a dimer composed of identical subunits and therefore has two identical active sites, interestingly only one site is activated in the presence of PFL-AE (16). The active site of PFL is ~ 8 Å from the surface of the enzyme suggesting that large conformational changes are required for the active site finger loop to unfold and emerge from the core of the protein to bind PFL-AE and become activated (17). Experimental evidence confirms that the core of PFL unfolds during PFL-AE binding

which leads to large conformational changes in the enzyme (17). Modeling studies suggest that after PFL is active, it may take on a new conformation that is different from the inactive enzyme (6). It seems reasonable to speculate that there may be an allosteric effect caused by PFL-AE binding and PFL activation leading to the availability of only one active site on the PFL dimer.

Our goals are to overexpress and purify flavodoxin, NADP+ flavodoxin oxidoreductase, pyruvate:flavodoxin oxidoreductase, pyruvate formate-lyase activating enzyme, and pyruvate formate-lyase to study protein-protein interactions, electron transfer, and activation of the pyruvate formate-lyase system.

Experimental Procedures

Materials

The pET-14b plasmid used in *fpr* and *fldA* cloning was obtained from Novagen and the *Escherichia coli* cell lines BL21(DE3)pLysS and XL-1 Blue Supercompetent cells were obtained from Stratagene. The PFL plasmid (pKK223-3) pKK-PFL was obtained as a generous gift from John Kozarich (Merck). The PFL-AE plasmid, pCal-n-EK was obtained from Stratagene. Primers were purchased from Integrated DNA technologies. Restriction enzymes and T4 DNA ligase were purchased form New England Biolabs and Pfu Turbo polymerase was purchased from Agilent. NovaBlue Gigasingles competent cells were purchased form EMD4 Biosciences. Other chemicals used were of the highest available purity and commercially available.

Growth and Expression of FNR

The gene for $NADP^+$ flavodoxin oxidoreductase (FNR, gene symbol *fpr*) was cloned from *Escherichia coli* strain B genomic DNA using the following primers: forward 5'-AGACCATGGCTGATTGGGTAA-3' and reverse 5'-CGAGGATCCTTACCAGTAATG-3'. The PCR product was digested in conjunction with the pET-14b plasmid using NcoI and BamHI restriction enzymes. The gene and plasmid were purified and ligated using DNA ligase and then used to transform XL-1 Blue Supercompetent cells. The entire *fpr* gene was sequenced by Nevada Genomics Center. The plasmid DNA was then purified and used to transform BL21(DE3)pLysS cells. A single colony was used to inoculate 50 mL of LB media containing 50 μg/mL ampicillin and grown overnight for ~16 hours. The culture was then added to 10 L of LB/Ampicillin media inside a sterile fermentor (New Brunswick) and grown at 37 °C with agitation set to 300 rpm with and air flow rate of 5 L/min. Optical density of the growth was monitored until $O.D._{600\ nm} \sim 0.6 - 0.8$, at which time expression was induced by the addition of 1 mM isopropyl-β-thiogalactopyranoside (IPTG). The culture was grown for an additional two hours before being harvested by centrifugation at 6,000 rpm (FIBERLite rotor, F9-4X1000Y) for 10 minutes; cells were then flash frozen in liquid nitrogen and stored at -80 °C.

Purification of FNR

$NADP^+$ flavodoxin oxidoreductase was purified from *Escherichia coli* BL21(DE3)pLysS cells. Flash frozen cell pellets were agitated using a stir bar in lysis buffer containing 20 mM HEPES, 1% (w/v) TritonX-100, 5% (w/v) glycerol, 10 mM

$MgCl_2$, 1 mM PMSF, 8 mg lysozyme, 0.1 mg DNAse I, and 0.1 mg RNAse A, pH 7.2 for 30 minutes. Cells were then put on ice for 30 minutes with stirring and cells were broken up using a syringe with a 16 gauge needle. The cell lysate was centrifuged at 18,000 rpm (FIBERLite rotor, F21-8 x 50) for 30 minutes and the supernatant was pipetted into a beaker for ammonium sulfate precipitation (18). The majority of the FNR protein pelleted out in the 60-100% ammonium sulfate fraction. The Superdex-75 column (5 x 60 cm) was equilibrated in gel filtration buffer (50 mM Tris, 200 mM NaCl, pH 8.5) and the 60-100 % ammonium sulfate pellet was dissolved in 10 mL volume and loaded onto the superloop to be injected onto the column. Flavodoxin reductase was run over the column once and fractions containing the most intense yellow color were collected corresponding to holo-flavodoxin reductase. Fractions were then concentrated using an Amicon Ultra 10 kDa MWCO filter.

Growth and Expression of Fld

The gene for flavodoxin (*fldA*) was cloned from *Escherichia coli* strain B genomic DNA using the following primers: forward GGACCATGGCTATCACTGGCA and reverse GCAGGATCCTCAGGCATTGAG. The *fldA* gene was digested in conjunction with the pET-14b vector using NcoI and BamHI restriction enzymes followed by DNA purification. The *fldA* gene and pET-14b vector were ligated and used to transform XL-1 Blue Supercompetent cells. The entire *fldA* gene was sequenced by the Nevada Genomics Center. The plasmid DNA was then purified from the propagation cell line and used to transform the BL21(DE3)pLysS cells. One colony was used to inoculate 50 mL of LB media containing 50 µg/mL of ampicillin and grown overnight for ~ 16

hours. The overnight growth was then added to 10 L of LB/ampicillin media in a sterile fermentor (New Brunswick). The fermentor agitation was set to 300 rpm with an air flow rate of 5 L/minute at 37 °C. Optical density of the growth was monitored until $O.D._{600\ nm}$ ~ 0.6 – 0.8 when it was induced with 1 mM IPTG and grown for an additional two hours. The cells were pelleted by centrifugation at 6,000 rpm (FIBERLite rotor, F9-4X1000Y) for 10 minutes and then flash frozen using liquid nitrogen and stored at -80 °C.

Purification of Fld

Flavodoxin was purified from cell paste from *Escherichia coli* BL21(DE3)pLysS cells using an enzymatic lysis buffer for 30 minutes. The buffer was composed of 20 mM HEPES, 1% (w/v) TritonX-100, 5% (w/v) glycerol, 10 mM $MgCl_2$, 1 mM PMSF, 8 mg lysozyme, 0.1 mg DNAse I, and 0.1 mg RNAse A, pH 7.2. The cell lysate was centrifuged at 18,000 rpm (FIBERLite rotor, F21-8 x 50) for 30 minutes and the supernatant was decanted into a beaker for ammonium sulfate precipitation (18). The flavodoxin was contained in the 60-100% fraction, which was re-dissolved in gel filtration buffer (50 mM Tris, 200 mM NaCl, pH 8.5) then pipetted into a superloop and loaded onto the Superdex-75 column (5 x 60 cm). The column was previously equilibrated with gel filtration buffer and flavodoxin fractions were collected and samples were taken for SDS-PAGE analysis. The purest fractions with the most intense color were pooled and concentrated using a 10 kDa Amicon Ultra 10 kDa MWCO filter, then flash frozen in liquid nitrogen and stored at -80 °C.

Growth and Expression of PFL

Cells expressing pyruvate formate-lyase (PFL) was grown from a single colony of transformed cells. A single colony of *Escherichia coli* BL21(DE3)pLysS containing the pKK-PFL plasmid was used to inoculate 50 mL of LB media containing ampicillin (50 μg/mL). The culture was grown overnight to saturation for at least 16 hours before being added to 10 L of sterile LB media containing 50 μg/mL ampicillin in a fermentor. The agitation on the fermentor was set to 250 rpm at 37 °C with a constant air purge of 5 L/min. Optical density was monitored until $O.D._{600\ nm}$ was in the range of 0.6 - 0.8, at which time IPTG was added at a 1 mM concentration. The growth was continued for an additional two hours before cells were harvested by centrifugation at 6,000 rpm (FIBERLite rotor, F9-4X1000Y). Cell paste was flash frozen in liquid nitrogen and stored at -80 °C in falcon tubes.

Purification of PFL

PFL was purified from *Escherichia coli* cell paste from the BL21(DE3)pLysS cell line containing the pKK-PFL plasmid. Approximately 25 grams of cells were added to 50 mL of enzymatic lysis buffer composed of 20 mM HEPES, 1% (w/v) TritonX-100, 5% (w/v) glycerol, 10 mM $MgCl_2$, 1 mM PMSF, 8 mg lysozyme, 0.1 mg DNAse I, and 0.1 mg RNAse A, pH 7.2. Cells were lysed at room temperature with a stir bar for 30 minutes then put on ice for an additional 30 minutes and broken up with a syringe with an 18 gauge needle. The lysate was centrifuged at 18,000 rpm (FIBERLite rotor, F21-8 x 50) for 30 minutes and the supernatant was decanted and a 25 mL volume was pipetted into a superloop and loaded on an AP5 Ion exchange column (Accell Plus QMA Anion

Exchange Column, Quaternary methylamine 300A Waters Corporation, 5 x 30 cm). The column was previously equilibrated with buffer A (20 mM Tris, pH 7.2) and a linear gradient was set up from 0 % Buffer A to 100 % Buffer B (20 mM Tris, 0.5 M NaCl, pH 7.2) for 900 mL. PFL eluted from the column at approximately 240 mM NaCl and fractions with the highest purity as judged by SDS-PAGE were pooled and concentrated. PFL was buffer exchanged into Buffer C (40 mM Tris, 1 M ammonium sulfate, pH 7.2) and then 25 mL was loaded onto a phenyl-sepharose column (Pharmacia 16/10) equilibrated with Buffer C, using a superloop. A gradient was run from 0 % Buffer C to 100 % Buffer A over 50 mL and fractions of the highest purity enzyme were concentrated to 5 mL using a Amicon Ultra 10 kDa MWCO filter. Samples were flash frozen using liquid nitrogen and stored at -80 °C.

Growth and Expression of PFL-AE

A single colony of *Escherichia coli* BL21(DE3)pLysS/pCALnAE3 cells were used to inoculate 50 mL of LB media containing ampicillin (50 μg/mL). The cell culture was grown overnight (at least 16 hours) at 37 °C in a shaker with agitation set to 250 rpm. The next day, the culture was added to 10 L of sterile media composed of 110 grams of casamino acids, 84.2 grams of MOPS, 8 grams of tricine, 29.3 grams of NaCl, 16 grams of KOH, 5.1 grams of NH_4Cl, 50 grams of glucose in 200 mL water, 25 mL of O solution (0.1 grams of $FeCl_2 \bullet 4H_2O$ in 10 mL of 12M HCl, plus 10 mL of water), 1mL of T solution (18.4 mg $CaCl_2 \bullet 2H_2O$, 64 mg of H_3BO_3, 40 mg of $MnCl_2 \bullet 4H_2O$, 18 mg of $CoCl_2 \bullet 6H_2O$, 4 mg of $CuCl_2 \bullet 2H_2O$, 340 mg of $ZnCl_2$, 605 mg of $Na_2MoO_4 \bullet 2H_2O$, dilute to 100 mL with water), 2.68 grams of $MgCl_2 \bullet 6H_2O$ in 50 mL of water. Ampicillin and

chloramphenicol were added to the fermentor to a final concentration of 50 μg/mL and 34 μg/mL, respectively. The following vitamins were added (10 mg each): biotin, pantothenic acid, vitamin B12, thiamine, folic acid, riboflavin, niacinamide, thioctic acid, and pyridoxine before inoculation of the fermentor (New Brunswick). The cells were grown in the fermentor at 37 °C with the agitation set to 300 rpm with air flow at 5 L/ minute. The optical density of the growth was monitored until O.D. $_{600\ nm}$ was approximately 0.5, at which time expression was induced by the addition of IPTG to a final concentration of 0.5 mM; 0.75 grams of ferrous ammonium sulfate was added to the fermentor and the growth was continued for two hours after induction. After two hours, cooling of the fermentor was started; when it reached 30 °C the air purge was turned off and replaced by N_2 gas at 5 L/minute. After 20 minutes of purging with N_2 gas, another addition of 0.75 grams of $Fe(NH_4)_2(SO_4)_2 \bullet 6H_2O$ was added. After the temperature decreased to 20 °C, the fermentor was placed in a deli fridge and purged with N_2 gas overnight for at least 14 hours. Cells were then harvested by centrifugation at 6,000 rpm (FIBERLite rotor, F9-4X1000Y) for 10 minutes and flash frozen in liquid nitrogen and stored at -80 °C.

Purification of PFL-AE

The PFL-AE purification was performed using *Escherichia coli* BL21(DE3)pLysS/pCALnAE3 cell paste. The purification was done in a single day under strict anaerobic conditions in a Coy chamber (Coy Laboratories, Grass Lake, MI). Lysis buffer was thoroughly degassed on a schlenk line and gel filtration buffer was purged with N_2 gas for one hour before they were brought into the Coy chamber. PFL-AE cell

paste was lysed in an enzymatic lysis buffer (2 mL of buffer/gram of cells) containing 50 mM Tris, 200 mM NaCl, 1% Triton X-100, 5% glycerol, 10 mM $MgCl_2$, 1 mM DTT, 8 mg lysozyme, 1 mM PMSF, ~0.1 mg of RNAse A and DNAse I, pH 7.5 for 30 minutes at room temperature. The lysis mixture was then put on ice for an additional 30 minutes and cells were broken up using a syringe with a 16 gauge needle. The lysate was then centrifuged at 18,000 rpm (FIBERLite rotor, F21-8 x 50) for 30 minutes and the supernatant was decanted into a beaker for ammonium sulfate precipitation (18). The PFL-AE was in the 20 – 60% ammonium sulfate fraction. The protein was re-dissolved using gel filtration buffer (50 mM Tris, 200 mM NaCl, 1 mM DTT, pH 8.5) and all the protein was pipetted into a superloop and loaded on the Superdex-75 column (5 x 60 cm). The column was previously equilibrated using gel filtration buffer. The PFL-AE was run over the Superdex-75 column twice to obtain protein of the highest purity. The purest fractions with the darkest brown color or highest 426 nm/280 nm ratio were pooled and concentrated using a Amicon Ultra 10 kDa MWCO filter. Samples were flash frozen in liquid nitrogen and stored at -80 °C.

Growth and Expression of PFOR

The gene for pyruvate:flavodoxin oxidoreductase (PFOR, gene designation *ydbK*) was cloned from *Escherichia coli* strain B genomic DNA using the following primers: forward 5'-CGG CTC TAG AAT GAT TAC TAT TGA CGG TAA TGG C-3' and reverse 5'-GAG CGT ATA CTT AAT CGG TGT TGC TTT TTT CCG C-3'. The *E. coli* PFOR gene *ydbK* was digested using XbaI and NdeI restriction enzymes in conjunction with the pET-14b vector followed by DNA purification by agarose gel electrophoresis.

The digested pET-14b vector was ligated to digested *ydbK* using DNA ligase which was allowed to incubate overnight at 4 °C before they were used to transformation with Nova Blue GigaSingles. The plasmid DNA for *ydbK*-pET-14b was subsequently purified using a miniprep kit from Quiagin. The *ydbK* entire gene was sequenced by the Nevada Genomics Center. Pure plasmid DNA was used to transform BL21(DE3)pLysS cells and pilot expressions were performed to detect overexpression of the *ydbK* gene (Figure 2).

Large-scale growths were performed using minimal media under identical growth conditions used for PFL-AE. Overnight growths were composed of 50 mL of LB media with 50 μg/mL of ampicillin and 34 μg/mL chloramphenicol and were inoculated using a single colony from a plate. The overnight growth was then added to a sterile fermentor (New Brunswick) containing 10 L of minimal media:110 grams casamino acids, 84.2 grams of MOPS, 8 grams of tricine, 29.3 grams of NaCl, 16 grams of KOH, 5.1 grams of NH_4Cl, 50 grams of glucose in 200 mL water, 25 mL of O solution (0.1 grams of $FeCl_2 \bullet 4H_2O$ in 10 mL of 12M HCl, plus 10 mL of water), 1 mL of T solution (18.4 mg $CaCl_2 \bullet 2H_2O$, 64 mg of H_3BO_3, 40 mg of $MnCl_2 \bullet 4H_2O$, 18 mg of $CoCl_2 \bullet 6H_2O$, 4 mg of $CuCl_2 \bullet 2H_2O$, 340 mg of $ZnCl_2$, 605 mg of $Na_2MoO_4 \bullet 2H_2O$, dilute to 100 mL with water), 2.68 grams of $MgCl_2 \bullet 6H_2O$, bring to 50 mL with water. Ampicillin and chloramphenicol were added to the growth at 50 μg/mL and 34 μg/mL final concentrations, respectively, and 10 mg of each of the following vitamins were added: biotin, pantothenic acid, vitamin B12, thiamine, folic acid, riboflavin, niacinamide, thioctic acid, and pyridoxine. The fermentor agitation was set to 300 rpm at a temperature of 37 °C with air flow rate of 5 L/minute. The growth was given two hours before optical

density was measured. When the cells reached an O.D. $_{600\ nm}$ ~ 0.8, gene expression was induced using 100 μM IPTG and the cells were grown for an additional two hours. The cells were pelleted by centrifugation at 6,000 rpms (FIBERLite rotor, F9-4X1000Y) for 10 minutes and then flash frozen in liquid N_2 and stored at -80 °C.

Purification of PFOR

Pyruvate:flavodoxin oxidoreductase was purified from *Escherichia coli* BL21(DE3)pLysS cell paste using an enzymatic lysis buffer for 30 minutes at room temperature followed by 30 minutes on ice. The buffer was composed of 20 mM HEPES, 1% (w/v) TritonX-100, 5% (w/v) glycerol, 10 mM $MgCl_2$, 1 mM PMSF, 8 mg lysozyme, 0.1 mg DNAse I, and 0.1 mg RNAse A, pH 7.2. The cell lysate was centrifuged at 18,000 rpm (FIBERLite rotor, F21-8 x 50) for 30 minutes and the supernatant was decanted into a beaker for ammonium sulfate precipitation (18). Ammonium sulfate cuts were performed over the range of 0-30% and 30-60% saturation and the PFOR was located in the 30-60% cut; which was then dissolved in 20 mL of buffer (20 mM HEPES, 250 mM NaCl, 1 mM DTT, pH 7.4) and injected over a Superdex-75 column (5 x 60 cm) (Figure 14). The column was previously equilibrated with gel filtration buffer: 20 mM HEPES, 250 mM NaCl, 1 mM $MgCl_2$, 1 mM DTT, pH 7.4 and PFOR fractions were collected from the column. The fractions with most intense color were pooled and concentrated using a 10 kDa Amicon Ultra 10 kDa MWCO filter, then flash frozen in liquid N_2 and stored at -80 °C. Pure PFOR was analyzed by SDS-PAGE for size and purity (Figure 15).

Protein Assays

Protein concentrations for PFL-AE were determined using the Bradford assay with bovine serum albumin as a standard (19). Amino acid hydrolysis was performed at the MCB Core facility, University of Massachusetts, Amherst, to provide a correction factor of 0.65 for Bradford assays (20). Extinction coefficients at 280 nm were determined for PFL-AE (39.4 mM^{-1} cm^{-1}), apo-flavodoxin (30.9 mM^{-1} cm^{-1}), and PFL (178 mM^{-1} cm^{-1}) using the ExPASy protparam tool http://web.expasy.org/protparam/. The extinction coefficient for PFL-AE was verified using the Bradford assay with correction factor. For apo-Fld concentrations derived from the above extinction coefficient were compared to stoichiometry in ITC experiments to verify the concentration of apo-Fld knowing that the stoichiometry should be 1:1 (chapter 3). The PFL extinction coefficient was verified using the Bradford assay. Extinction coefficients for holo-flavodoxin ($\varepsilon_{467\ nm}$ = 8250 $M^{-1}cm^{-1}$) and flavin mononucleotide ($\varepsilon_{445\ nm}$ = 12.5 mM^{-1} cm^{-1}) were available in the literature (14,21).

Iron Assays

Iron assays on PFL-AE and PFOR were performed using the Beinert method (22). A standard solution of iron used for atomic absorption spectroscopy was obtained by dilution from 1015 µg/mL to 10.15 µg/mL in 0.1 M H_2SO_4. Iron standard was added to Falcon tubes (USA Scientific) from 0 µL to 200 µL and brought up to a total volume of 1 mL using MQ water. Purified PFL-AE was diluted ten fold and aliquots were added to Falcon tubes and brought to 1 mL volume with MQ water. Reagent A (45% w/v $KMnO_4$/1.2 N HCl; 1:1) was then added to tubes (500 µL) containing iron standard or

purified PFL-AE. Samples were incubated at 65 °C in a hot water bath for 2 hours and then 100 μL of Reagent B (8.8 g Ascorbic acid, 9.7 g $(NH_4)OAc$, 80 mg ferrozine, and 80 mg neocuproine, in water with a final volume of 25 mL) was added. The samples were allowed to incubate at room temperature for 30 minutes, after which, absorbance measurements were taken at 562 nm. PFL-AE iron number was obtained by dividing the iron concentration by PFL-AE protein concentration.

EPR Spectroscopy

EPR spectroscopy was carried out by Dr. Eric Shepard using a Bruker ER-200D-SRC spectrometer equipped with a liquid He cryostat with a temperature controller from Oxford instruments. Spectra were obtained at X-band and all measurements were recorded at 12 K for PFL-AE containing $[3Fe\text{-}4S]^{1+}$ clusters and $[4Fe\text{-}4S]^{1+}$ clusters. Measurements were recorded at 60 K for glycyl radical signals on PFL or the flavodoxin semiquinone. Spin quantification on PFL-AE and PFL was performed as described previously (11). Double integrals of EPR signals were evaluated and spin concentrations of the protein samples were calculated by calibrating double integrals under non-saturating conditions with standards. A Cu(II) and 1 mM EDTA solution was used as a standard to determine PFL-AE iron spin concentrations and a solution of $K_2(SO_3)_2NO$ was used for glycyl radical spin quantification. Concentrations of the $K_2(SO_3)_2NO$ standard were calculated using the optical extinction coefficient (23).

Results and Discussion

Expression and Purification of FNR

$NADP^+$ dependent flavodoxin oxidoreductase (FNR) was cloned from the *fpr* gene from *Escherichia coli* strain B genomic DNA. Primers were designed to incorporate NcoI and BamHI restriction endonuclease sites. The genes were digested, purified, and ligated into the pET-14b vector and the placement of the gene inside the vector was verified by PCR with T7 and *fpr* primers (Figure 2.1). A pilot expression was performed to ensure that FNR was expressed in BL21(DE3)pLysS cells (Figure 2.2). FNR was purified from BL21(DE3)pLysS cells containing the pET-14b FNR plasmid and cells were enzymatically lysed. Ammonium sulfate precipitation was performed and FNR was present in the 60-100% fraction. FNR was further purified using a Superdex-75 size exclusion column (Figure 2.3). The purest fractions with the most intense yellow color were pooled and concentrated (Figure 2.4). Protein yield was approximately 10 mg/L of bacterial culture.

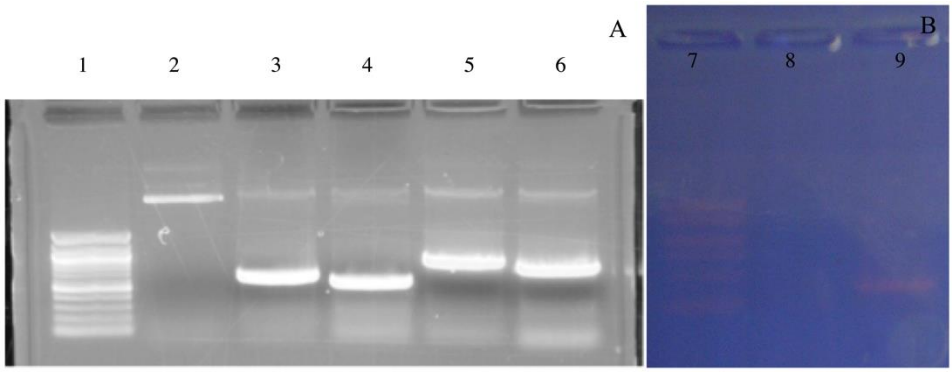

Figure 2.1: A) PCR of Fld and FNR in the pET-14b plasmid. Lane 1) Standards, Lane 2) pET-14b plasmid with the *fldA* gene inserted, Lane 3) Fld amplified using T7 primer, Lane 4) Fld amplified using *fldA* primer, Lane 5) FNR amplified using T7 primer, Lane 6) FNR amplified using *fpr* primer. B) PCR gel of PFOR amplification from *E. coli* the pET-14b/PFOR plasmid. Lane 7) Standards 8) empty lane 9) amplified PFOR

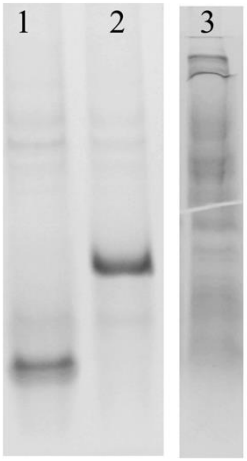

Figure 2.2: 12 % SDS-PAGE gel showing expression of Fld, FNR and PFOR. Lane1) Expression of Fld, Lane 2) Expression of FNR Lane 3) Expression of PFOR.

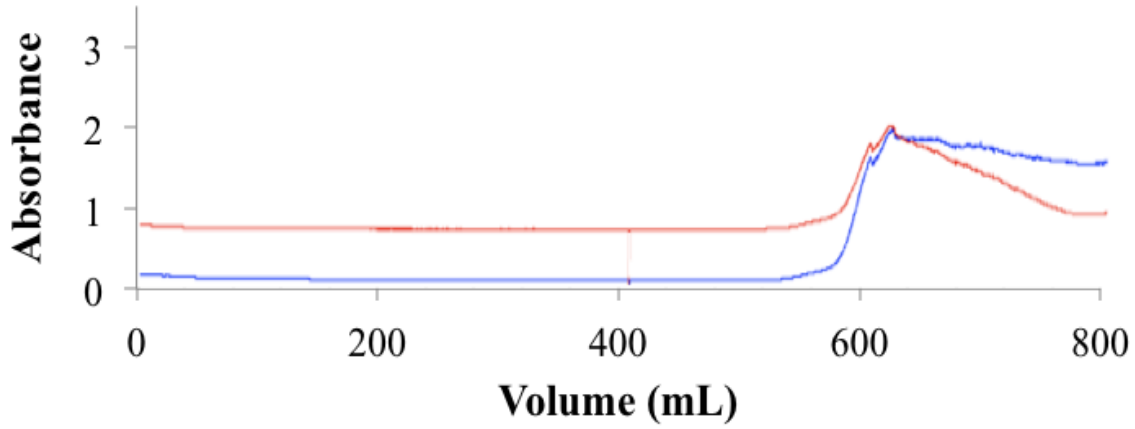

Figure 2.3: Chromatogram of FNR purification using the Superdex-75 column. Red trace: 260 nm absorbance, Blue trace: 280 nm absorbance. FNR eluted from 600-700 mL using an isocratic gradient of 20 mM HEPES, 50 mM NaCl, pH 8.0.

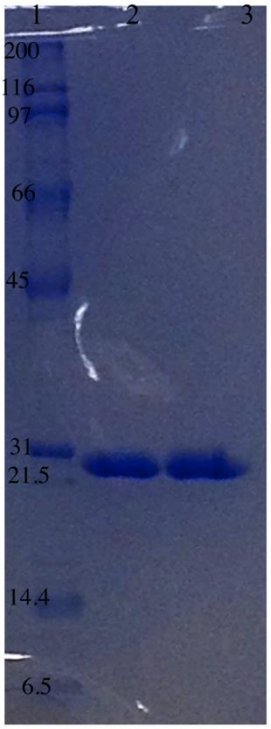

Figure 2.4: 12% SDS-PAGE gel of purified FNR. Lane 1) Standards, Lane 2) Pure FNR, Lane 3) Pure FNR. Fractions were pooled from 600-700 mL and concentrated using a YM-10 MWCO filter. The flow rate was 5 mL/minute.

Expression and Purification of Fld

Flavodoxin was cloned from the *fldA* gene from *Escherichia coli* strain B genomic DNA. Primers were designed for the *fldA* gene to include NcoI and BamHI restriction endonuclease sites. The *fldA* gene and pET-14b vector were digested and purified before ligation and gene insertion into the pET-14b vector was verified by PCR using T7 and *fldA* primers (Figure 2.1). Pilot expressions were then performed to ensure that flavodoxin was expressed in BL21(DE3)pLysS cells (Figure 2.2). Flavodoxin was purified by enzymatic lysis from *Escherichia coli* BL21(DE3)pLysS cells containing the pET-14b vector with the *fldA* gene inserted. Ammonium sulfate precipitation was performed as a first step in protein purification and Fld was found primarily in the 60 - 100% fraction. The protein was then run over a Superdex-75 size exclusion chromatography column (Figure 2.5). The purest fractions with the most intense orange color were pooled and concentrated (Figure 2.6). Total protein yield for flavodoxin was approximately 10 mg/L of bacterial culture.

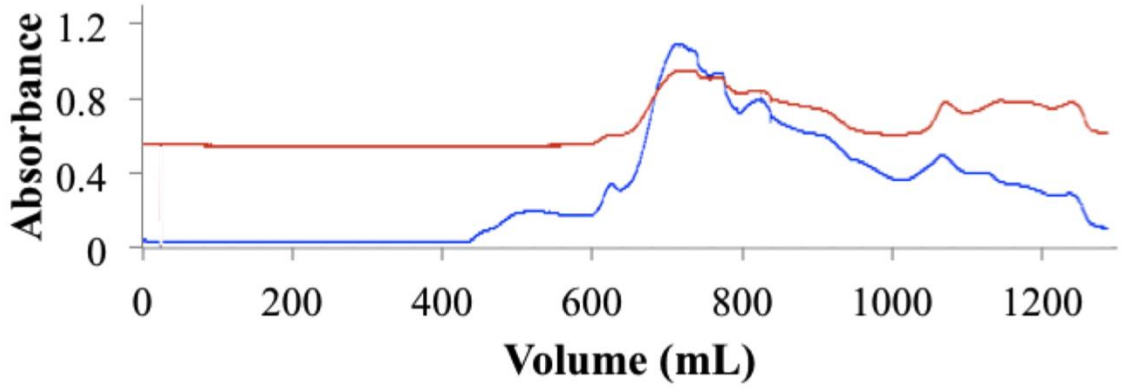

Figure 2.5: Chromatogram of Fld purified on the Superdex-75 column using 20 mM HEPES, 50 mM NaCl, pH 8.0 with an isocratic gradient. Blue trace: 280 nm, Red trace: 466 nm. Fld eluted in the 650-800 mL range. The flow rate was 5 mL/minute.

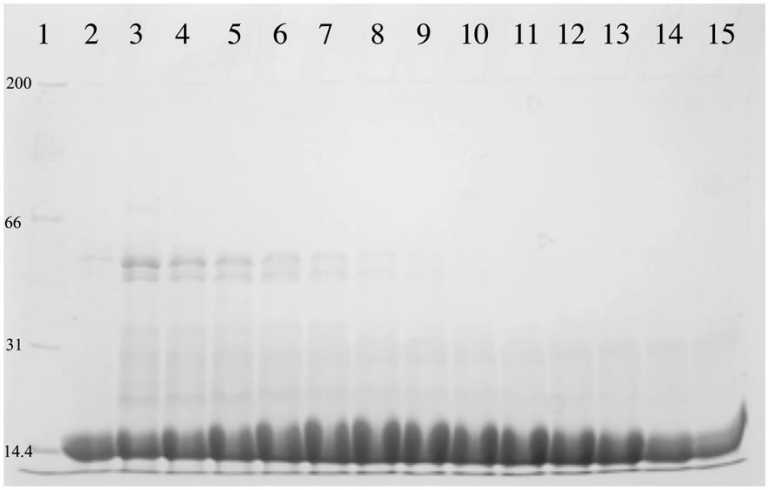

Figure 2.6: 12 % SDS-PAGE gel of purified Fld. Fractions taken from Fld purification from 650-800 mL.

Expression and Purification of PFL

PFL was purified from *Escherichia coli* BL21(DE3)pLysS/pKK-PFL cells. The cells were lysed enzymatically and the lysate volume was divided in half to ensure that the column was not overloaded. Each half was loaded separately onto a Q-sepharose

anion exchange column (Figure 2.7) and then run on an SDS-PAGE gel (Figure 2.8). The purest protein was pooled and buffer exchanged and run over a hydrophobic phenyl-sepharose column (Figure 2.9) to yield protein with high purity, which was run on an SDS-PAGE gel (Figure 2.10). PFL protein yield was approximately 50 mg/L of bacterial culture.

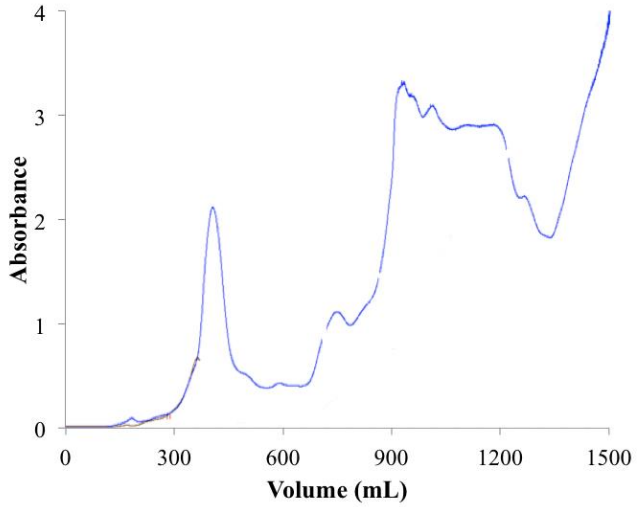

Figure 2.7: Chromatogram of PFL purification using a Q-sepharose column. Blue trace: 280 nm. Half of the PFL cell lysate was loaded (30-50 mL). Gradient: 300 mL 20 mM HEPES, pH 7.2 (no salt buffer), followed by 900 mL of starting with no salt buffer and ending at 100% 20 mM HEPES, 500 mM NaCl, pH 7.2 (high salt buffer) then 300 mL high salt buffer. PFL eluted from 1000-1200 mL. The flow rate was 5 mL/minute.

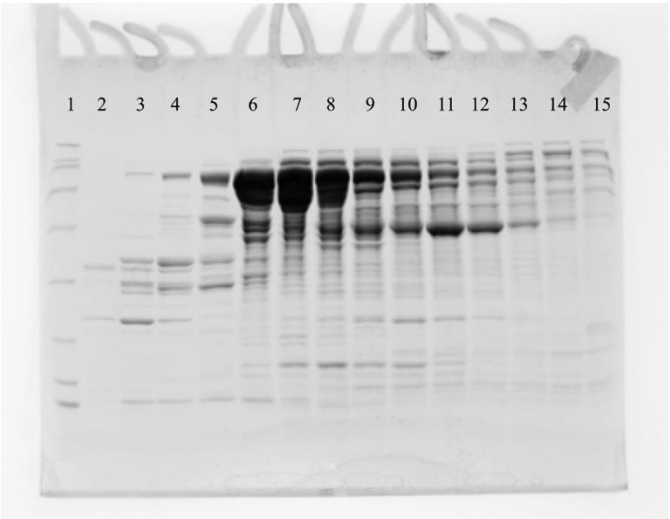

Figure 2.8: 12% SDS-PAGE gel of PFL purified on a Q-sepharose column. Lane 1) Standards, Lanes 2-15 Fractions taken during PFL purification from 1000 mL to 1200 mL.

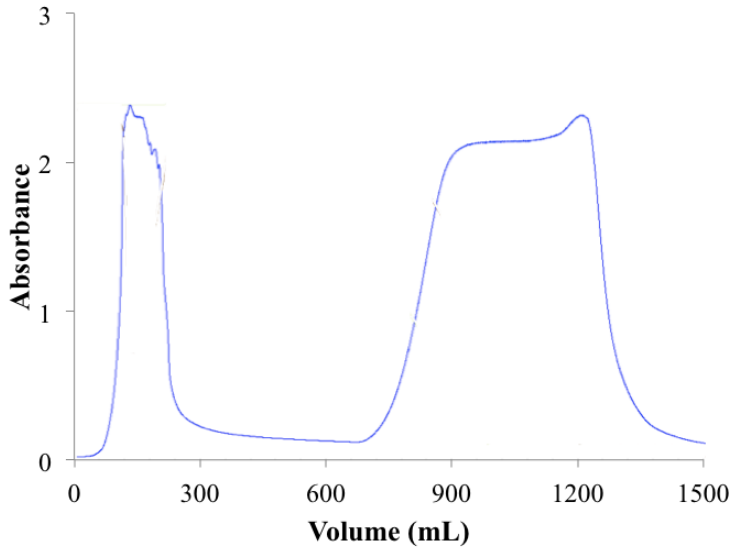

Figure 2.9: Chromatogram of PFL purification using the phenyl-sepharose column. Blue trace: 280 nm. PFL eluted from 1050-1150 mL. Gradient: 100% buffer B (20 mM HEPES, 1 M $(NH_4)_2SO_4$, pH 7.2) for 50 mL, followed by 50 mL starting at 100% buffer B and ending at 100% buffer A (20 mM HEPES, pH 7.2), then 50 mL of buffer A. The flow rate was 1 mL/minute. All the protein from the Q-sepharose purification above was loaded.

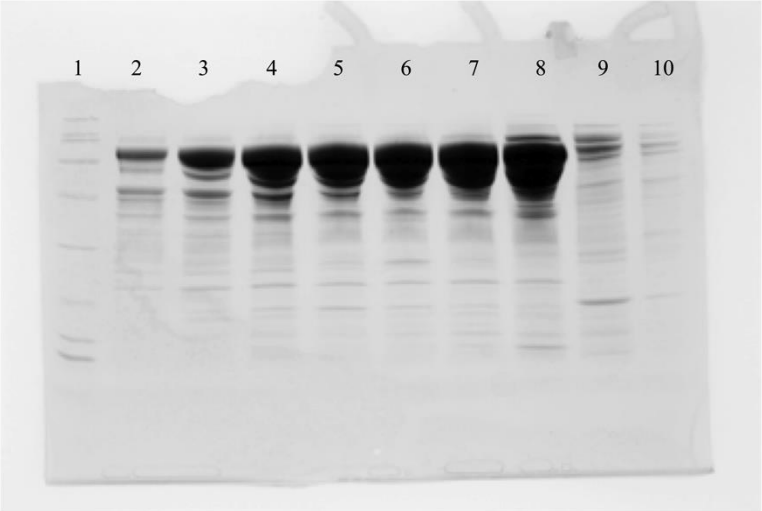

Figure 2.10: 12 % SDS-PAGE gel of PFL purified on a phenyl-sepharose column. Lane 1) Standards, Lanes 2-10 Fractions taken during PFL purification from 1050-1150 mL.

Expression and Purification of PFL-AE

PFL-AE was purified from *Escherichia coli* BL21(DE3)pLysS cells containing the pCal-n-AE3 plasmid. Cells were lysed enzymatically and the protein was first purified using ammonium sulfate precipitation. PFL-AE was present in the 20-60% fraction, which was re-dissolved in buffer and loaded onto a Superdex-75 size exclusion column (Figure 2.11). Fractions with the darkest brown color eluted from the column were pooled and concentrated before being loaded onto the Superdex-75 column for a second round of purification (Figure 2.12). Fractions were analyzed based on 426 nm/280 nm absorbance ratio and this was compared to SDS-PAGE gels for protein purity (Figure 2.13). PFL-AE with the highest 426 nm/280 nm ratio with the highest purity were pooled and concentrated, then flash frozen in liquid N_2 and stored at -80 °C. Typical yield of PFL-AE was 40 mg/L of bacterial culture.

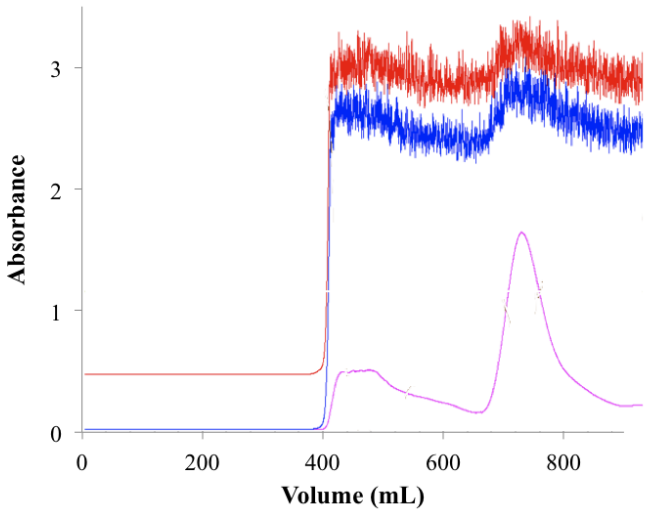

Figure 2.11: Chromatogram of PFL-AE purification on a superdex-75 column after ammonium sulfate precipitation (first elution). The entire cell lysate was loaded onto the column (~100 mL) Blue trace: 280 nm, Red trace: 266 nm, Magenta trace: 426 nm. An isocratic gradient was used with 20 mM HEPES, 200 mM NaCl, 1 mM DTT, pH 7.4 with a flow rate of 5 mL/minute. PFL-AE eluted from 700-800 mL.

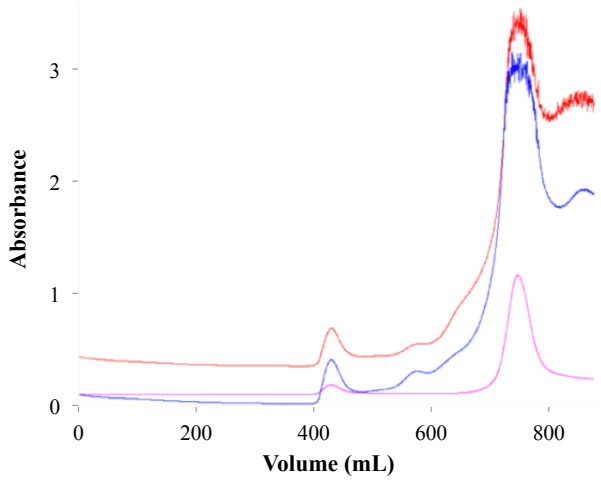

Figure 2.12: Chromatogram of PFL-AE purification on a superdex-75 column (second elution). Blue trace: 280 nm, Red trace: 266 nm, Magenta trace: 426 nm. The pure PFL-AE that eluted from 700-800 mL above was concentrated down to 10 mL using a YM-10 MWCO filter and loaded onto the column. An isocratic gradient was used with 20 mM HEPES, 200 mM NaCl, 1 mM DTT, pH 7.4 and PFL-AE eluted from 700-800 mL.

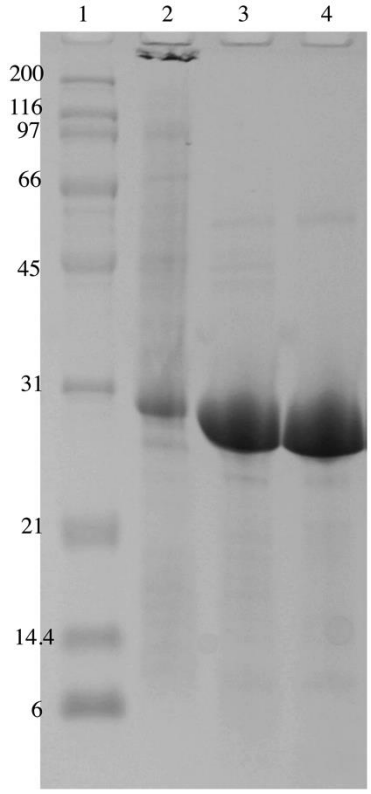

Figure 2.13: 12 % SDS-PAGE gel of PFL-AE. Lane one: molecular weight marker, lane two: cell lysate, lane three: PFL-AE after elution number one on the Superdex-75 size exclusion column, lane four: PFL-AE after elution two on the Superdex-75 column. Fractions of PFL-AE were pooled and concentrated using a YM-10 MWCO filter.

Expression and Purification of PFOR

PFOR was purified from chemically lysed cells from *Escherichia coli* strain B and subjected to ammonium sulfate precipitation. PFOR was located in the 30 – 60 % saturation fraction of the ammonium sulfate precipitation and the pellet was re-dissolved in 20 mM HEPES, 250 mM NaCl, 1mM $MgCl_2$, 1mM DTT, pH 7.4 and ran over the Superdex-75 column (Figure 2.14). The protein with the most intense brown color was collected and pooled and then concentrated using a 10 kDa MWCO filter and run on an SDS-PAGE gel. The purification did not yield protein of high purity (data not shown). The protein was flash frozen with liquid N_2 and stored at -80 °C. The as isolated enzyme

was determined to be inactive during Fld reduction and PFL activity assays. PFOR was then reconstituted to incorporate [4Fe-4S] clusters in a solution of 2.5 µM PFOR homodimer, 1mM TPP, 5 mM $MgCl_2$, in 20 mM HEPES, 250 mM NaCl, 10 mM DTT, pH 7.4. Stock solutions were made of 50 mM $FeCl_3$ and 50 mM Na_2S and iron was added first in 5 µL aliquots, ten times, while spacing each addition by one minute. Na_2S was then added in the same manner with the exception of smaller additions of 1.5 µL each for a total of seven additions. The protein incubated at room temperature for 2.5 hours before it was centrifuged at 13,000 rpm for 10 minutes at 4 °C to remove iron sulfur precipitates. The protein was then loaded onto a G-25 desalting column to separate residual iron sulfur clusters and other material from PFOR. The protein was collected as it came off the column and was subsequently concentrated using a 10 kDa MWCO filter and flash frozen with liquid N_2 before storage at -80 °C.

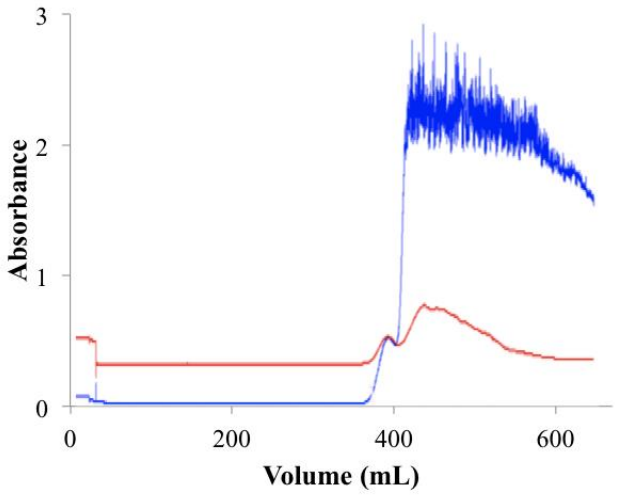

Figure 2.14: PFOR purification using a Superdex-75 column with an isocratic gradient of 20 mM HEPES, 250 mM NaCl, 1mM $MgCl_2$, 1mM DTT, pH 7.4. Blue trace: 280 nm, Red trace: 426 nm. PFOR eluted from 425-500 mL. The flow rate was 5 mL/minute.

Characterization of Purified PFL-AE

Purified PFL-AE in the presence of DTT has been previously shown to contain primarily $[4Fe\text{-}4S]^{2+}$ clusters with a small contribution from $[3Fe\text{-}4S]^{1+}$ clusters (24). Since $[4Fe\text{-}4S]^{2+}$ clusters are EPR silent, the only signal present in as isolated PFL-AE is due to the contribution of the $[3Fe\text{-}4S]^{1+}$ clusters. Photoreduction of PFL-AE affords complete conversion from the $[3Fe\text{-}4S]^{1+}$ cluster to the catalytically active $[4Fe\text{-}4S]^{1+}$ cluster (Figure 2.15). Iron assays yield iron numbers of 3-3.8 irons/protein for different purifications.

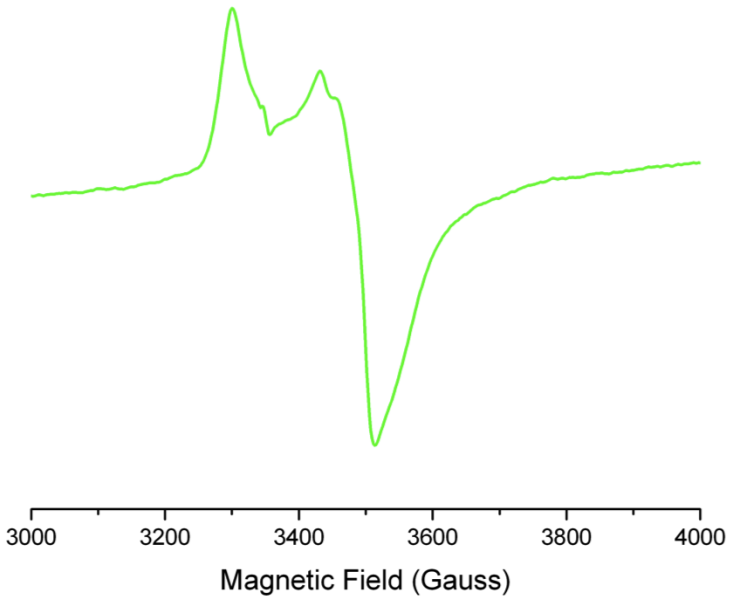

Figure 2.15: X-band EPR spectrum of PFL-AE in the reduced state ($[4Fe\text{-}4S]^{1+}$) at 12 K. The spectrum was measured on a Bruker ER-200D-SRC spectrometer with a frequency of 9.37 GHz, a microwave power of 1.59 mW, a 100 kHz modulation frequency, a 5 G modulation amplitude, and the spectrum was the sum of 4 scans. PFL-AE (100 μM) was reduced using 50 μM 5-deazariboflavin for 30 minutes using a 500 W halogen lamp.

Characterization of Purified Fld

Purified flavodoxin has three oxidation states for the flavin mononucleotide cofactor, fully oxidized, one electron reduced (semiquinone), and two electron reduced (hydroquinone). Of these three oxidation states, there is only one EPR active oxidation state, corresponding to the one electron reduced or semiquinone oxidation state. Photoreduction of the as isolated fully oxidized flavodoxin affords complete conversion to the semiquinone oxidation state (Figure 2.16). Extended incubation times with strong reducing agents such as sodium dithionite or prolonged photoreduction will produce the two electron reduced or hydroquinone oxidation state, which is EPR silent (Figure 2.17).

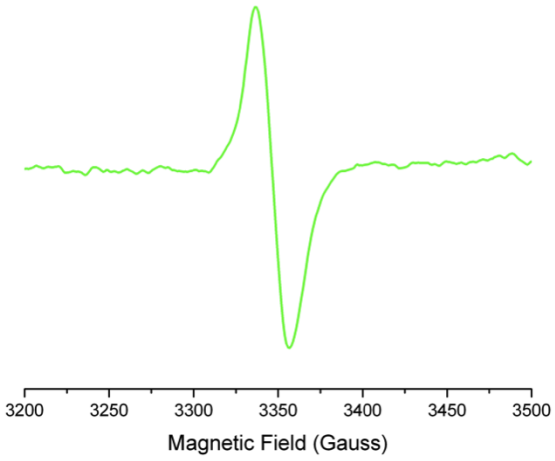

Figure 2.16: X-band EPR spectrum of Fld in the semiquinone oxidation state in 100 mM tris, pH 7.6. The spectrum was measured on a Bruker ER-200D-SRC spectrometer at 60 K with a frequency of 9.37 GHz, a microwave power of 0.06 mW, a modulation frequency of 100 KHz, with a 5G modulation amplitude, the spectrum was the sum of 4 scans. The protein was reduced using 50 μM 5-deazariboflavin with a 500 W halogen lamp for 30 minutes.

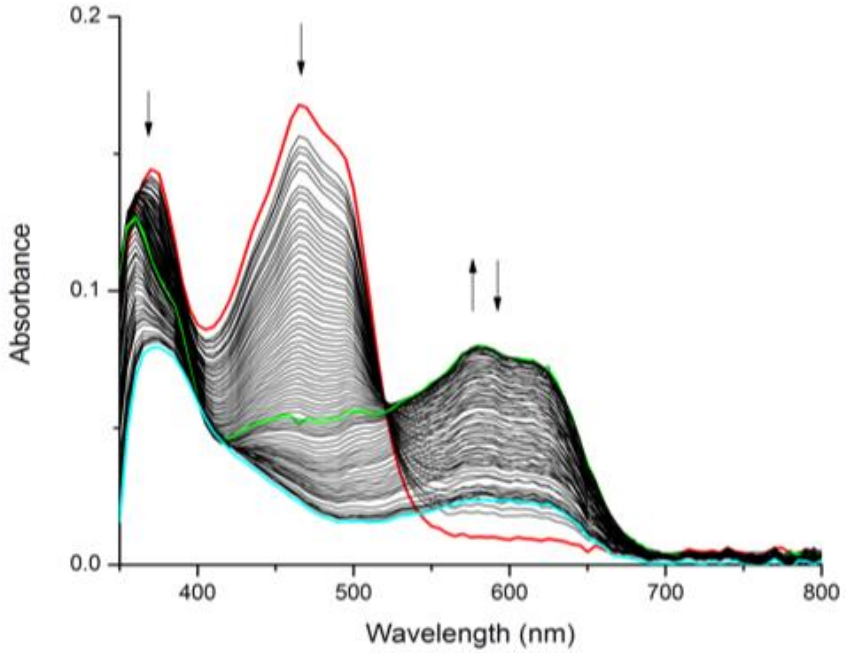

Figure 2.17: UV-Vis of 20 μM Fld in the presence of 1 mM sodium dithionite in 20 mM HEPES, 50 mM NaCl, pH 8.0 buffer. Absorbance scans were monitored as a function of time. Red: fully oxidized flavodoxin, Green: semiquinone flavodoxin (20 minutes incubation time), Cyan: hydroquinone flavodoxin (2 hours incubation time)

Characterization of PFOR

PFOR was found in the 30 – 60% saturated fraction during ammonium sulfate precipitation. PFOR eluted from the column around 400 mL and had an absorbance at 426 nm, typical of an iron sulfur cluster containing enzyme. Iron assays on as isolated PFOR from *E. coli* show that the enzyme has an iron number of 1.24 ± 0.2 Fe/subunit. Under ideal conditions, PFOR should contain 12 Fe/subunit so not surprising, this enzyme was inactive. After reconstitution, PFOR was determined to have an iron number of 15.9 ± 0.7, indicating that there is probably some residual iron sulfur precipitates, which are evident by absorbance above baseline at 800 nm in UV-vis (Figure 2.18). The

reconstituted PFOR was determined to be active in Fld reduction and PFL activation using UV-vis activity assays.

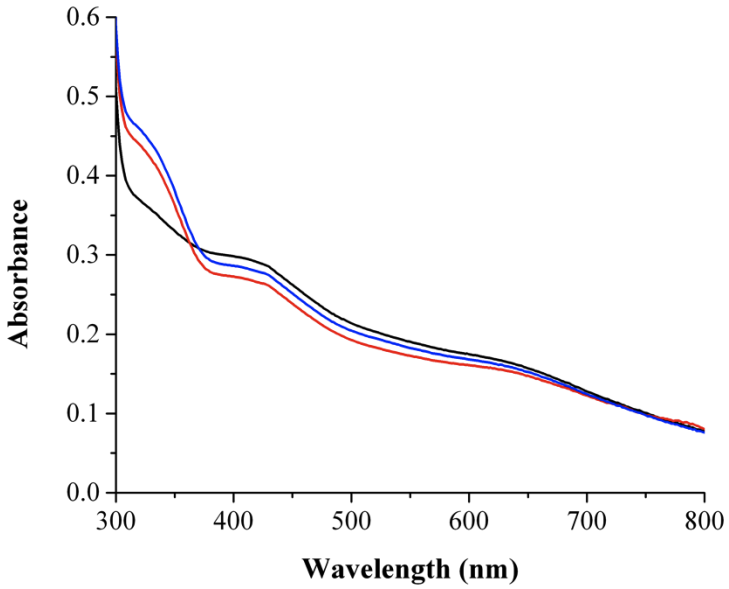

Figure 2.18: UV-vis data of the as isolated and reconstituted PFOR. Both the as isolated and reconstituted PFOR are at 1 µM dimer. Magenta line: As isolated PFOR, Black line: reconstituted PFOR, Blue line: Reconstituted PFOR plus 10 mM pyruvate, Red line: reconstituted PFOR plus 10 mM pyruvate and 100 µM CoA.

Conclusion

Cloning of Fld and FNR was performed in our laboratory and growth and purification conditions were optimized to produce high quality, pure proteins. The growth and purification conditions for PFL and PFL-AE was previously optimized to produce large amounts of active protein with high purity. We attempted to overexpress PFOR from *E. coli* for the first time, however, based on SDS-PAGE gels, PFOR does not appear to be very pure. As isolated PFOR was inactive in Fld reduction and PFL activity assays,

however after reconstitution, the enzyme was capable of reducing Fld and activating the PFL system in the presence of pyruvate, CoA, $MgCl_2$ and TPP. Extinction coefficients were calculated for apo-Fld, PFL-AE, and PFL to obtain accurate concentrations for enzymatic assays. Accurate extinction coefficients already exist for holo-flavodoxin and the Bradford assay works well for quantification of PFOR and FNR for assays. All purified proteins appear to be active, pure, and correctly folded and with reliable extinction coefficients that can be used to easily and accurately calculate protein concentrations. The addition of Fld and FNR or Fld and PFOR to the PFL system in our laboratory provides the opportunity to study the entire PFL system from electron transfer reactions, to PFL activation by PFL-AE and ending with the PFL reaction of pyruvate + CoA ⇆ acetyl-CoA + formate.

References

1. Knappe, J., Bohnert, E., and Brümmer, W. (1965) *Biochim. Biophys. acta* 107, 603-608

2. Knappe, J., and Blaschkowski, H., P. (1975) *Pyruvate Formate-Lyase from Escherichia coli and its Activation System*, Academic Press Inc., New York

3. Knappe, J., and Sawers, G. (1990) *FEMS Microbiol. Rev.* 75, 383-398

4. Knappe, J., Neugebauer, F. A., Blaschkowski, H., P., and Gänzler, M. (1984) *Proc. Natl. Acad. Sci. U.S.A.* 81, 1332-1335

5. Conradt, H., Hohmann-Berger, M., Hohmann, H.-P., Blaschkowski, H., P., and Knappe, J. (1984) *Arch. Biochem. Biophys.* 228, 133-142

6. Frey, M., Rothe, M., Volker Wagner, A. F., and Knappe, J. (1994) *J. Biol. Chem.* 269, 12432-12437

7. Broderick, J. B., Duderstadt, R. E., Fernandez, D. C., Wojtuszewski, K., Henshaw, T. F., and Johnson, M. K. (1997) *J. AM. Chem. Soc.* 119, 7396-7397

8. Sofia, H., J., Chen, G., Hetzler, B., G., Reyes-Spindola, J., F., and Miller, N., E. (2001) *Nucleic Acids Res.* 29, 1097-1106

9. Krebs, C., Broderick, W. E., Henshaw, T. F., Broderick, J. B., and Hanh Huynh, B. (2002) *J. Am. Chem. Soc.* 124, 912-913

10. Walsby, C. J., Ortillo, D., Broderick, W. E., Broderick, J. B., and Hoffman, B. M. (2002) *J. Am. Chem. Soc.* 124, 11270-11271

11. Henshaw, T. F., Cheek, J., and Broderick, J. B. (2000) *J. Am. Chem. Soc.* 122, 8331-8332

12. Blaschkowski, H., P., Neuer, G., Ludwig-Festl, M., and Knappe, J. (1982) *Eur. J. Biochem.* 123, 563-569

13. Knappe, J., Blaschkowski, H., P., Grobner, P., and Schmitt, T. (1974) *Eur. J. Biochem.* 50, 253-263

14. Vetter, H., Jr., and Knappe, J. (1971) *H-Z Physiol. Chem.* 352, 433-446

15. Knappe, J., Schacht, J., Möckel, W., Höpner, T., Vetter, H., Jr., and Edenharder, R. (1969) *European J. Biochem.* 11, 316-327

16. Unkrig, V., Neugebauer, F. A., and Knappe, J. (1989) *Eur. J. Biochem.* 184, 723-728

17. Peng, Y., Veneziano, S. E., Gillispie, G. D., and Broderick, J. B. (2010) *J. Biol. Chem.* 285, 27224-27231

18. Englard, S., and Seifter, S. (1990) *Method. Enzymol.* 182, 291

19. Bradford, M., M. (1976) *Anal. Biochem.* 72, 248-254

20. Broderick, J. B., Henshaw, T., F., Cheek, J., Wojtuszewski, K., Smith, S., R., Trojan, M., R., McGhan, R., M., Kopf, A., Kibbey, M., and Broderick, W., E. (2000) *Biochem. Bioph. Res. Co.* 269, 451-456

21. Muralidhara, B. K., and Wittung-Stafshede, P. (2004) *Biochemistry* 43, 12855-12864

22. Beinert, H. (1978) *Methods Enzymol.* 54, 435-445

23. Murib, H., J., and Ritter, D., M. (1952) *J. AM. Chem. Soc.* 74, 3394-3398

24. Yang, J., Naik, S., G., Ortillo, D., O., Garcia-Serres, R., Li, M., Broderick, W., E., Hanh Huynh, B., and Broderick, J., B. (2009) *Biochemistry* 48, 9234-9241

CHAPTER 3

FLAVODOXIN COFACTOR BINDING INDUCES STRUCTURAL CHANGES THAT ARE REQUIRED FOR PROTEIN-PROTEIN INTERACTIONS WITH $NADP^+$ OXIDOREDUCTASE AND PYRUVATE FORMATE-LYASE ACTIVATING ENZYME

Contribution of Authors and Co-Authors

Manuscripts in Chapters 1, 3, 4, 5, 6

Author Adam V. Crain

Contributions: Conceived and implemented the study, analyzed that data, and wrote the manuscript

Co-Author: Dr. Joan B. Broderick

Contributions: Provided oversight and guidance in experimental design and interpretation. Provided all funding and resources for the projects. Advised on manuscript preparation and edited manuscript drafts.

Flavodoxin Cofactor Binding Induces Structural Changes that are Required for Protein-Protein Interactions with $NADP^+$ Oxidoreductase and Pyruvate Formate-Lyase Activating Enzyme

Adam V. Crain and Joan B. Broderick

From the Department of Chemistry & Biochemistry and the Astrobiology Biogeocatalysis Research Center
Montana State University, Bozeman, MT 59717

To whom correspondence should be addressed: Joan B. Broderick, Department of Chemistry & Biochemistry, Montana State University, Bozeman, MT 59717, Tel: (406) 994-6160; E-mail: jbroderick@chemistry.montana.edu.

Keywords: flavodoxin, $NADP^+$ oxidoreductase, pyruvate formate-lyase activating enzyme, protein-protein interactions, surface plasmon resonance (SPR), circular dichroism (CD), Isothermal titration calorimetry (ITC)

Abstract

Flavodoxin (Fld) conformational changes, thermal stability, and cofactor binding were studied using circular dichroism (CD) and isothermal titration calorimetry (ITC), and limited proteolysis. Thermodynamics of apo and holo-Fld folding were examined to discern the features of this important electron transfer protein and to provide data on apo-Fld. With the exception of fluorescence and UV-vis binding experiments with its cofactor flavin mononucleotide (FMN), apo-Fld is almost completely uncharacterized in *Escherichia coli*. Fld is more structured and stable when the FMN cofactor is bound; the association is tight and driven by enthalpy of binding. Surface plasmon resonance binding experiments were carried out under anaerobic conditions for both apo- and holo-Fld and demonstrate the importance of structure and conformation for interaction with binding partners. Holo-Fld is capable of associating with $NADP^+$-dependent flavodoxin

oxidoreductase (FNR) and pyruvate formate-lyase activating enzyme (PFL-AE) whereas there is no detectable interaction between apo-Fld and either protein. Limited proteolysis experiments followed by LC-MS identified the regions in Fld that are involved in conformations changes upon cofactor binding. Docking software was used to model a Fld/PFL-AE complex to understand the interactions between these two proteins and gain insight into electron transfer reactions from Fld to PFL-AE.

Introduction

Flavodoxins are small acidic electron transfer proteins that utilize a flavin mononucleotide cofactor (FMN). Flavodoxins are widespread in bacteria and are present in some red and green algae [1-3]. In higher eukaryotes, proteins with sequence homology to flavodoxin and its reductase are fused to multidomain proteins as in methionine synthase reductase, which reductively activates methionine synthase [4-6]. Flavodoxins exhibit low reduction potentials making them ideal electron donors for a number of biological redox reactions, including those catalyzed by the radical *S*-adenosylmethionine (SAM) superfamily enzymes. Several studies have shown that flavodoxin (Fld) is capable of activating the pyruvate formate-lyase and anaerobic ribonucleotide reductase activating enzymes (PFL-AE and RNR-AE) as well as biotin synthase (BioB), presumably by reducing the [4Fe-4S] cluster that binds and reductively cleaves SAM [7-9]. The details of these interactions, however, are not well understood.

In addition to interacting with PFL-AE, RNR-AE, and BioB, *Escherichia coli* Fld serves as an electron transfer partner with $NADP^+$-dependent flavodoxin reductase (FNR), methionine synthase, ferredoxin, pyruvate dependent flavodoxin oxidoreductase,

and probably other unknown proteins, and thus plays integral roles in metabolism [7]. Crystal structures are available for holo-Fld from *Escherichia coli*, however there is no structure for apo-Fld [10]. Residues involved in the binding site interface of Fld with SAM binding domain of methionine synthase and FNR have been mapped onto the crystal structure of *E. coli* Fld, showing several residues in common, all located near the FMN binding site [11]. These results suggest that both methionine synthase and FNR bind the same face of Fld and thus presumably bind sequentially [11]. Further support for sequential binding to a single face of Fld comes from the observation of competitive binding between FNR and methionine synthase in spectrophotometric assays [12]. Fld binds the cofactor FMN with an equilibrium constant of 1 nM and a 1:1 stoichiometry, using multiple hydrogen bonds, salt bridges, and stacking interactions between the isoalloxazine ring and aromatic residues [10]. These interactions are extremely important for determining the reduction potentials of the FMN cofactor once bound to the protein [13, 14].

Pyruvate formate-lyase activating enzyme (PFL-AE) is a 28 kDa monomer that contains a [4Fe-4S] cluster and utilizes *S*-adenosylmethionine (SAM) to activate pyruvate formate-lyase (PFL), a central enzyme in anaerobic glycolysis [15]. The SAM cofactor coordinates the unique iron of the [4Fe-4S] cluster via amino and carboxylate moieties [16, 17]. In the reduced $[4Fe\text{-}4S]^{+}$ state, the cluster donates an electron to SAM, thus promoting homolytic cleavage of the S-C(5') bond to generate methionine and a 5'-deoxyadenosyl radical; this adenosyl radical abstracts a hydrogen atom from G734 of PFL to generate the active enzyme [15, 18, 19]. Knappe and coworkers have shown that

Fld can be used in the activation of PFL, presumably as an electron donor for PFL-AE [20]. When the crystal structure of PFL-AE was solved, a conserved region opposite the PFL binding site was proposed to act as the Fld binding site on PFL-AE [21].

In this work we provide insights into the apo- and holo- forms of *E. coli* Fld, and their interactions with protein partners, PFL-AE and FNR. Stability and conformational changes associated with Fld cofactor binding were examined to understand how changes in structure affect protein-protein interactions. We utilize surface plasmon resonance under anaerobic conditions to examine the interactions between the air-sensitive PFL-AE and Fld and FNR. Limited proteolysis followed by LC-MS was used to determine the regions in Fld that were involved in conformational changes. The goal of this work was to understand the interactions involved in the PFL-AE system in relation to electron donors and the structural changes induced by cofactor binding that are necessary for these interactions to occur.

Experimental Procedures

Cloning, Expression, and Purification of Fld and FNR

PFU-Turbo DNA polymerase and restriction enzymes NcoI and BamHI were purchased from New England Biolabs. FMN was purchased from MP Biomedicals, LLC, and was used without further purification. Fld (*fldA*) and FNR (*fpr*) were separately cloned using PCR to amplify the *fldA* and *fpr* genes from *E. coli* strain B genomic DNA. The PCR products were separately inserted into pET-14b using BamHI and NcoI restriction sites that were incorporated into the ends of the PCR product. The *fldA* and *fpr*

genes were completely sequenced at Nevada Genomics Center. The purified DNA was used to transform the BL21(DE3)pLysS expression cell line. For protein expression, cells were grown in LB media at 37 °C in Fernbach flasks with agitation at 250 rpm. When cultures reached an O.D. of 0.8, protein production was induced by addition of IPTG to 100 μM final concentration. Cells were harvested three hours later by centrifugation at 6,000 rpm for 10 minutes.

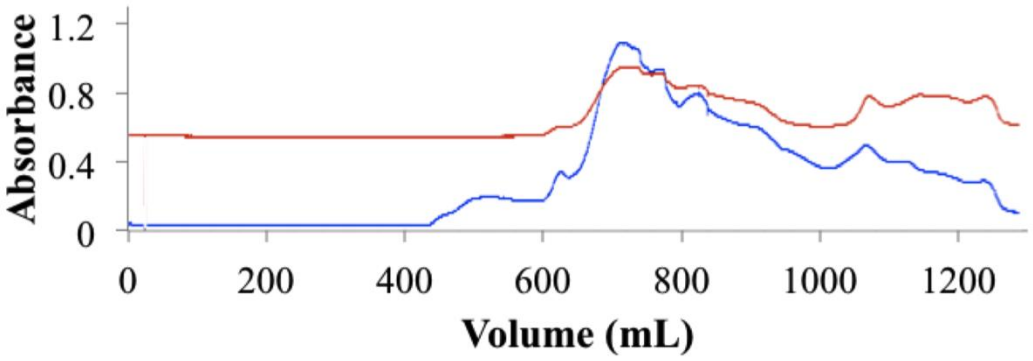

Figure 3.1: FPLC chromatogram of a Fld purification using the Superdex-75 size exclusion column. Blue trace corresponds to 280 nm absorbance and red trace corresponds to 466 nm absorbance of Fld. Fractions were collected from 650 – 790 mL in 10 mL increments.

Cells were lysed by chemical lysis (~ 23 grams of cells in 50 mL of lysis buffer: 20 mM HEPES, 1% w/v Triton X-100, 5% w/v glycerol, 10 mM $MgCl_2$ pH 7.2 with 9 mg PMSF dissolved in 100 μL methanol, 8 mg lysozyme, 1 mg of DNAse and RNAse; cells were lysed for one hour followed by centrifugation at 18,000 rpm for 30 minutes) and Fld and FNR were purified using ammonium sulfate precipitation. Fld and FNR precipitated out in the 60-100% fraction and were subsequently purified using a Superdex-75 size exclusion column (Figure 3.1). Fractions of the highest purity with the

most intense color were pooled and concentrated and then flash frozen and stored at -80 °C (Figure 3.2). Holo-Fld was quantified using a previously determined extinction coefficient of $\varepsilon_{467\ nm} = 8{,}250\ M^{-1}\ cm^{-1}$ [22].

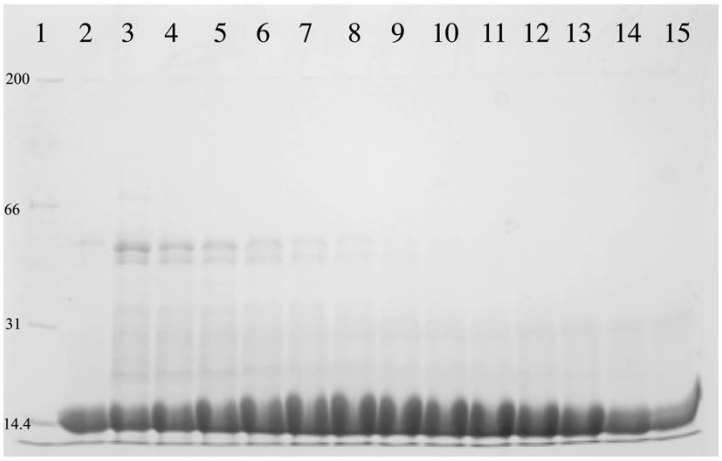

Figure 3.2: 12 % SDS-PAGE gel of a Fld purification. Lane one is the molecular weight marker. Each lane is from one 10 mL fraction starting at 650 mL and going to 790 mL from left to right.

Apo-Fld was prepared using trichloroacetic acid precipitation as described previously [23]. This technique was found to be satisfactory previous studies [10, 23-26]. Apo-Fld was quantified using $\varepsilon_{280nm} = 30{,}900\ M^{-1}\ cm^{-1}$, which was calculated using the protparam tool in ExPASy (http://www.expasy.org). The concentration of the FMN cofactor was determined using $\varepsilon_{445nm} = 12{,}500\ M^{-1}\ cm^{-1}$ [27]. To ensure that the apo-Fld was capable of cofactor binding, a single titration of concentrated apo-Fld was added to a UV-vis cuvette containing FMN show the 20 nm shift in λ_{max} from 445 nm to 465 nm, characteristic of holo-Fld formation (Figure 3.3) [22]. PFL-AE was grown and purified as described previously [28]. An extinction coefficient of $\varepsilon_{280nm} = 39{,}400\ M^{-1}\ cm^{-1}$ was

calculated using ExPASy and correlated well with results from Bradford protein assays [29] after applying a previously-determined correction factor of 0.65 [30].

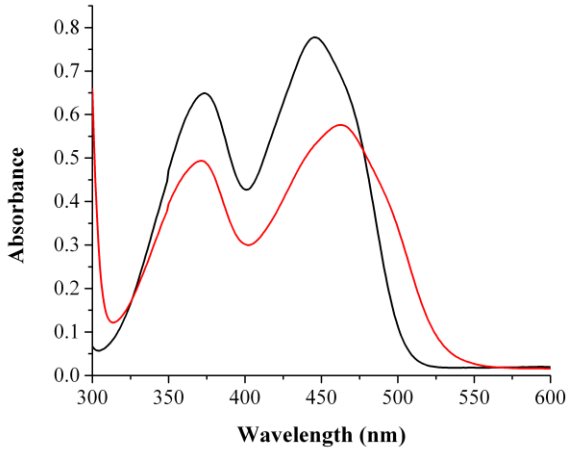

Figure 3.3: UV-vis data of Fld binding its cofactor FMN. Scans were taken in the visible region at 25 °C, from 300 – 800 nm. The buffer used was 20 mM HEPES, 50 mM NaCl, pH 8.0. Black: 62.2 µM FMN, Red: 64 µM apo-Fld plus 61.6 µM FMN.

CD Spectroscopy

Secondary structure and thermal unfolding experiments were carried out using circular dichroism spectroscopy (CD). Spectra were measured with a Jasco-710 spectropolarimeter using either 0.1 mm or 1 cm pathlength cuvettes. Far-UV measurements were in the range of 195 - 260 nm and near–UV measurements were in the range of 240 – 800 nm. Sensitivity was 100 millidegrees, data pitch was 0.1 nm, using a continuous scan mode with a speed of 100 nm/minute, response was 4 seconds, bandwidth was 1.0 nm, with an accumulation of 3 scans. The buffer used for secondary structure and thermal unfolding experiments was 20 mM HEPES, 50 mM NaCl, pH 8.0. Protein concentrations of 30 µM were used for far-UV measurements and 30 µM or 75

μM for near-UV and visible region measurements. The Fld unfolding curves were independent of protein concentration under the conditions studied. Temperature was maintained for thermal unfolding experiments using an endocal refrigerated circulating water bath from NESLAB model RTE-5. Temperature was increased or decreased at a rate of 0.5 K/minute for unfolding or folding, respectively.

Circular dichroism binding studies were performed on a Jasco-810 spectropolarimeter using a 1 cm cuvette. Scans were taken from 240-800 nm using the same parameters as above. The buffer used for CD binding experiments was 20 mM HEPES, 10 mM NaCl, pH 7.4. In these experiments FNR was held constant at 30 μM while Fld was titrated into the FNR. Spectra were also measured for the Fld titration into buffer alone and the contribution of both proteins was subtracted out of the mixture to create difference spectra to visualize changes in visible and near-UV regions as a result of binding. All CD experiments were run in triplicate.

Analysis of Thermal Unfolding Data

Thermal denaturation of Fld was assessed at pH 8.0 using far-UV (222 nm), near-UV (296 nm), and visible regions (496 nm) of circular dichroism. Thermal unfolding curves were first fit to a two state unfolding model to obtain initial thermodynamic parameters of unfolding (Figure 3.6, Equations 1 and 2). The spectroscopic signals of the native (S_N) and unfolded (S_U) states with respective slopes m_N and m_U, are presumed to vary linearly with temperature. The change in enthalpy, heat capacity, and thermal melting point of the transition correspond to ΔH_m, ΔC_p, and T_m, respectively. The ΔC_p for Fld unfolding was not reported since it has been determined to be unreliable [31, 32].

Apo-Fld and holo-Fld unfolding curves were subsequently fit to a three state unfolding model using a global fit (Figure 3.6, Equation 3). ΔG for the three state unfolding model follows expressions analogous to Equation 2 in Figure 3.6. The signal of the intermediate (S_I) and its associated slope (m_I) at T = 0 K are also presumed to vary linearly in relation to temperature. ΔG_1 and ΔG_2 correspond to differences in free energy between the native/intermediate and intermediate/unfolded equilibria, respectively. Thermodynamic parameters of unfolding are reported with subscripts NI, IU, and NU corresponding to the transition from native to intermediate, intermediate to unfolded, and native to unfolded Fld; NU is reported as the sum of NI and IU.

Isothermal Titration Calorimetry

Experiments were performed on a VP-ITC (Microcal LLC, Northampton, MA) using 25 μM apo-Fld in the cell with 600 μM FMN cofactor in the syringe. Experimental parameters were as follows: 26 injections, reference power of 10 μcal/second, initial delay of 300 seconds, stir speed of 510 rpm, feedback mode/gain was high and automatic with fast equilibration. Injection duration was 24 seconds, spacing was 300 seconds, and filter period was 2 seconds. All experiments were performed in triplicate at either 25 °C or 37 °C. All Binding isotherm data was analyzed using a best fit to a single-site binding model by Marquardt nonlinear least-squares analysis (Origin 5.0) with VP-ITC software.

Surface Plasmon Resonance Binding Studies

Surface plasmon resonance experiments were performed under anaerobic conditions in a Coy chamber (Coy Laboratories, Grass Lake, MI) using a Biacore X-100 with the plus package. FNR or PFL-AE was immobilized to a CM5 sensor chip using

thiol coupling as recommended by the manufacturer. Apo-Fld, holo-Fld, or FNR was injected as the analyte at a flow rate of 30 μL/minute using single cycle kinetics. Contact time was 60 seconds, dissociation time was 120 seconds, and regeneration time was 120 seconds. The running buffer was 20 mM HEPES, 10 mM NaCl, pH 7.4 and the regeneration buffer was 20 mM HEPES, 500 mM KCl, 0.005% polysorbate 20, 200 mM imidazole, pH 7.4, all experiments were performed in triplicate at 25 °C. All data was fit using affinity mode in the data analysis software on the Biacore X-100 plus package.

Limited Proteolysis of Fld

Samples of apo- and holo-Fld were prepared under aerobic conditions in a total volume of 20 μL each. All samples contained 450 μM apo-Fld in 20 mM HEPES, 250 mM NaCl, pH 8.0. Holo-Fld samples were prepared for comparison to apo-Fld by the addition of a 1:1 ratio of the FMN cofactor. Trypsin was added in a 1:500 ratio (mg/mL) to apo- and holo-Fld and each sample was digested for 10 minutes. Samples were then boiled for 10 minutes and flash frozen using liquid N_2 and stored until LC-MS analysis using an Agilent 1100 HPLC-ESI-MS using a linear gradient of 100 % H_20/0.1 % FA, to 95 % acetonitrile/0.1 % FA for 0-7 minutes and held at 95 % acetonitrile/0.1 % FA, from 7-8 minutes, followed by re-equilibration with 100 % H20/0.1 % FA for 8-10 minutes using a reverse phase Phenomenex Jupiter Proteo C12 column at 25 °C (50 mm L x 1 mm inner diameter, pore size 4 μm, 90 Å pore size) at a flow rate of 400 μL/minute. Peptides eluted at 18 % and 55 % acetonitrile/0.1 % FA. Mass spectrometry was preformed using a Bruker MicroTOF mass spectrometer with an ESI source. Source parameters: drying gas 7 L/minute, nebulizer 4 bar, capillary voltage 4500 V., spectra

were collected in positive mode from 300-300 m/z at a rate of 1 Hz. All samples were analyzed at the Montana State University mass spectrometry core facility.

Docking of Fld and PFL-AE

A sequence alignment was performed using Clustal Omega to determine the residues involved in the Fld binding site on PFL-AE (http://www.clustal.org/). The amino acid sequences for PFL-AE from the following organisms was aligned and FASTA ID is listed: *Escherichia coli* (P0A9N6), *Clostridium pasteurianum* (Q46267), *Haemophilus influenzae* (P43751), *Listeria innocua* (P0A443), *Staphylococcus aureus* (Q2FK43), *Staphylococcus epidermidis* (Q5HKI0), *Streptococcus mutans* (O68575), *Clostridium novyi* (A0Q1M3), *and Shewanella sp.* (A0KVG9). The residues with 100% sequence conservation were then mapped onto the structure of PFL-AE and the structure was examined to determine which residues were likely to be involved in the interface between PFL-AE and Fld. Previous work has been done to determine the residues involved in Fld binding with FNR and the SAM binding domain of methionine synthase [11]. The residues thought to be involved in the binding site for Fld and PFL-AE were used to construct an *in silico* rigid body complex between the two proteins using ZDOCK software [33].

Results

Secondary Structure of *E. coli* Fld

The secondary structure of Fld was examined by far-UV circular dichroism to determine if FMN cofactor binding to the apo-Fld resulted in changes in secondary

structure. For these experiments, FMN was added to apo-Fld to generate the holo-Fld. Native apo-Fld was compared to native holo-Fld and our date shows that cofactor binding does not appear to change the secondary structure of the protein (Figure 3.4). Apo- and holo-Fld both contain features at 220 and 208 nm, which correspond to alpha helical structure, suggesting that they are both well folded. After the native apo- and holo-Fld proteins were thermally unfolded, far-UV CD was compared to show that unfolded apo- and holo-Fld are very similar and exhibit features at 203 nm characteristic of an unfolded protein [34].

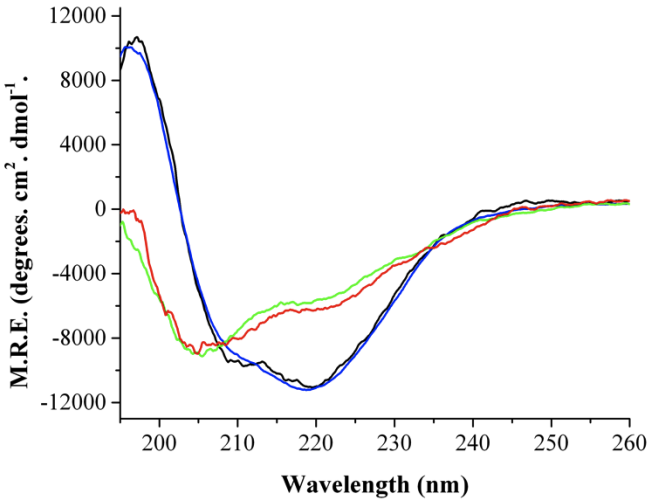

Figure 3.4: Secondary Structure of *E. coli* Fld as determined by far-UV CD. Black: Native apo-Fld at 24 °C, Blue: □□□□□□ holo-Fld at 24 °C, Red: Unfolded apo-Fld at 86 °C, Green: Unfolded holo-Fld at 94 °C. Protein concentrations were 30 μM, 0.1 mm cuvette, 195-260 nm, Sensitivity = 100 millidegrees, data pitch = 0.1 nm, accumulation of 4 scans.

Cofactor Binding Increases the Thermal Stability of Fld

The thermal stability of Fld was measured using circular dichroism in the far-UV and near-UV regions (Figure 3.5). Two thermal transitions were evident for apo-Fld

unfolding, the first one was in the near-UV region at 323.6 ± 0.7 K and the second was in the far-UV region at 326.3 ± 0.5 K (Figure 3.5A). The superposition test was used to show that Fld unfolds via a three state mechanism based on non-superimposable unfolding curves where an intermediate accumulates in the transition region [35-37] and thermodynamics of unfolding have been determined for each transition (Table 3.1). The enthalpy of unfolding from the native state to the completely unfolded state (ΔH_m NU) of the apo-protein was determined to be 77 ± 4.6 kcal/mol•K, which agrees well with the previously determined values for apo-Fld from *D. desulfuricans* and Anabaena [27, 38]. Refolding of apo-Fld was also examined by circular dichroism by cooling unfolded samples to determine whether signal intensity can be restored. Both unfolding and refolding curves were superimposable and the signal intensity was completely restored upon sample cooling, therefore the three state unfolding process for apo-Fld is reversible under the conditions studied.

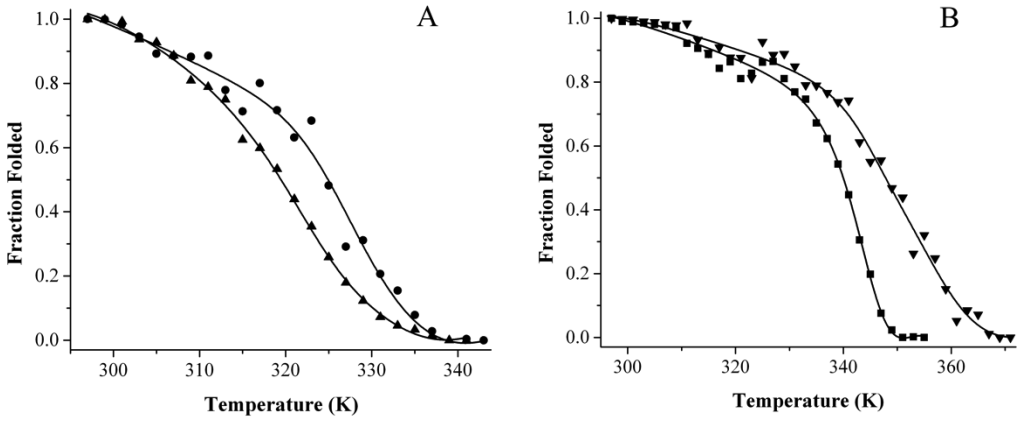

Figure 3.5: Thermal unfolding curves for holo-Fld as monitored in the near-UV, and far-UV regions by CD. A) Apo-Fld near-UV (▲) and far-UV (●) unfolding curves. B) Holo-Fld near-UV (■) and far-UV (▼) unfolding curves. The unfolding curves were globally fit to a three state folding model.

The thermal unfolding of holo-Fld produces two different melting transitions, one at 345.9 ± 0.4 K observed in the near-UV and visible regions of the CD spectrum, and the second at 352.8 ± 0.4 K observed in the far-UV (Figure 3.5B). The near-UV and visible region unfolding curves overlay well, whereas the far-UV unfolding curve is not super-imposable with these, indicating that holo-Fld, much like apo-Fld unfolds via a three state mechanism that involves an intermediate. The ΔH_m NU of the holo-protein is 105.1 ± 3 kcal/mol•K, indicating that the holo-protein is more stable and structured than the apo-protein; the thermodynamics of both transitions have been determined (Table 3.1). This value agrees well with that determined for *D. desulfuricans* holo-Fld [27]. After holo-Fld was unfolded, the samples were slowly cooled to monitor refolding of the protein. Based on far-UV, near-UV and visible region data, signal intensity can be restored and protein folding is a reversible equilibrium process provided that the sample is not heated much above the thermal melting point, similar to observations for *D. desulfuricans* Fld [27]. Both apo- and holo-Fld unfold to the same extent albeit at different temperatures and have features at 203 nm similar to other unfolded proteins (Figure 1) [34].

Table 3.1: Thermodynamics of Fld folding calculated using the three state equation.

Apo-Fld		Holo-Fld	
H_m NI (kcal/mol)	46.1 ± 4.1	H_m NI (kcal/mol)	65.5 ± 1.7
T_m NI (K)	323.6 ± 0.7	T_m NI (K)	345.9 ± 0.4
H_m IU (kcal/mol)	30.9 ± 2.1	H_m IU (kcal/mol)	39.6 ± 2.4
T_m IU (K)	326.3 ± 0.5	T_m IU (K)	352.8 ± 0.4

When unfolding curves are compared between the apo and holo-protein, it is obvious that there is a large increase in stability upon cofactor binding. Increased unfolding enthalpy and thermal melting points suggest that the native and intermediate states of apo-Fld are both stabilized upon interaction with the FMN cofactor. Thermal transitions are independent of protein concentration under these conditions and increased thermal melting points for both holo-Fld unfolding transitions suggest that the FMN cofactor is bound during both unfolding transitions.

$$S = \frac{S_N + m_N T + (S_U + m_U T)\exp^{-(\Delta G/RT)}}{1 + \exp^{-(\Delta G/RT)}} \quad (1)$$

$$\Delta G(T) = H_m(1 - (T/T_m)) - C_p((T_m - T) + T\ln(T/T_m)) \quad (2)$$

$$S = \frac{S_N + m_N T + (S_I + m_I T)\exp^{-(\Delta G1/RT)} + (S_U + m_U T)\exp^{-(\Delta G1 + \Delta G2)/RT}}{1 + \exp^{-(\Delta G1/RT)} + \exp^{-(\Delta G1 + \Delta G2)/RT}} \quad (3)$$

Figure 3.6: Two state and three state unfolding equations

Thermodynamics of Binding of FMN to apo-Fld

FMN binding to apo-Fld was measured using isothermal titration calorimetry at 25 °C and 37 °C to determine the affinity and thermodynamics of interaction (Figure 3.7). At 25 °C the K_D was 5.6 ± 1.2 nM. UV-vis and fluorescence binding assays have been performed previously on *E. coli* apo-Fld, yielding equilibrium constants of 1 nM, which is in agreement with our ITC data [10]. The ΔH of binding was -21.6 ± 0.6 kcal/mole and ΔS = -34.4 ± 1.6 cal/mol•K with a stoichiometry of 0.93 ± 0.01 and a ΔG = -11.3 ± 0.1 kcal/mol. At 37 °C cofactor binding was slightly weaker exhibiting a K_D = 8.2 ± 0.8 nM and a stoichiometry of 0.92 ± 0.08. The ΔH of binding was -31.9 ± 3.3

kcal/mol with a $\Delta S = -65.6 \pm 10.4$ cal/mol•K and a $\Delta G = -11.5 \pm 0.1$ kcal/mol and a $\Delta Cp = -802 \pm 200$ cal/mol•K. It is clear from this data that FMN binding to apo-Fld is driven by enthalpy and that there is an unfavorable contribution from entropy of binding. To ensure that FMN was indeed binding apo-Fld, a control experiment was performed using UV-vis in the visible region where FMN was added to buffer and a scan was measured followed by the addition of apo-Fld (Figure 3.3). This data clearly shows a 20 nm shift in λ_{max} from 445 nm to 465 nm characteristic of apo-Fld binding the FMN cofactor resulting in holo-protein formation [22].

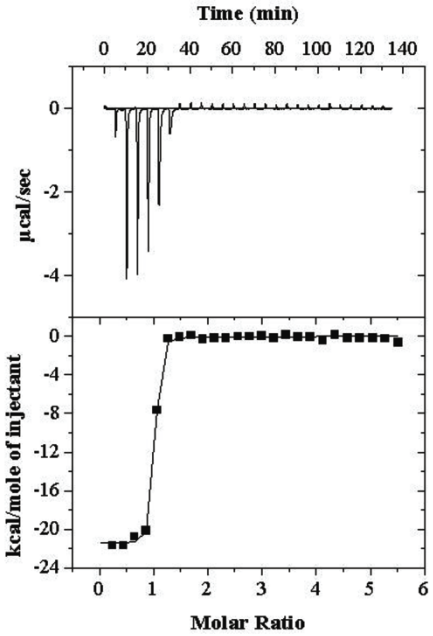

Figure 3.7: Isothermal titration calorimetry of apo-Fld binding FMN at 37 °C. Injections (26 at 10 µL each and the first one at 2 µL) of FMN (600 µM stock concentration) were added to 25 µM apo-Fld in the cell. The reference power was 10 µcal/second, initial delay of 300 seconds, stir speed of 510 rpm, feedback mode/gain was set to high and automatic with fast equilibration, duration of 24 seconds, spacing of 300 seconds, with a filter period of 2 seconds.

Binding Interactions Perturb FNR CD Spectra

FNR is a $NADP^+$-dependent reductant for Fld in *E. coli.* Previous work on FNR has provided evidence that upon interaction with Fld or ferredoxin, the visible absorbance is perturbed and has been attributed to changes in the electronic environment of the FAD cofactor [39-41]. In Figure 3.8 we show CD spectra of holo-Fld alone (green trace), FNR alone (blue trace), and a spectral addition of these two spectra (red trace). We also show the CD spectrum obtained for a 1:1 mixture of Fld and FNR (black trace). It is clear from comparison of the black and red traces that the physical mixture of Fld and FNR produces a different CD spectrum than that obtained by spectral addition of the data for the isolated proteins, indicating that protein-protein interactions are perturbing the CD spectra of one or both proteins in the mixture. As another way to illustrate these effects, we titrated Fld into a solution of FNR and monitored changes by CD spectroscopy; the contribution of Fld and FNR was subtracted out from each titration spectrum in order to emphasize the changes in FNR upon Fld binding. As expected, both near-UV and visible regions monitored by circular dichroism exhibited changes characteristic of binding (Figure 3.8), indicating that when Fld and FNR interact, aromatic residues and the FAD cofactor experience a change in environment. These changes were determined to be proportional to the amount of titrated flavodoxin in the mixture. The difference spectrum shows decreased intensity and a red shift in the near-UV region as well as intensity changes in the visible region (Figure 3.8 inset). It is not known whether conformational changes cause the electronic environment of the FAD cofactor to be perturbed or if the close proximity of cofactors during binding causes this phenomenon.

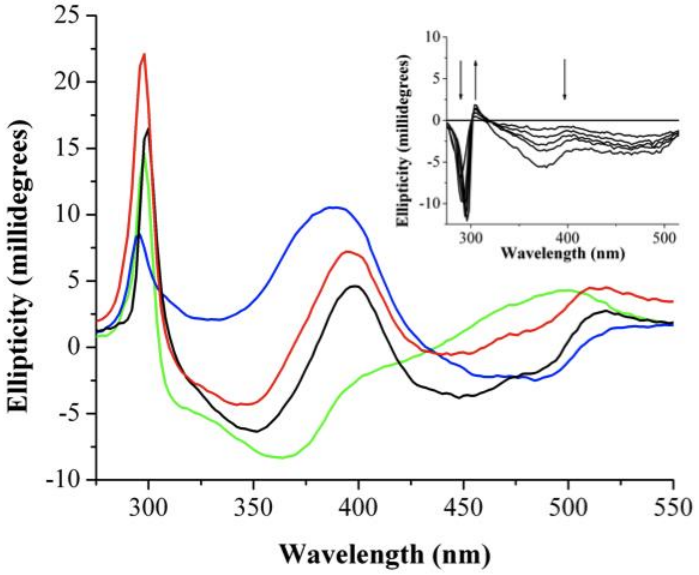

Figure 3.8: Binding of holo-Fld to FNR as monitored by CD spectroscopy. Blue: 30 μM FNR; Green: 30 μM Fld; Red: spectral addition of FNR and Fld; Black: Mixture of 30 μM FNR and 30 μM Fld. Inset shows difference spectra corresponding to a titration of (0 μM, 7.5 μM, 15 μM, 22.5 μM, 30 μM, 60 μM) Fld into FNR (30 μM) to show changes in the near-UV and visible regions as a result of Fld binding FNR.

Fld Binding to FNR and PFL-AE

FNR and Fld have been shown to be capable of supplying low-potential electrons for radical SAM enzymes such as PFL-AE, with the electrons originating from NADPH [7, 9, 42, 43]. In order to probe the interactions between Fld and its partners FNR and PFL-AE, we have utilized surface plasmon resonance studies under anaerobic conditions; anaerobic conditions were required in order to maintain the integrity of the [4Fe-4S] cluster of PFL-AE. A K_D of 3.7 ± 1.6 μM was determined for holo-Fld binding with FNR; this agrees well with the previously determined value of 2.0 ± 1 μM [39]. Interestingly, apo-Fld was found to be inert as a binding partner for FNR. Holo-Fld interacts with PFL-AE with a K_D of 23.3 ± 3.8 μM (Figure 3.9). When apo-Fld was

substituted for holo-Fld, there was no interaction between these two proteins. The observation that holo-Fld binds to both FNR and PFL-AE with micromolar affinity, while binding of apo-Fld cannot be detected for either protein, suggests that Fld cofactor binding produces a conformational change in Fld rendering it capable of interacting with binding partners.

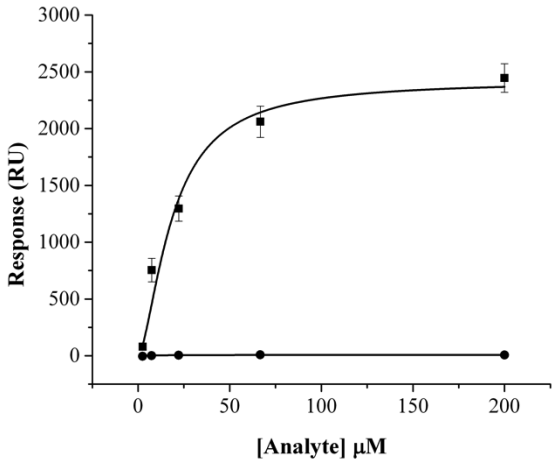

Figure 3.9: Binding of PFL-AE to apo- and holo-Fld using surface plasmon resonance under anaerobic conditions. Single cycle kinetics mode was used at 25 °C and PFL-AE was covalently attached to a CM5 sensor chip using thiol coupling. Either apo-Fld (●) or holo-Fld (■) was titrated over PFL-AE at concentrations of 2.47, 7.41, 22.2, 66.7, and 200 µM. The running buffer used was 20 mM HEPES, 10 mM KCl, pH 7.4 with a flow rate of 30 µL/minute used in assays with a contact time of 60 seconds and dissociation time of 120 seconds. The regeneration buffer was 20 mM HEPES, 500 mM KCl, 0.005% Polysorbate 20, 200 mM imidazole, pH 7.4 and the regeneration time was 120 seconds.

Fld Conformational Changes Upon FMN Cofactor Binding

Conformational changes in Fld were examined using limited proteolysis to determine which regions in the protein change in conformation as a result of FMN cofactor binding. Samples were digested using trypsin and peptides were analyzed by

LC-MS and identified using Mascot. Peptides that were unique to Apo- and holo-Fld were considered to be involved in conformational changes involved in FMN cofactor binding. One unique peptide was observed for each sample, indicating that cofactor binding alters the conformation of the Fld protein. The unique peptide observed in the holo-Fld sample corresponds to S38-R111 and the peptide that was unique to apo-Fld was determined to be G112-K161 (Figure 3.10).

Figure 3.10: Regions of Fld that are involved in conformational changes upon FMN cofactor binding monitored by trypsin digestion followed by LC-MS. Red: unique peptide in trypsin digestion of holo-Fld corresponding to S38-R111, Blue: unique peptide in trypsin digestion of apo-Fld corresponding to G112-R111. The FMN cofactor was colored orange.

Docking of Fld with PFL-AE

When the structure of PFL-AE was solved, a sequence alignment was performed that showed an area of 100% sequence conservation, which was proposed to be the Fld binding site [21]. We have reproduced and analyzed this alignment in order to determine

the residues that were likely to be involved in the interface between PFL-AE and Fld (Figure 3.11 A). PFL-AE residues Q27, G28, C29, R32, H37, N38, D40, T41, W42, E79, Q83, F86, and K208 were 100 % sequence conserved and confined to a region where the [4Fe-4S] cluster is close to the surface of the enzyme. Previous studies suggest that electrostatic interactions are important for Fld binding and that Fld binding partners contain positively charged residues at the binding site interface [44, 45]. However, hydrophobic residues are thought to contribute the bulk of binding energy to Fld protein-protein interactions [11, 46]. Electrostatic mapping results show that there is only one location where there is a large positively charged patch on the surface of PFL-AE and this positively charged area largely overlays the region of 100% conservation. When hydrophobic residues were mapped on PFL-AE, there was a large hydrophobic patch that coincided with the 100% conserved residues and positively charges residues. These findings were used in conjunction with results from a previous study that identified Fld residues involved in interactions with FNR and the SAM binding domain from methionine synthase [11] to produce a docked structure using ZDOCK software (Figure 3.11 B). The Fld binding site on PFL-AE is the only location other than the PFL binding site where the [4Fe-4S] cluster is close to the surface of the enzyme, which would be necessary for efficient electron transfer from Fld to PFL-AE. There are also aromatic residues between the FMN cofactor in Fld and the [4Fe-4S] cluster in PFL-AE that may be involved in the electron transfer pathway. In the Fld/PFL-AE complex, FMN is located 10.7 Å from the [4Fe-4S] cluster in PFL-AE (Figure 3.11 C). In the Fld crystal structure, W57 stacks with the FMN cofactor 3.8 Å away. In Fld, W57 is within 3.3 Å of

W42 from PFL-AE forming a bridge between the two cofactors. In PFL-AE, W42 is located 3.1 Å from the [4Fe-4S] cluster. Indeed, tryptophan and tyrosine are greatly enriched at binding site interfaces and tryptophan can act an electron donor/acceptor between cofactors and significantly increase long distance electron transfer rates [47, 48].

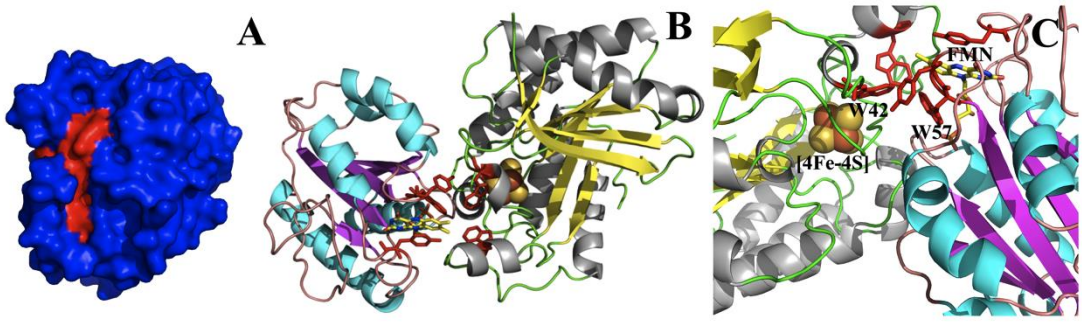

Figure 3.11: A) Surface representation of PFL-AE with 100 % sequence conserved residues highlighted in red B) Docked structure of Fld bound to PFL-AE constructed using ZDOCK. Fld (1AHN), PFL-AE (3C8F) and C) Zoomed in view of the active sites in the Fld/PFL-AE complex. Aromatic residues that form a bridge between cofactors are highlighted in red. The FMN cofactor and W57 from flavodoxin and W42 from PFL-AE and the [4Fe-4S] cluster are all labeled.

Discussion

In this study, we set out to determine whether cofactor binding induces changes in stability and conformation in apo-Fld and what effects these structural changes would have on protein-protein interactions. The far-UV region of circular dichroism shows that native apo- and holo-Fld have features that correspond to structured, well-folded proteins and FMN cofactor binding does not appear to alter protein secondary structure. At high temperatures, both apo- and holo-Fld exhibit features corresponding to an unfolded protein. Thermal unfolding studies support the idea that holo-Fld is more structured than apo-Fld and that it exhibits a large increase stability upon cofactor binding. Both apo-Fld

and holo-Fld unfold via a three state unfolding mechanism that involves an intermediate. Fld unfolding studies show that binding of the cofactor causes a large increase in stability of both the native protein as well as the intermediate. Overall, the unfolding of apo-Fld and holo-Fld from *E. coli* are in very nice agreement with the results obtained for the Fld protein from *D. desulfuricans* [27].

Isothermal titration calorimetry data clearly shows that Fld cofactor binding is a favorable process. The binding is driven by enthalpy and exhibits an unfavorable entropy contribution that may correspond to a decrease in conformational freedom of the cofactor and cofactor binding loops, much like in *H. pylori* [24]. The unfavorable entropy contribution is larger at *in vivo* temperatures, indicating that Fld cofactor binding regions are most likely more disordered and dynamic at higher temperatures. The crystal structure from *Anabaena* PCC 7119 clearly shows that when Fld binds its cofactor, W57 and Y94 swing back into the interior of the protein and hold the isoalloxazine ring in place using stacking interactions [49]. It is likely that *Escherichia coli* Fld uses the same mechanism for binding FMN.

Association experiments between Fld and FNR show that when the proteins interact, aromatic residues experience a change in environment (based on near-UV CD changes) that may be a result of conformational changes or an altered environment at the interface of the complex. The electronic environment of the FAD cofactor is also perturbed during binding, which may be due to conformational changes that alter the cofactor environment. However, it believed that when these proteins bind, their cofactors are juxtaposed for electron transfer such that the FMN cofactor in Fld fits into a cavity

near the FAD cofactor in FNR, possibly contributing to the perturbed visible region spectrum [11]. Surface plasmon resonance experiments demonstrate the functional significance of conformational changes associated with cofactor binding in Fld. Holo-Fld interacts with PFL-AE and FNR, however in absence of the FMN cofactor, Fld is no longer capable of binding either protein. Activity assays demonstrate that Fld is the electron donor for PFL-AE and that FNR reduces Fld [7].

Limited proteolysis of Fld in the presence and absence of the FMN cofactor analyzed by LC-MS shows conformational changes in Fld upon cofactor binding and identifies the regions involved. The crystal structure of *E. coli* holo-Fld shows that residues in the 50's and 90's loops that are involved in hydrogen bonding interactions with the FMN cofactor as well as π-stacking interactions with W57 and Y94 that hold the isoalloxazine ring of FMN in the binding pocket of Fld [10]. Fld residues involved in binding FNR or the SAM binding domain of methionine synthase were located in the same region identified in cofactor binding in the crystal structure and include S40, Y58, Y59, A62, D68, D93, Y94, A95, F127, K131, and Q149 [11]. Our results show that the regions identified in FMN cofactor binding and protein-protein interactions experience conformational changes, which explain why cofactor binding would affect protein-protein interactions.

The interaction between PFL-AE and Fld has been modeled using ZDOCK software. The rigid body model of the Fld/PFL-AE complex was generated based on bioinformatic data of PFL-AE and previous studies of Fld because experimental data was not available. A distance of 10.7 Å is estimated between the FMN cofactor and the [4Fe-

4S] cluster, which puts the two relatively close, however this distance would ensure an outer sphere electron transfer mechanism. The docked structure of the Fld/PFL-AE complex shows Fld bound to the side opposite the PFL binding site on PFL-AE, which is the only other location on PFL-AE where the [4Fe-4S] cluster is located close to the surface of the enzyme. Sequence alignments performed on other radical SAM enzymes have shown that this region is conserved and is thought to be a common binding site for electron donors [50]. Additionally aromatic residues were found between the Fld (W57) and PFL-AE (W42) cofactors that may be involved in electron transfer from the FMN cofactor to the [4Fe-4S] cluster.

Overall our data suggests that cofactor binding in Fld is required to alter Fld structure and stability, which is necessary for protein-protein interactions. Interaction regions between FNR and methionine synthase overlap on Fld suggesting that in the PFL system, FNR would first bind and reduce Fld before Fld interacts with and presumably reduces PFL-AE. PFL-AE can then activate PFL in the presence of SAM and PFL substrates to produce active PFL.

Conclusions

Fld cofactor binding is not only required for a functional Fld that is capable of transferring electrons, but it also induces conformational changes that increase protein stability and facilitate protein-protein interactions. Fld interacts with FNR and PFL-AE with low micromolar affinity that would be expected for electron donor and acceptor proteins involved in PFL activation. Bioinformatic data on PFL-AE in conjunction with previous Fld studies suggest that PFL-AE binds Fld at a site that is separate from the PFL

binding site, therefore making it possible for Fld to reduce PFL-AE when it is bound to SAM, PFL, and PFL substrates.

Acknowledgments

We are grateful to GE Biacore for the Biacore X-100 Inspiration Contest that provided the Biacore X-100 plus machine and materials for the surface plasmon resonance experiments. I would also like to thank Dave Dooley's group at Montana State University and Michele McGuirl's group at the University of Montana for use of their circular dichroism instruments.

Footnotes

This work was supported by NIH grant 2R01GM054608.

References

1. Sancho, J. (2006) *Cell. Mol. Life Sci.* 63, 855-864

2. Peleato, M., L., Ayora, S., Inda, L., A., and Gomez-Moreno, C. (1994) *Biochem. J.* 302, 807-811

3. Fukuyama, K., Matsubara, H., and Rodgers, L., J. (1992) *J. Mol. Biol.* 225, 775-789

4. Olteanu, H., and Banerjee, R. (2001) *J. Biol. Chem.* 276, 35558-35563

5. Zhao, Q., Modi, S., Smith, G., Paine, M., McDonage, P., D., Wolf, R., C., Tew, D., Lian, L.-y., Roberts, G., C.K., and Driessen, H., P.C. (1999) *Protein Sci.* 8, 298-306

6. Paine, M., J.I., Garner, A., P., Powell, D., Sibbald, J., Sales, M., Pratt, N., Smith, T., tew, D., G., and Wolf, R., C. (2000) *J. Biol. Chem.* 275, 1471-1478

7. Blaschkowski, H., P., Neuer, G., Ludwig-Festl, M., and Knappe, J. (1982) *Eur. J. Biochem.* 123, 563-569

8. Bianchi, V., Eliasson, R., Fontecave, M., Mulliez, E., Hoover, D., M., Matthews, R., G., and Reichard, P. (1993) *Biochem. Biophys. Res. Commun.* 197, 792-797

9. Ifuku, O., Koga, N., Haze, S.-i., Kishimoto, J., and Wachi, Y. (1994) *Eur. J. Biochem.* 224, 173-178

10. Hoover, D., M., and Ludwig, M., L. (1997) *Protein Sci.* 6, 2525-2537

11. Hall, D., A., Vander Kooi, C., W., Stasik, C., N., Stevens, S., Y., Zuiderweg, E., R., and Matthews, R., G. (2001) *Proc Natl Acad Sci U S A* 98, 9521-9526

12. Hoover, D., M., Jarrett, J., T., Sands, R., H., Dunham, W., R., Ludwig, M., L., and Matthews, R., G. (1997) *Biochemisty* 36, 127-138

13. Zhou, Z., and Swenson, R., P. (1995) *Biochemistry* 34, 3183-3192

14. Kasim, M., and Swenson, R., P. (2001) *Biochemistry* 40, 13548-13555

15. Henshaw, T., F., Cheek, J., and Broderick, J., B. (2000) *J. Am. Chem. Soc.* 122, 8331-8332

16. Krebs, C., Broderick, W., E., Henshaw, T., F., Broderick, J., B., and Huynh, B. H. (2002) *J. Am. Chem. Soc.* 124, 912-913

17. Walsby, C., J., Ortillo, D., Broderick, W., E., Broderick, J., B., and Hoffman, B., M. (2002) *J. Am. Chem. Soc.* 124, 11270-11271

18. Frey, M., Rothe, M. A. F., Wagner, V., and Knappe, J. (1994) *J. Biol. Chem.* 269, 12432-12437

19. Volker Wagner, A. F., Frey, M., Meugebauer, F., A., Schäfer, W., and Knappe, J. (1992) *Proc. Natl. Acad. Sci.* 89, 996-1000

20. Knappe, J., Schacht, J., Möckel, W., Höpner, T., Vetter, H., Jr., and Edenharder, R. (1969) *European J. Biochem.* 11, 316-327

21. Vey, J., L., Yang, J., Li, M., Broderick, W., E., Broderick, J., B., and Drennan, C., L. (2008) *Proc. Natl. Acad. Sci. U S A* 105, 16137-16141

22. Vetter, H., Jr., and Knappe, J. (1971) *H-Z Physiol. Chem.* 352, 433-446

23. Mayhew, S., G., and Massey, V. (1969) *J. Biol. Chem.* 244, 794-802

24. Credmades, N., Velazquez-Campoy, A., Freire, E., and Sancho, J. (2008) *Biochemistry* 47, 627-639

25. Cremades, N., and Sancho, J. (2008) *Biophys. J.* 95, 1913-1927

26. D'Anna, J., A., and Tollin, G. (1972) *Biochemistry* 11, 1073-1080

27. Muralidhara, B. K., and Wittung-Stafshede, P. (2004) *Biochemistry* 43, 12855-12864

28. Broderick, J., B., Henshaw, T., F., Cheek, J., Wojtuszewski, K., Smith, S., R., Trojan, M., R., McGhan, R., M., Kopf, A., Kibbey, M., and Broderick, W., E. (2000) *Biochem. Biophys. Res. Commun.* 269, 451-456

29. Bradford, M., M. (1976) *Anal. Biochem.* 72, 248-254

30. Broderick, J., B., Duderstadt, R., E., Fernandez, D., C., Wojtuszewski, K., Henshaw, T., F., and Johnson, M., K. (1997) *J. Am. Chem. Soc.* 119, 7396-7397

31. Privalov, P., L., and Potekhin, S., A. (1986) *Methods Enzymol.* 131, 4-51

32. Privalov, P., L. (1997) *J. Chem. Thermodyn.* 29, 447-474

33. Chen, R., Li, L., and Weng, Z. (2003) *Proteins* 52, 80-87

34. Chen, L., Jiang, Z., G., Khan, A., A., Chishti, A., H., and McKnight, C. J. (2009) *Protein Sci.* 18, 629-636

35. Irún, M., P., Garcia-Mira, M., M., Sanchez-Ruiz, J., M., and Sanch, J. (2001) *J. Mol. Biol.* 306, 877-888

36. Maldonado, S., Jimènez, M., Á., Langdon, G., M., and Sancho, J. (1998) *Biochemistry* 37, 10589-10696

37. Luo, Y., Kay, M., S., and Baldwin, R., L. (1997) *Nature Struct. Biol.* 4, 925-930

38. Campos, L., and Sancho, J. (2006) *Proteins* 63, 581-594

39. Wan, J., T., and Jarrett, J., T. (2002) *Arch. Biochem. Biophys.* 406, 116-126

40. Jung, Y.-S., Roberts, V., A., Stout, D., C., and Burgess, B., K. (1999) *J. Biol. Chem.* 274, 2978-2987

41. Lambeth, D., J., Seybert, D., W., and Kamin, H. (1980) *J. Biol. Chem.* 255, 4667-4672

42. Sanyal, I., Gibson, K., J., and Flint, D., H. (1996) *Arch. Biochem. Biophys.* 326, 48-56

43. Mulliez, E., Padovani, D., Atta, M., Alcouffe, C., and Fontecave, M. (2001) *Biochemistry* 40, 3730-3736

44. Hall, D., A., Jordan-Starck, T., C., Loo, R., O., Ludwig, M., L., and Matthews, R., G. (2000) *Biochemistry* 39, 10711-10719

45. Medina, M., Peleato, L., M., Mendez, E., and Gomez-Moreno, C. (1992) *Eur. J. Biochem.* 203, 373-379

46. Nogués, I., Martinez-Júlvez, M., Navarro, J., A., Hervás, M., Armenteros, L., Angel de la Rosa, M., Brodie, T., B., Hurley, J., K., Tollin, G., Gómez-Moreno, C., and Medina, M. (2003) *Biochemistry* 42, 2036-2045

47. Bogan, A., A., and Thorn, K., S. (1998) *J. Mol. Biol.* 280, 1-9

48. Shih, C., Museth, A., K., Abrahamsson, M., Blanco-Rodriguez, A., M., Di Bilio, A., J., Sudhamsu, J., Crane, B., R., Ronayne, K., L., Towrie, M., Vlček, A., Jr., Richards, J., H., Winkler, J., R., and Gray, H., B. (2008) *Science* 320, 1760-1762

49. Genzor, C., G., Perales-Alcón, A., Sancho, J., and Romero, A. (1996) *Nat. Struct. Biol.* 3, 329-332

50. Vey, J., L., and Drennan, C., L. (2011) *Chem. Rev.* 111, 2487-2506

CHAPTER 4

PYRUVATE FORMATE-LYASE: PROTEIN-PROTEIN INTERACTIONS AND ACTIVATION BY PYRUVATE FORMATE-LYASE ACTIVATING ENZYME

Contribution of Authors and Co-Authors

Manuscripts in Chapters 1, 3, 4, 5, 6

Author Adam V. Crain

Contributions: Conceived and implemented the study, analyzed that data, and wrote the manuscript

Co-Author: Dr. Joan B. Broderick

Contributions: Provided oversight and guidance in experimental design and interpretation. Provided all funding and resources for the projects. Advised on manuscript preparation and edited manuscript drafts.

PYRUVATE FORMATE-LYASE: PROTEIN-PROTEIN INTERACTIONS AND ACTIVATION BY PYRUVATE FORMATE-LYASE ACTIVATING ENZYME

Adam V. Crain and Joan B. Broderick

From the Department of Chemistry & Biochemistry and the Astrobiology Biogeocatalysis Research Center
Montana State University, Bozeman, MT 59717

To whom correspondence should be addressed: Joan B. Broderick, Department of Chemistry & Biochemistry, Montana State University, Bozeman, MT 59717, Tel: (406) 994-6160; E-mail: jbroderick@chemistry.montana.edu.

Keywords: Pyruvate Formate-Lyase Activating Enzyme, Pyruvate formate-Lyase, Protein-Protein Interactions, Enzyme Activation

Abstract

The activation of pyruvate formate-lyase (PFL) by pyruvate formate-lyase activating enzyme (PFL-AE) was examined to understand and determine the necessary components for activation. Surface plasmon resonance (SPR) experiments were performed under anaerobic conditions on the oxygen sensitive PFL-AE to determine the kinetics of its interaction with PFL. These experiments show that the interaction is very slow and the rate of association is limited by large conformational changes. A peptide binding experiment was performed using a 12-*mer* peptide analogue of the PFL active site that clearly demonstrates the importance of full length PFL and residues outside the active site loop increase binding affinity by ~ 20 fold. A novel *S*-adenosylmethionine (SAM) binding assay was used to accurately determine the equilibrium constants for SAM binding to as isolated PFL-AE and the PFL-AE/PFL complex. The PFL-AE/PFL

complex bound SAM with the same affinity as PFL-AE alone with a dissociation constant of ~ 6 μM. *In vivo* concentrations of the entire PFL system were calculated to estimate the amount of bound protein in the cell. PFL, PFL-AE, and SAM are essentially fully bound *in vivo*, whereas electron transfer proteins are partially bound. The role of PFL substrates in activation was examined to determine if they are necessary and if they have any direct effect on glycyl radical formation. PFL activated in the presence of pyruvate or oxamate resulted in stoichiometric conversion of the $[4Fe\text{-}4S]^{+}$ cluster to the glycyl radical on PFL. When PFL was activated with CoA or no substrate the concentration of glycyl radical was identical, but 3.7 fold lower than in the presence of oxamate or pyruvate; indicating that PFL substrates/analogue are not required for PFL activation, but optimal activation only occurs in the presence of pyruvate or oxamate.

Introduction

Pyruvate formate-lyase (PFL) is an important enzyme involved in anaerobic metabolism of *Escherichia coli*. PFL supplies the citric acid cycle with acetyl-CoA during anaerobic glycolysis by catalyzing the reaction of pyruvate + CoA acetyl-CoA + formate. PFL is purified in an inactive state when expressed under aerobic conditions and must be activated before catalysis can occur (1-3). PFL is expressed under aerobic conditions in *E. coli*, however under anaerobic conditions PFL is up-regulated 10 - 12 fold and the percent soluble protein and number of polypeptides per cell has been determined for the entire PFL system (3,4). Pyruvate formate-lyase activating enzyme (PFL-AE) is an iron-sulfur cluster containing enzyme that activates pyruvate formate-lyase (PFL) via pro-*S* hydrogen abstraction on glycine 734 (5,6). Crystal structure and

crosslinking data clearly show PFL is composed of two identical subunits, each containing an active site with substrate bound and analytical ultracentrifugation (AUC) data shows that the enzyme is exclusively in the dimeric state (3,7,8). Based on these observations, it would be reasonable to assume that each monomer is capable of catalyzing the PFL reaction. However, studies have been performed to examine glycyl radical formation by EPR using spin quantitation and results show PFL exhibits half-site reactivity (4,9-11).

Another interesting feature of the PFL crystal structure is that each active site is buried ~ 8 Å from the surface of the enzyme, suggesting that a large conformational change would be required for interaction with PFL-AE (7-9). Indeed, in the presence of a 1:1 ratio of PFL to PFL-AE, glycyl radical formation initially increases until all PFL is active, but over time solvent quenches the glycyl radical (9). Changes in secondary structure of PFL in the presence of PFL-AE in conjunction with a decreased thermal melting point and glycyl radical quenching suggest that PFL is in an open conformation in the presence of its activase (9). The PFL substrate pyruvate and its analogue oxamate, is thought to be required for PFL activation, and in the presence of oxamate, reduced PFL-AE is stoichiometrically converted to the PFL glycyl radical (2,5,10,12). However, the exact role of PFL substrates/analogue in activation remains to be elucidated.

PFL-AE contains a [4Fe-4S] cluster ligated by a conserved CX_3CX_2C motif where the cysteine amino acids in the motif coordinate the iron atoms of the cluster with the exception of the unique iron, which is chelated by *S*-adenosylmethionine (SAM) (12,13). The unique iron in PFL-AE is coordinated by the amino and carboxylate

moieties of SAM, thus protecting it from oxidative degradation and anchoring it within van der Waals distance to G734 on PFL for hydrogen abstraction (14,15). The equilibrium constant for SAM binding with PFL-AE has been determined to be in the range of 3 - 5 μM and SAM binding was only detected for holo-PFL-AE, indicating that the cluster is required for SAM binding (12,16). PFL-AE cycles between two different oxidation states during hydrogen abstraction, $[4Fe\text{-}4S]^{2+/1+}$, but only the $[4Fe\text{-}4S]^{1+}$ state was found to be the catalytically active state of the enzyme (10). *In vivo*, it is believed that PFL-AE is reduced by flavodoxin, which is first reduced by either $NADP^+$:flavodoxin oxidoreductase (FNR) or pyruvate:flavodoxin oxidoreductase (PFOR) (1,2,17-19).

Pyruvate formate-lyase activating enzyme is one of the best-characterized radical SAM enzymes. However the activation process is not fully understood, making it an exciting area of research and a perfect model system for other radical SAM enzymes. In this publication we show the first direct evidence of protein-protein interactions between PFL and the oxygen sensitive PFL-AE using surface plasmon resonance under anaerobic conditions. We also developed a novel SAM binding assay to determine if the as isolated PFL-AE binds SAM with the same affinity as the PFL-AE/PFL complex. *In vivo* concentrations of the PFL system were calculated and this information was used to estimate the amount of bound complex in the cell to provide a more complete understanding of the conditions under which PFL activation occurs. The role of PFL substrates/analogue in activation was also explored by measuring glycyl radical concentrations during PFL activation studies in the presence and absence of PFL

substrates/analogue. The aggregate data provide a more complete understanding of PFL activation by PFL-AE and the necessary components involved in activation.

Experimental Procedures

Preparation of Proteins and Small Molecules

PFL-AE and PFL was grown and purified as previously published (10,20-22). PFL-AE was quantified using $\varepsilon_{280\ nm} = 39.4\ mM^{-1}\ cm^{-1}$ (Chapter 3). Iron assays were performed on PFL-AE and an iron number of 2.83 ± 0.03/protein was determined according to a previously published method (23). PFL was quantified using either the Bradford assay or $\varepsilon_{280\ nm} = 178\ mM^{-1}\ cm^{-1}$, both techniques gave identical values (24). The PFL-AE and PFL extinction coefficients were obtained using the ExPASy protparam tool (http://www.expasy.org/tools/protparam.html). *S*-adenosylmethionine was synthesized using SAM synthetase and purified as done previously (25). Small molecule substrates pyruvate, oxamate, and coenzyme A used in PFL activation assays were obtained from Sigma Aldrich and were of the highest commercially available quality and used without further purification.

PFL and PFL-AE Binding Studies

All experiments were carried out in triplicate under anaerobic conditions using a Biacore X-100 with the plus package in a Coy chamber (Coy Laboratories, Grass Lake, MI). The ligand protein (PFL-AE) was attached to a CM5 sensor chip using standard thiol coupling procedures as recommended by the manufacturer. Experiments were ran at 25 °C in 20 mM HEPES, 10 mM NaCl, pH 7.4. Analytes were injected at a flow rate of

30 μL/min with a contact time of 180 seconds, and a dissociation time of 60 seconds. The regeneration buffer was 20 mM HEPES, 500 mM KCl, 0.005% polysorbate 20, 200 mM imidazole, pH 7.4 and the regeneration time was 180 seconds. Sensograms for PFL-AE and PFL binding were fit to a 1:1 kinetics model and peptide-binding experiments were fit using the affinity model available in the Biacore X-100 plus software package.

PFL-AE Structure and SAM Binding Studies

CD Experiments were run in triplicate under anaerobic conditions using a Jasco-710 spectropolarimeter at room temperature. Visible region measurements were collected using a 1 cm pathlength cuvette and far-UV measurements were collected using a 0.1 mm pathlength cuvette. The sensitivity of the Jasco-710 was set to 100 millidegrees, with a data pitch of 0.1 nm, in continuous scan mode at a speed of 100 nm/minute, with a response of 1 second, a bandwidth of 1.0 nm, and an accumulation of 3 scans. The buffer used for all CD experiments was 20 mM HEPES, 250 mM NaCl, 1 mM DTT, pH 7.4 and PFL-AE concentrations were in the range of 50-120 μM in the visible region and 30 μM in the far-UV region. During SAM binding experiments, small volumes of concentrated SAM were titrated into the cuvette and the CD spectrum was scanned from 300-800 nm. A control experiment was also performed where buffer was titrated in the place of SAM to show SAM binding was responsible for the changes in the CD spectrum and to provide data for dilution correction. SAM binding data are an average of triplicate data analyzed using change in ellipticity at 400 nm, which was divided by the maximum change in ellipticity and fit to Equation 1. The total PFL-AE concentration is represented by the

variable Et in the equation below. Lt represents the total SAM concentration titrated during the assay, and K_D is the equilibrium constant.

Limited proteolysis experiments were performed in triplicate at 37 °C in 20 mM sodium phosphate, 20 mM NaCl, pH 7.4 with PFL-AE at 300 μM or 8.5 mg/mL and mass spectrometry grade trypsin gold was used at a ratio of 1:500, with respect to PFL-AE. Samples were digested in the presence and absence of 7 mM SAM over a time course of 0, 5, 10, 20, 30, 60, and 120 minutes before the reaction was quenched by boiling and later analyzed by SDS-PAGE using Coomassie and silver stains.

$$y = \frac{[Et] + [Lt] + K_D - ([Et]^2 - 2[Et][Lt] + 2[Et]K_D + [Lt]^2 + 2[Lt]K_D + K_D^2)^{1/2}}{2[Et]} \quad (1)$$

Figure 4.1: Quadratic binding equation used to fit PFL-AE and SAM binding data.

PFL Activation Studies

EPR spectra were measured on a Bruker ER-200D-SRC spectrometer at 12 K and 60 K for PFL-AE and PFL, respectively with a frequency of 9.37 GHz. The EPR microwave power for glycyl radicals was set to 0.06 mW and 1.59 mW for iron sulfur cluster signals on PFL-AE with a modulation frequency of 100 kHz and a 5-G modulation amplitude for all samples; all spectra were the sum of four scans. PFL activation reactions were carried out under anaerobic conditions in an mBraun box with <1 ppm O_2. PFL-AE was added to an EPR tube at 100 μM with a volume of 350 μL in 100 mM Tris, 250 mM NaCl 10 mM DTT, 100 μM 5-deazariboflavin, pH 7.4 and photoreduced for a time course of 0, 5, 10, 20, 30, and 60 minutes with a 500 W halogen

bulb. Photoreduced PFL-AE was then added to PFL to make a 1:1 ratio at a final concentration of 50 μM each of PFL-AE and PFL dimer in the presence of 500 μM SAM. One PFL substrate was then added to each EPR sample (10 mM pyruvate, 10 mM oxamate, 100 μM CoA, or no substrate) and components were mixed. Samples were pipetted into a clean EPR tube and wrapped in foil before being incubated for 20 minutes to provide time for the reaction to go to completion. EPR samples were then flash frozen in liquid N_2 and stored in a liquid N_2 dewar until the EPR spectrum could be measured. The concentration of the PFL glycyl radical was determined using a $K_2(SO_3)_2NO$ standard according to previously described methods (9,10,26).

Results

PFL-AE Binding Interactions with PFL

Previous work in our lab, using circular dichroism and thermal unfolding experiments led to an estimated K_D for PFL and PFL-AE in the low micromolar range < 10 μM (27). Surface plasmon resonance binding experiments were performed under anaerobic conditions to elucidate the interaction between PFL and the oxygen sensitive PFL-AE. The K_m for PFL-AE and PFL has been determined to be 1.4 μM (28), which is in very close agreement with our calculated K_D value of 1.14 ± 0.2 μM (Figure 4.2). Indicating that the PFL active site is likely in perfect orientation for activation upon binding, thus providing a very efficient system for glycyl radical formation on PFL. The association rate for complex formation was determined to be 1028.4 +/- 34 (1/Ms). When compared to other biological systems, this rate is very slow and on the low end for protein-protein interactions and indicates that the association rate is limited by large

conformational changes rather than by diffusion (29). Indeed, conformational changes are evident in the crystal structure of PFL-AE upon binding of SAM and the 7-*mer* peptide analogue of the PFL active site (15). Conformational changes have also been detected in PFL upon binding of PFL-AE where the active site loop on PFL must unfold to interact with the binding site in PFL-AE (9). Based on the slow rate of binding, it is reasonable to assume that electrostatic interactions play no role in binding (29). This data is further corroborated by activity assay data that shows ionic strength does not affect PFL activity in the range of 0.1-1.6 M KCl (16). The dissociation rate for the PFL-AE/PFL complex was determined to be 1.17 +/- 0.16 x 10^{-3} (1/s); indicating that the complex exhibits reasonable stability.

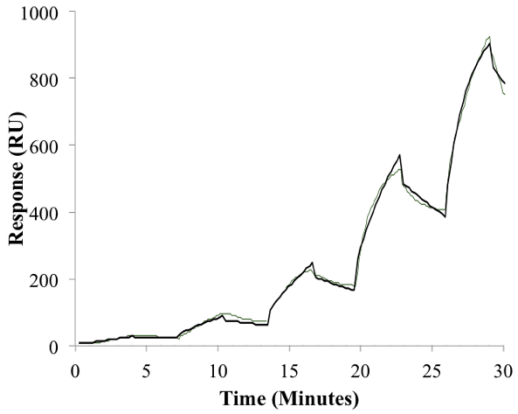

Figure 4.2: PFL-AE and PFL binding kinetics using surface plasmon resonance under anaerobic conditions. PFL-AE was covalently attached to a CM5 biochip using thiol-coupling procedures and PFL was injected at a rate of 30 µL/minute in 20 mM HEPES, 10 mM NaCl, pH 7.4 at 25 °C. The Biacore X-100 plus model was in single cycle kinetics mode and the data was fit to a 1:1 binding model.

Previous studies have been performed using peptide analogues of the PFL active site in activity assays (5). The K_m for the 12-*mer* peptide was determined to be 40 μM, which is in reasonable agreement with the K_D of 24.6 ± 16 μM that we determined for the C-terminal acetylated 12-*mer* peptide interacting with PFL-AE. As expected the affinity of PFL-AE for its natural substrate PFL is ~ 20 fold higher than for that of the peptide. The differences in K_D and K_m in full length PFL compared to a peptide active site model underscores the importance of key residues in PFL outside the active site, which interact with PFL-AE for tight binding and orient the two active sites for efficient catalysis. In addition to the increase in K_D and K_m observed for PFL-AE and the 12-*mer* peptide as compared with PFL, not surprisingly, PFL is significantly more active than the peptide, which is explained by the completeness of the substrate (5).

PFL-AE Structure and SAM Binding Studies

We wondered if SAM binding interactions with the [4Fe-4S] cluster in PFL-AE would produce a change in the visible region CD signal that could be exploited to examine SAM binding under anaerobic conditions. The CD spectrum of PFL-AE is robust with λ_{max} values of 305 and 430 nm with shoulders at 345 and 630 nm and λ_{min} values of 380 and 550 nm. When SAM is titrated into a solution of PFL-AE there are dramatic changes in the CD spectrum with multiple isosbestic points (Figure 4.3 A). The CD spectrum of PFL-AE with SAM bound has λ_{max} values of 305, 410, 495 and 690 nm with shoulders at 365 and 630 nm and λ_{min} values of 345 and 560 nm. PFL-AE in the as isolated form binds SAM with a K_D of 7.6 ± 1.9 μM (Figure 4.3 B). Activity assays have been used to determine the K_m for PFL-AE and SAM yielding values of 2.8 - 7 μM

(16,18). Because PFL has no cofactor, it was possible to set up binding experiments where PFL-AE was essentially fully bound to PFL and SAM was titrated into the cuvette to monitor SAM binding to the PFL-AE/PFL complex. In this case, PFL-AE exhibited the same affinity for SAM when PFL was already bound with a K_D of 5.7 μM ± 1.7; agreeing with the K_m value in both cases.

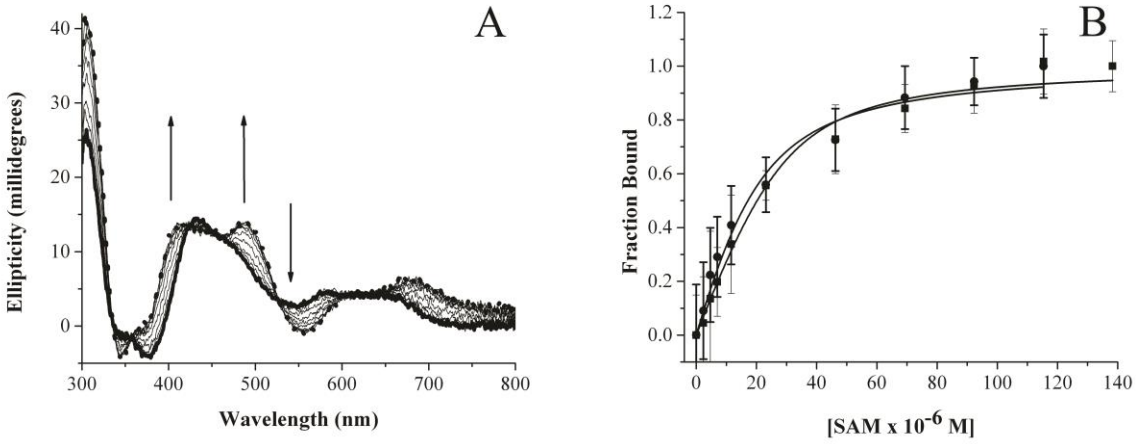

Figure 4.3: A) Visible region circular dichroism of PFL-AE showing the [4Fe-4S] cluster is perturbed upon SAM binding. Solid bold line represents as isolated PFL-AE and the bold dotted line represents PFL-AE that is fully bound by SAM. The PFL-AE concentration was 120 μM and SAM concentrations were in the range of 0 - 140 μM; the assay was performed in 20 mM HEPES, 250 mM NaCl, 1 mM DTT, pH 7.4 at 25 °C. B) SAM binding data for as isolated PFL-AE (●) and SAM binding to the PFL-AE/PFL complex (■). The data was analyzed using changes in ellipticity at 400 nm divided by total change in ellipticity, which was then plotted as function of SAM concentration and fit to the quadratic binding equation. CD parameters were set to a sensitivity of 100 millidegrees, with a data pitch of 0.1 nm, in continuous scan mode with a scan rate of 100 nm/minute, a scan range of 300 - 800 nm, response of 1 second, bandwidth of 1.0 nm, and an accumulation of 3 scans; all measurements were performed using a 1 cm pathlength cuvette.

We were interested in determining if SAM binding to PFL-AE would stabilize the enzyme to limited proteolysis. Limited proteolysis of PFL-AE over a two-hour time

period shows that the enzyme is digested reasonably well by trypsin protease. However in the presence of SAM, PFL-AE is significantly more stable to proteolytic digestion based on qualitative examination of the protein bands on SDS-PAGE (Figure 4.4 A). To further characterize the interaction between PFL-AE and SAM, we used far-UV circular dichroism studies to see if changes in secondary structure occur during SAM binding. Interestingly, there was no difference in PFL-AE secondary structure in the presence or absence of SAM (Figure 4.4 B). The aggregate data suggests that while SAM binding does increase PFL-AE stability, there is no change in secondary structure.

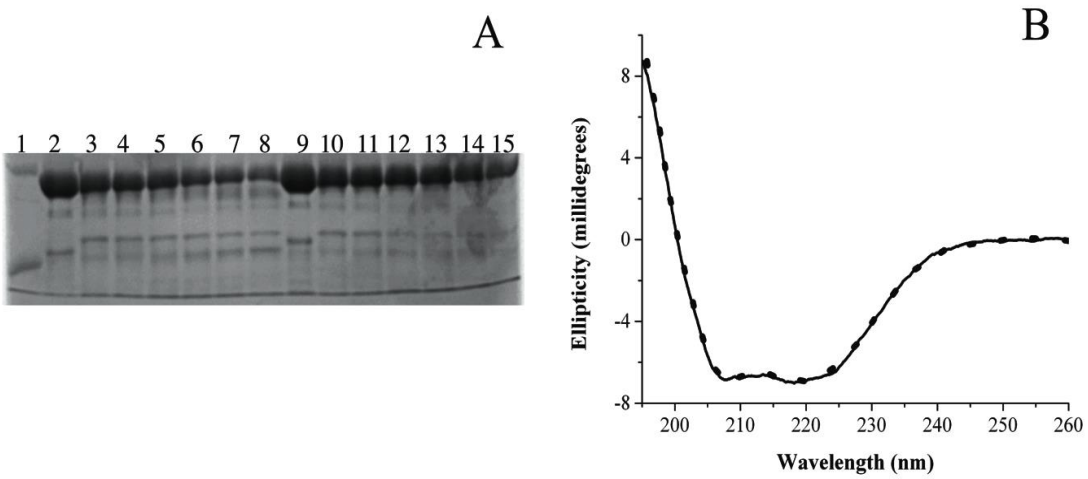

Figure 4.4: A) SDS PAGE gel showing PFL-AE digested by trypsin in the absence (lanes 2-8) and presence of SAM (lanes 9-15) Experiments were run at 37 °C and digested for 0, 5, 10, 20, 30, 60 and 120 minutes in 20 mM sodium phosphate, 20 mM NaCl, pH 7.4 with a PFL-AE concentration of 300 μM or 8.5 mg/mL with a 1:500 ratio of trypsin to PFL-AE. Lane 1 is the SDS-PAGE molecular weight standard. The proteolysis reaction was quenched by boiling the samples for 5 minutes; followed by SDS-PAGE analysis. The gel was stained using Coomassie stain and silver stain. B) Far-UV CD of PFL-AE in the absence (dotted line) and presence of SAM (solid line) in 20 mM HEPES, 250 mM NaCl, pH 7.4 at 25 °C. CD parameters were as follows: sensitivity was 100 millidegrees, data pitch was 0.1 nm, scan range was 195-260 nm, in continuous scan mode at a rate of 50 nm/minute, response of 4 second, bandwidth of 0.1 nm, and an accumulation of 3 scans; all measurements were performed using a 0.1 mm pathlength cuvette.

PFL Activation Studies

Our goal was to understand what role, if any, each PFL substrate/analogue had in PFL activation. Samples containing either pyruvate or oxamate exhibited a stoichiometric conversion of $[4Fe\text{-}4S]^{+}$ cluster of PFL-AE to the glycyl radical on PFL and were identical with respect to glycyl radical concentration (Figure 4.5). After PFL-AE was photoreduced for 60 minutes and mixed with PFL in the presence of pyruvate, the concentration of the glycyl radical was determined to be 44 ± 5 μM, and in the presence of oxamate the glycyl radical was calculated to be 46 ± 5 μM. PFL was then activated in the presence of CoA and the concentration of glycyl radical was determined to be 12.4 ± 3 μM, and in the absence of substrate the concentration of the glycyl radical was 12.5 ± 3 μM. PFL incubated in the presence of either CoA or no substrate resulted in 3.7 fold less active enzyme than when compared to PFL activated in the presence of pyruvate or oxamate (Figure 4.5). The K_m values for PFL substrates have been previously determined to be 2 mM for pyruvate and 7 μM for CoA (4). Equilibrium constants have also been determined for these substrates of 2 mM for oxamate and 100 μM for pyruvate (8). Under the conditions employed during these experiments we can therefore confidently say that the substrates are at high enough concentrations to interact with PFL and should produce the desired effect.

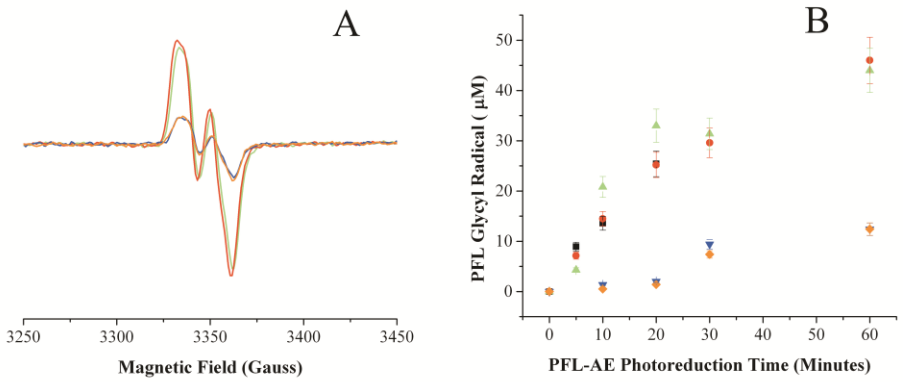

Figure 4.5: PFL activation by photoreduced PFL-AE in the presence of SAM and different PFL substrates. A) EPR data of the PFL glycyl radical in the presence of different PFL substrates after being mixed with PFL-AE that was photoreduced for 60 minutes, red: 10 mM oxamate, green: 10 mM pyruvate, blue: 100 μM CoA, and orange: no substrate. B) The graph shows glycyl radical formation on PFL with PFL-AE that has been photoreduced over a time course of 0-60 minutes monitored using EPR. Color is the same as above with the addition of a PFL-AE standard in black that was spin quantified for $[4Fe\text{-}4S]^{+}$ content using a copper/EDTA standard and PFL was spin quantitated using a $K_2(SO_3)_2NO$ standard. Each experimental sample contained 50 μM PFL dimer and 50 μM PFL-AE in 20 mM HEPES, 250 NaCl, pH 7.4 with 50 μM 5-deazariboflavin and either pyruvate, oxamate, CoA, or no substrate. Samples were photoreduced for 0, 10, 20, 30, and 60 minutes before being frozen in liquid N_2 and later analyzed by EPR. Glycyl radical signals were measured at 60 K and the [4Fe-4S] cluster signals were measured at 12 K to ensure that there would be no overlapping signals. EPR parameters: Microwave frequency, 9.37 GHz; modulation frequency, 100 kHz; microwave power for PFL-AE was 1.59 mW and 0.06 mW for PFL; modulation amplitude, 5G.

In Vivo Protein and Small Molecule Concentrations

In vivo concentrations of the proteins and small molecules involved in the PFL system were calculated for this study to provide a context for dissociation constants and estimate the fraction of bound proteins and small molecules *in vivo*. Calculations were performed using data from Joachim Knappe's lab where the amount of protein per cell was quantified for the PFL system (4). Advances in cellular microscopy have allowed for the accurate determination of cytosolic volumes of *E. coli* cells (30). When combined this

data has allowed us to calculate the *in vivo* concentrations of the proteins involved in the PFL system. Unfortunately error calculations were not available for the polypeptide or percent soluble protein measurements in the PFL system, so we are unable to calculate errors associated with *in vivo* concentrations. The *in vivo* concentration of PFL under anaerobic conditions was determined to be 14.5 μM dimer. The PFL-AE concentration was determined to be 830 nM, flavodoxin was 2.1 μM, FNR was 1.7 μM, and PFOR was 470 nM. The *in vivo* concentration of SAM has been estimated to be in the range of 50 - 400 μM (31-33). Under these conditions and assuming a SAM concentration of 50 μM, PFL, PFL-AE, and SAM would be essentially fully bound (Table 4.1). *In vivo* concentrations have been calculated for pyruvate of 7.5 ± 0.5 mM (34). We calculated the *in vivo* concentration of CoA in *E. coli* to be 9 - 100 μM based on previous measurements (error calculations were not available) (35,36) with an assumed cell volume of 4.0 ± 1.3 fL (30).

Table 4.1: Equilibrium constants and *in vivo* concentrations for the PFL system. Equilibrium constants were taken from chapter 3*. *In vivo* concentrations for the PFL family were calculated using previously determined polypeptide measurements and combined with cell volume measurements of 4.0 ± 1.3 fL (4,30). *In vivo* concentrations under anaerobic conditions were as follows: [PFL-AE] = 830 nM, [PFL] = 14.5 μM, [Fld] = 2.1 μM, [FNR] = 1.7 μM, [PFOR] = 470 nM. Error calculations could not be performed since error information was not available for polypeptide measurements (4,37).

Sample	K_D (μM)	[Bound *in vivo*] (nM)	% Bound *in vivo*
FNR: Fld*	3.7 ± 1.6 μM	511	30 % of FNR
PFL-AE: PFL	1.14 ± 0.2 μM	766	92% of PFL-AE
PFL-AE: Fld*	23.3 ± 3.8 μM	66.6	8% of PFL-AE
PFL-AE: SAM	7.6 ± 1.9 μM	719	87% of PFL-AE
PFL-AE/PFL: SAM	5.7 ± 1.7 μM	744	90% of PFL-AE

Discussion

The activation of PFL was studied in this work providing the first available information on the interactions between PFL and its activase, PFL-AE. Surface plasmon resonance binding experiments were carried out under anaerobic conditions and the data was fit to a 1:1 binding model with good fits. The K_D value of 1.14 ± 0.2 μM, calculated for PFL and PFL-AE is nearly identical to the K_m value previously reported of 1.4 μM and agrees well with previous estimates of the K_D (5,9). The association rate between PFL-AE and PFL was extremely slow and on the low end for biological interactions indicating that the rate of binding is limited by large conformational changes (29). Binding of the 12-*mer* peptide, an analogue of the PFL active site exhibited a ~ 20 fold decreased binding affinity when compared to the intact enzyme, suggesting that there are residues outside of the peptide that are important in binding interactions. Our data is in nice agreement with activity assays performed with either the 12-*mer* peptide or PFL that show a reduced V_{max} and an increased K_m value when the peptide is substituted for PFL (5).

The [4Fe-4S] cluster in PFL-AE undergoes dramatic changes to its CD spectrum as a direct consequence of SAM binding. Limited proteolysis data in this work shows that PFL-AE is more stable to protease digestion in the presence of SAM, however no changes in secondary structure occurred upon SAM binding based on far-UV CD measurements. Therefore, it is assumed that this effect is caused by the direct coordination of SAM to the unique iron of the [4Fe-4S] cluster (14,15). These changes in the visible region CD of PFL-AE can be used to accurately determine dissociation

constants for SAM binding in the presence and absence of PFL. PFL-AE binds SAM with the same affinity within error regardless of PFL binding to PFL-AE, indicating that PFL binding to PFL-AE does not affect SAM binding affinity. This data suggests that *in vivo*, the order of interaction for SAM binding to PFL-AE or the PFL-AE/PFL complex does not matter.

In vivo concentrations for PFL-AE, PFL, Fld, PFOR, and FNR were calculated in this work and compared with K_D values to estimate the amount of bound protein *in vivo*. Under these conditions, PFL-AE is almost completely bound to PFL (Table 4.1). *In vivo* concentrations of SAM have been determined to be in the 50 - 400 μM, (31-33) however there may be less available SAM for PFL-AE given the wide spread use of SAM in many enzymatic reactions in *E. coli* (17,38-41). SAM binds to both PFL-AE and the PFL-AE/PFL complex with the same affinity of ~ 6 μM, assuming an *in vivo* SAM concentration of 50 μM, PFL-AE would be essentially completely bound with SAM *in vivo* regardless of whether PFL is bound. Based on previous experiments with Fld and FNR, we calculate that this complex is 30 % bound *in vivo* and the Fld/PFL-AE complex was estimated to be 8% bound (Chapter 3) (Table 4.1).

PFL substrates pyruvate and its analogue oxamate have been suggested to act as allosteric effectors required for PFL activation (2,5,10,12). We monitored PFL activation by EPR in the presence of substrates to determine if they are required for PFL activation and if they have any direct affect on the amount of active enzyme produced. Our data shows that while PFL substrates are not required for activation, they do play a very significant role in activation. When pyruvate and oxamate are incubated with PFL there is

a stoichiometric conversion of the $[4Fe\text{-}4S]^{+}$ cluster from PFL-AE to the glycyl radical in PFL. PFL activated in the presence of CoA or no substrate results in 3.7 fold less glycyl radical than in the presence of pyruvate or oxamate. The signal for the $[4Fe\text{-}4S]^{+}$ cluster in PFL-AE is absent when PFL is included in the experiments, indicating that all the reduced PFL-AE activates PFL, however, given the lower quantities of glycyl radical formed with CoA and no substrate, a portion of the glycyl radical must be quenched by solvent. Our data suggests that pyruvate and oxamate aid in PFL radical domain reinsertion into the core of the enzyme forming a stable glycyl radical. It is interesting to note that pyruvate and oxamate bind to the PFL active site, whereas CoA binds much further away from the active site and has no affect on PFL activation.

Acknowledgements

We are grateful to GE Biacore for the Biacore X-100 Inspiration Contest and for the use of the Biacore X-100 plus model and materials for anaerobic surface plasmon resonance experiments. We would like to thank the Dooley lab at Montana State University for the use of their CD instrument.

Footnotes

This work was supported by NIH grant 2R01GM054608-14.

References

1. Knappe, J., Schacht, J., Möckel, W., Höpner, T., Vetter, H., Jr., and Edenharder, R. (1969) *European J. Biochem.* 11, 316-327

2. Knappe, J., Blaschkowski, H., P., Grobner, P., and Schmitt, T. (1974) *Eur. J. Biochem.* 50, 253-263

3. Conradt, H., Hohmann-Berger, M., Hohmann, H.-P., Blaschkowski, H., P., and Knappe, J. (1984) *Arch. Biochem. Biophys.* 228, 133-142

4. Knappe, J., and Sawers, G. (1990) *FEMS Microbiol. Rev.* 75, 383-398

5. Frey, M., Rothe, M., Volker Wagner, A. F., and Knappe, J. (1994) *J. Biol. Chem.* 269, 12432-12437

6. Broderick, J. B., Duderstadt, R. E., Fernandez, D. C., Wojtuszewski, K., Henshaw, T. F., and Johnson, M. K. (1997) *J. AM. Chem. Soc.* 119, 7396-7397

7. Becker, A., and Kabsch, W. (2002) *J. Biol. Chem.* 277, 40036-40042

8. Becker, A., Fritz-Wolf, K., Kabsch, W., Knappe, J., Schultz, S., and Wagner, V., A. (1999) *Nat. Struct. Biol.* 6, 969-975

9. Peng, Y., Veneziano, S. E., Gillispie, G. D., and Broderick, J. B. (2010) *J. Biol. Chem.* 285, 27224-27231

10. Henshaw, T. F., Cheek, J., and Broderick, J. B. (2000) *J. Am. Chem. Soc.* 122, 8331-8332

11. Plaga, W., Frank, R., and Knappe, J. (1988) *Eur. J. Biochem.* 178, 445-450

12. Kulzer, R., Pils, T., Kappl, R., Huttermann, J., and Knappe, J. (1998) *J. Biol. Chem.* 273, 4897-4903

13. Krebs, C., Broderick, W. E., Henshaw, T. F., Broderick, J. B., and Hanh Huynh, B. (2002) *J. Am. Chem. Soc.* 124, 912-913

14. Walsby, C. J., Ortillo, D., Broderick, W. E., Broderick, J. B., and Hoffman, B. M. (2002) *J. Am. Chem. Soc.* 124, 11270-11271

15. Vey, J. L., Yang, J., Li, M., Broderick, W. E., Broderick, J. B., and Drennan, C. L. (2008) *Proc. Natl. Acad. Sci. U.S.A.* 105, 16137-16141

16. Wong, K., K., Murray, B., W., Lewisch, S., A., Baxter, M., K., Ridky, T., W., Ulissi-DeMario, L., and Kozarich, J., W. (1993) *Biochemistry* 32, 14102-14110

17. Blaschkowski, H., P., Neuer, G., Ludwig-Festl, M., and Knappe, J. (1982) *Eur. J. Biochem.* 123, 563-569

18. Knappe, J., and Blaschkowski, H., P. (1975) *Pyruvate Formate-Lyase from Escherichia coli and its Activation System*, Academic Press Inc., New York

19. Vetter, H., Jr., and Knappe, J. (1971) *H-Z Physiol. Chem.* 352, 433-446

20. Nnyepi, M., R., Peng, Y., and Broderick, J., B. (2007) *Arch. Biochem. Biophys.* 459, 1-9

21. Krebs, C., Broderick, W., E., Henshaw, T., F., Broderick, J. B., and Huynh, B. H. (2002) *J. Am. Chem. Soc.* 124, 912-913

22. Broderick, J. B., Henshaw, T., F., Cheek, J., Wojtuszewski, K., Smith, S., R., Trojan, M., R., McGhan, R., M., Kopf, A., Kibbey, M., and Broderick, W., E. (2000) *Biochem. Bioph. Res. Co.* 269, 451-456

23. Beinert, H. (1978) *Methods Enzymol.* 54, 435-445

24. Bradford, M., M. (1976) *Anal. Biochem.* 72, 248-254

25. Walsby, C., J., Hong, W., Broderick, W., E., Cheek, J., Ortillo, D., Broderick, J. B., and Hoffman, B., M. (2002) *J. Am. Chem. Soc.* 124, 3143-3151

26. Aasa, R., and Vänngård, T. (1975) *J. Magn. Res.* 19, 308-315

27. Yi Peng, S. E. V., Gregory D. Gillispie, and Joan Broderick. (2010) *J. Biol. Chem.* 285, 27224-27231

28. Manfred Frey, M. R., A. F. Volker Wagner, and Joachim Knappe. (1994) *J. Biol. Chem.* 269, 12432-12437

29. Schreiber, G., Haran, G., and Zhou, H. X. (2009) *Chem. Rev.* 109, 839-860

30. Volkmer, B., and Heinemann, M. (2011) *PLoS ONE* 6, e23126

31. Val, D., L., and Cronan, J., E. Jr. (1998) *J. Bacteriol* 180, 2644-2651

32. Halliday, N. M., Hardie, K. R., Williams, P., Winzer, K., and Barrett, D. A. (2010) *Anal. Biochem.* 403, 20-29

33. Bennett, B., D., Kimball, E., H., Gao, M., Osterhout, R., Van Dien, S., J., and Rabinowitz, J., D. (2009) *Nat. Chem. Biol.* 5, 593-599

34. Yang, Y.-T., Bennett, G., N., and San, K.-Y. (2001) *Metab. Eng.* 3, 115-123

35. Jackowski, S., and Rock, C., O. (1981) *J. Bacteriol.* 148, 926-932

36. Loewen, P., C. (1978) *Can. J. Biochem.* 56, 753-759

37. Pecher, A., Blaschkowski, H., P., Knappe, K., and Böck, A. (1982) *Arch. Microbiol.* 132, 365-371

38. Bianchi, V., Eliasson, R., Fontecave, M., Mulliez, E., Hoover, D., M., Matthews, R., G., and Reichard, P. (1993) *Biochem. Biophys. Res. Commun.* 197, 792-797

39. Ifuku, O., Koga, N., Haze, S.-i., Kishimoto, J., and Wachi, Y. (1994) *Eur. J. Biochem.* 224, 173-178

40. Hall, D., A., Vander Kooi, C., W., Stasik, C., N., Stevens, S., Y., Zuiderweg, E., R., and Matthews, R., G. (2001) *Proc Natl Acad Sci U S A* 98, 9521-9526

41. Sekowska, A., Kung, H.-F., and Danchin, A. (2000) *J. Mol. Mircobiol. Biotechnol.* 2, 145-177

CHAPTER 5

ELUCIDATING THE ROLE OF CATION BINDING IN PFL-AE

Contribution of Authors and Co-Authors

Manuscripts in Chapters 1, 3, 4, 5, 6

Author Adam V. Crain

Contributions: Conceived and implemented the study, analyzed that data, and wrote the manuscript

Co-Author: Stephanie J. Maiocco

Contributions: Performed electrochemistry experiments on PFL-AE in different cation conditions

Co-Author: Dr. Joan B. Broderick

Contributions: Provided oversight and guidance in experimental design and interpretation. Provided all funding and resources for the projects. Advised on manuscript preparation and edited manuscript drafts.

Co-Author: Sean J. Elliot

Contributions: Assisted with the interpretation of electrochemical data

CHAPTER 5

ELUCIDATING THE ROLE OF CATION BINDING IN PFL-AE

Adam V. Crain, Stephanie J. Maiocco, Sean J. Elliot, and Joan B. Broderick

From the Department of Chemistry & Biochemistry and the Astrobiology Biogeocatalysis Research Center
Montana State University, Bozeman, MT 59717

To whom correspondence should be addressed: Joan B. Broderick, Department of Chemistry & Biochemistry, Montana State University, Bozeman, MT 59717, Tel: (406) 994-6160; E-mail: jbroderick@chemistry.montana.edu.

Keywords: Pyruvate Formate-Lyase, Pyruvate Formate-Lyase Activating Enzyme, *S*-Adenosylmethionine, and Monovalent Cation

Abstract

Pyruvate formate-lyase activating enzyme (PFL-AE) has a monovalent cation-binding pocket of unknown function juxtaposed with *S*-adenosylmethionine and the [4Fe-4S] cluster. We examined the cation bound near the cluster in PFL-AE and found that it affects the enzyme in many different ways. UV-vis PFL-AE activity assays show that cation binding stimulates catalytic activity in dose response to sodium addition. The EPR signal of the [4Fe-4S] cluster of PFL-AE is drastically different in the absence of a bound cation. When SAM is bound to the cation free PFL-AE the EPR signal is significantly altered from either the sodium bound PFL-AE or the cation free PFL-AE in absence of SAM. CD experiments indicate that cation binding does not alter the secondary structure of PFL-AE. Electrochemistry was used to determine the affect of the cation on reduction potentials. PFL-AE was studied in NaCl, choline chloride, and a 1:1 mixture of NaCl and choline chloride to maintain ionic strength. It is expected that due to the large size of the

choline cation, that it would not be capable of binding the small cation binding pocket in PFL-AE. Preliminary data suggests that cation binding makes the reduction potential of PFL-AE more negative, making SAM cleavage and PFL activation possible.

Introduction

Pyruvate formate-lyase activating enzyme (PFL-AE) is a radical SAM enzyme that binds and post-translationally modifies Gly734 on its substrate pyruvate formate-lyase (PFL), an important enzyme in anaerobic glycolysis (1). PFL catalyzes the reaction of pyruvate + CoA ⇆ acetyl-CoA + formate, under anaerobic conditions (2). The active site of PFL is buried ~ 8 Å away from the surface of the protein and is thought to undergo large conformational changes where the active site loop unfolds from the core of the enzyme to be activated by PFL-AE (3). In the crystal structure of PFL-AE, a 7-*mer* peptide was used to model the PFL active site bound to PFL-AE to gain insight into PFL-AE activity (4). PFL-AE contains a CX_3CX_2C motif that binds three irons from the [4Fe-4S] cluster allowing one of the iron atoms to be unique and non-protein ligated (5). ENDOR and X-ray crystallography data show that the amino and carboxylate moieties from *S*-adenosylmethionine (SAM) chelate the unique iron in the [4Fe-4S] cluster of PFL-AE (6). The iron sulfur cluster in PFL-AE has two oxidation states $[4Fe\text{-}4S]^{1+/2+}$, however only the $[4Fe\text{-}4S]^{1+}$ cluster is the catalytically relevant oxidation state (7). Reduced PFL-AE in the presence of bound SAM efficiently activates PFL resulting in the oxidation of one $[4Fe\text{-}4S]^{+}$ cluster on PFL-AE for every glycyl radical generated on PFL (7). A 5'-deoxyadenosyl radical generated from SAM in the PFL-AE active site abstracts

the pro-*S* hydrogen of glycine 734 on PFL, creating a stable glycyl radical that is capable of undergoing many of rounds of catalysis before inactivation (8).

Early work on PFL-AE and PFL shows that the system can be activated by reduced flavodoxin (Fld), which presumably reduces PFL-AE (9-13). Fld can be reduced by pyruvate dependent flavodoxin oxidoreductase (PFOR) and $NADP^+$ dependent flavodoxin oxidoreductase (FNR) (9). Recently flavodoxin folding and cofactor binding thermodynamics were characterized to gain insight into the putative *in vivo* electron donor for PFL-AE that shows a likely Fld binding site on PFL-AE (Chapter 3). Interactions between PFL-AE with Fld in addition to FNR with Fld were characterized using surface plasmon resonance under anaerobic conditions (Chapter 3). Protein-protein interactions involved in PFL activation were characterized using anaerobic SPR to study the binding of PFL-AE with PFL and PFL-AE with the 12-*mer* active site peptide analogue for PFL demonstrating the importance of intact PFL (Chapter 4). A novel SAM binding assay for PFL-AE was also developed that shows that PFL binding to PFL-AE has no effect on SAM binding affinity (Chapter 4). Nuclear vibrational resonance spectroscopy (NRVS) experiments have shown that PFL-AE increases in structure and rigidity as a result of binding either SAM or SAM and YfiD (unpublished data).

When the crystal structure of PFL-AE was solved, electron density was found near the [4Fe-4S] cluster and *S*-adenosylmethionine and was assigned to a sodium cation of unknown function (4). Subsequent work in our lab showed that the sodium cation could be replaced with other monovalent cations such as K^+, Rb^+, Cs^+, and NH_4^+ while retaining activity, however PFL-AE was most active in K^+ and shows a dose response to

addition of the cation (unpublished data). In this work we set out to characterize PFL-AE in the absence of the monovalent cation to elucidate the role of cation binding in PFL-AE activity using choline chloride to maintain ionic strength; due to its large size, choline does not bind small cation binding pockets (14).

Experimental Procedures

Chemicals and Protein Purification

PFL-AE and PFL were expressed and purified as previously described (7,15-17). PFL and PFL-AE were quantified using calculated extinction coefficients from ExPASy protparam tool and verified using the Bradford assay for PFL and the Bradford assay plus a correction factor of 0.65 for PFL-AE (17,18). Iron assays were preformed as previously published (19). SAM was synthesized as previously described (20). All other small molecules and reagents used were of the highest purity available and used without further purification.

UV-vis PFL-AE Activity Assays

PFL-AE and PFL were vigorously buffer exchanged into 100 mM Tris, 100 mM choline chloride, 1 mM DTT, pH 7.6 (2.3 ± 0.16 Fe/PFL-AE). An activation mix was prepared that was composed of 50 nM PFL-AE and 5 μM PFL in 100 mM Tris, 8 mM DTT, 10 mM oxamate, 200 μM SAM, 50 μM 5-deazariboflavin, pH 7.6. Samples also contained 200 mM NaCl, 100 mM NaCl/100 mM choline chloride, or 200 mM choline chloride and were photoreduced using a 500 W halogen lamp for 5 minutes. After photoreduction 5 μL of the activation mix was added to 895 μL of the activity mix

containing 2 U/mL citrate synthase and 30 U/mL malic dehydrogenase with 10 mM malate, 10 mM pyruvate, 55 mM CoA, 0.1 mg/mL BSA, 3 mM NAD^+, 10 mM DTT, in 100 mM Tris, pH 8.1. The rate of NADH production was monitored at 340 nm as described previously (11,15) and converted to specific activity for PFL.

EPR Studies of PFL-AE in Absence of the Bound Sodium Cation

Samples for EPR spectroscopy contained 200 μM PFL-AE from the choline/Tris PFL-AE stock described in the previous section (2.3 ± 0.16 Fe/PFL-AE) in either 200 mM NaCl, 200 mM choline chloride, or 100 mM NaCl/100 mM choline chloride in 20 mM Tris, 5 mM DTT, 100 μM 5-deazariboflavin, pH 7.6. Samples were photoreduced for 45 minutes in an ice water bath inside an anaerobic chamber (mBraun) with < 1 ppm O_2. After photoreduction the samples were split in half and SAM was added to one of the samples to a final concentration of 1 mM. EPR samples were flash frozen in liquid N_2 and stored in a liquid N_2 dewar until EPR analysis.

CD Structural Studies of PFL-AE

All experiments were performed on a Jasco-710 spectropolarimeter with a 0.1 mm pathlength cuvette for far-UV studies. The sensitivity was set to 100 millidegrees, with a data pitch of 0.1 nm, in continuous scan mode, with a scan speed of 100 nm/minute, and a response of 4 seconds, and an accumulation of 5 scans. Experiments were carried out in an anaerobic cuvette with 25 μM PFL-AE (3.98 ± 0.01 Fe/PFL-AE) in 20 mM Tris, 200 mM NaCl, 1 mM DTT, pH 7.4, or 20 mM Tris, 200 mM choline chloride, 1 mM DTT, pH 7.4. Far-UV measurements were used to examine the secondary structure of PFL-AE

in the absence of a bound cation (200 mM choline chloride) compared with the enzyme with the cation presumably fully bound (200 mM NaCl).

Electrochemistry of PFL-AE

PFL-AE (3.98 ± 0.01 Fe/PFL-AE) was aliquotted into screw cap vials and sent to Dr. Sean Elliot's lab at Boston University for electrochemical analysis. The reduction potentials were determined for PFL-AE in the presence of 200 mM NaCl, 200 mM choline chloride, or 100 mM NaCl/100 mM choline chloride. Electrochemical experiments were carried out anaerobically in an MBraun Labmaster glovebox using a PGSTAT 12 potentiostat (EcoChemie). A three-electrode configuration was used in a water-jacketed glass cell. A platinum wire was used as the counter electrode and the reference electrode was a standard calomel electrode; potentials reported are relative to the standard hydrogen electrode. Baseline measurements were collected using a pyrolytic graphite edge (PGE) electrode polished with 1 μm alumina, rinsed, and placed into a glass cell containing a 10 °C mixed buffer solution (10 mM MES, CHES, TAPS, HEPES), pH 7.5 with 200 mM NaCl, 100 mM NaCl/100 mM choline chloride, or 200 mM choline chloride. A 2 μL aliquot of protein and 2 μL aliquot of 2 mg/mL neomycin were applied directly to the polished PGE electrode surface, removed, and the electrode was placed back into the buffer cell solution. Electrochemical signals were analyzed by subtraction of baseline electrochemical response of the electrode surface from the raw data using the SOAS package.

Results

PFL-AE Activity Assays in Choline Chloride and NaCl

The crystal structure of PFL-AE shows a sodium cation of unknown function bound near SAM and the iron sulfur cluster (Figure 5.1) (4). EPR spectroscopic studies carried out in our lab from our lab show that monovalent cation binding near the [4Fe-4S] cluster in PFL-AE perturbs the electronic environment of the cluster (J. Yang and R. Hutcheson, unpublished data). Monovalent cation binding can also result in altered PFL-AE activity, with K^+ exhibiting the highest activity among the cations Na^+, K^+, Cs^+, Rb^+, and NH_4^+ (R. Hutcheson, unpublished data). We set out to examine the [4Fe-4S] cluster in the absence of the bound cation while maintaining ionic strength using choline chloride to examine the role of the monovalent cation.

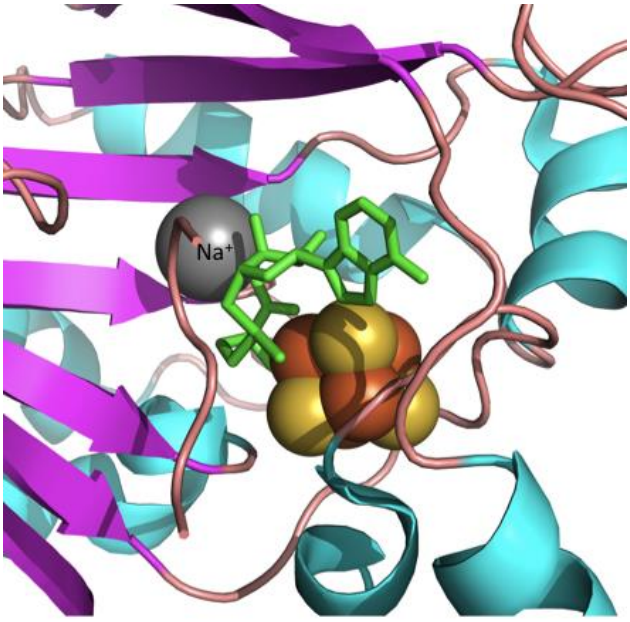

Figure 5.1: Active site of PFL-AE with SAM, the 7-*mer* peptide, and the cation bound. PDB ID 3C8F.

Choline chloride is a large monovalent cation that is precluded from binding small cation pockets that can be used to maintain ionic strength of a buffer while probing cation effects with a smaller cation (14). PFL-AE and PFL were thoroughly buffer exchanged into 20 mM Tris, 100 mM choline chloride, 1 mM DTT, pH 7.6 for activity assays. The PFL activation mixture contained 200 mM NaCl, 100 mM choline chloride/100 mM NaCl, or 200 mM choline chloride. PFL-AE was determined to be inactive in the absence of a bound cation in 200 mM choline chloride. When NaCl was supplemented into the activity assay at 100 mM NaCl/100 mM choline chloride, PFL-AE was able to activate PFL to an activity of 1.16 units. When activity assays were performed at 200 mM NaCl, PFL-AE activated PFL activity to 4.64 units, indicating apparent concentration dependence for the sodium cation. Our experiments suggest that the cation is required for PFL-AE activity (Figure 5.2), while work carried out by others in the lab indicate that the cation is important but not required (R. Hutcheson, unpublished results). Efforts are underway to resolve the discrepancy between my results and those of Dr. Hutcheson.

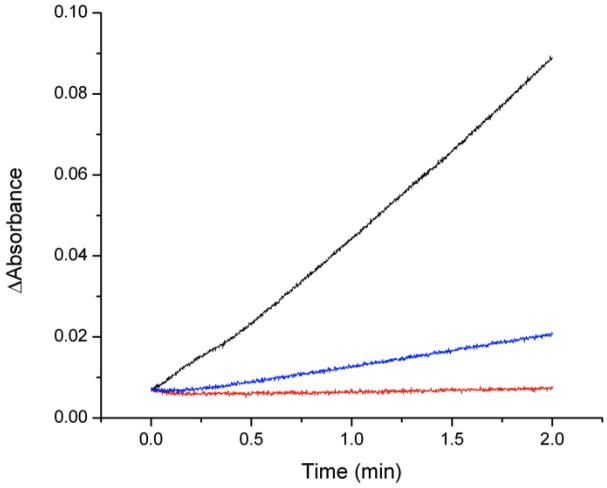

Figure 5.2: Assays of PFL activation by PFL-AE in NaCl (black), choline (red), and an NaCl/choline mixture (blue). In each case the total salt concentration was 200 mM. Other buffer components present during PFL activation included 100 mM Tris, pH 7.6 with 50 μM 5-deazariboflavin. Assays were performed by photoreducing PFL-AE in a mixture of SAM and PFL in the stated buffer for 5 minutes, at which point an aliquot was removed and added to an assay mix containing the substrates for PFL as well as coupling enzymes that ultimately report on PFL activity via rate of reduction of NAD^+ to NADH, which is monitored at 340 nm as shown here.

EPR of PFL-AE in the Absence and Presence of the Sodium Ion

EPR was used to examine the $[4Fe\text{-}4S]^+$ cluster in PFL-AE in the presence of 200 mM choline chloride, 100 mM NaCl/100 mM choline chloride, and 200 mM NaCl to determine the affect of monovalent cation binding near the cluster. The EPR spectrum for PFL-AE prepared in 200 mM NaCl or 100 mM NaCl/100 mM choline chloride are very similar, other than small changes in intensity. The EPR spectrum of PFL-AE in choline chloride however is considerably different (Figure 5.3 A). Similar trends were observed for EPR spectra of reduced PFL-AE prepared under the different salt conditions in the presence of SAM (Figure 5.3 B). It should be noted that in all three salt conditions

tested, SAM appears to bind, as significant changes in the EPR spectra indicative of SAM binding are observed (compare Figure 5.3 A and 5.3 B).

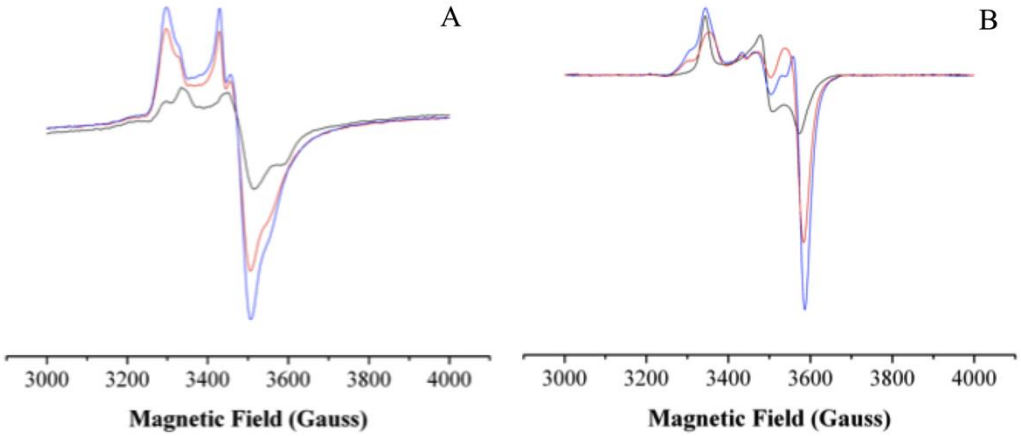

Figure 5.3: EPR of the [4Fe-4S] cluster in PFL-AE and the effect of sodium cation binding. PFL-AE in 200 mM choline chloride (black), 100 mM choline chloride/100 mM NaCl (red), and 200 mM NaCl (blue). Each experimental sample contained 100 µM PFL-AE in 100 mM Tris, pH 7.6 with 50 µM 5-deazariboflavin. Samples were photoreduced for 45 minutes before being frozen in liquid N_2 and later analyzed by EPR. A) PFL-AE B) PFL-AE plus SAM Signals from the [4Fe-4S] cluster in PFL-AE were measured at 12 K. EPR parameters: Microwave frequency, 9.37 GHz; power, 19 mW; modulation amplitude, 5G.

CD of PFL-AE to in the Absence and Presence of the Monovalent Cation

Far-UV circular dichroism has been used for many years to determine protein secondary structure (21). We used this technique to examine the secondary structure of PFL-AE in the presence and absence of a bound monovalent cation to determine if cation binding plays a structural role in PFL-AE. Comparison of the far-UV spectrum of PFL-AE in 200 mM choline chloride to PFL-AE in 200 mM NaCl reveals that cation binding has no influence on the secondary structure of PFL-AE (Figure 5.4). This data suggests that PFL-AE is similarly folded in the absence of the cation as well as in the presence of

NaCl. Therefore changes in secondary structure or protein denaturation cannot explain the inactivity of PFL-AE in choline chloride.

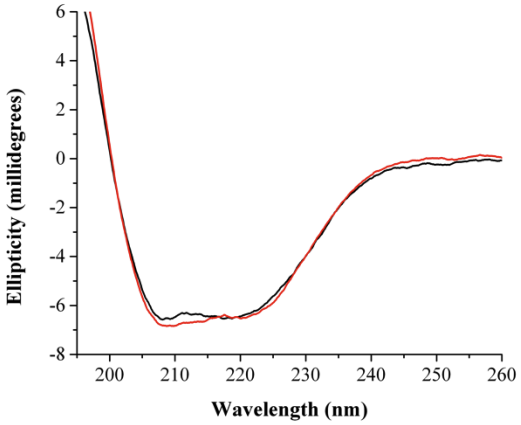

Figure 5.4: PFL-AE is well folded in absence of the bound cation as determined by far-UV CD. Black: PFL-AE in 200 mM choline chloride, Red: 100 mM choline chloride/100 mM NaCl, Blue: 200 mM NaCl. Samples were prepared in 20 mM HEPES, 1 mM DTT, pH 7.4 with the above salts. Protein concentrations were 25 μM, 0.1 mm cuvette, 195-260 nm, sensitivity = 100 millidegrees, data pitch = 0.1 nm, accumulation of 4 scans.

Electrochemistry of PFL-AE and the Role of the Cation

Monovalent cation binding in PFL-AE was examined using electrochemistry to see if cation binding would modulate the reduction potential of the [4Fe-4S] cluster. Activity assays clearly show a dose dependent increase in activity with sodium addition to PFL-AE and significantly less activity in the absence of the cation. To fully understand the effect of the cation on the [4Fe-4S] cluster of PFL-AE, electrochemistry was used to understand how favorable activation would be in the absence and presence of the bound cation. The reduction potential for PFL-AE in 200 mM NaCl at 4 °C pH 7.5 was determined to be -265 mV (Figure 5.5). The experiment was then performed using 100 mM NaCl/100 mM choline chloride to reduce the cation concentration while maintaining

ionic strength; in this case the reduction potential was determined to be -248 mV. When experiments were performed in 200 mM choline chloride, the reduction potential for PFL-AE was determined to be -234 mV.

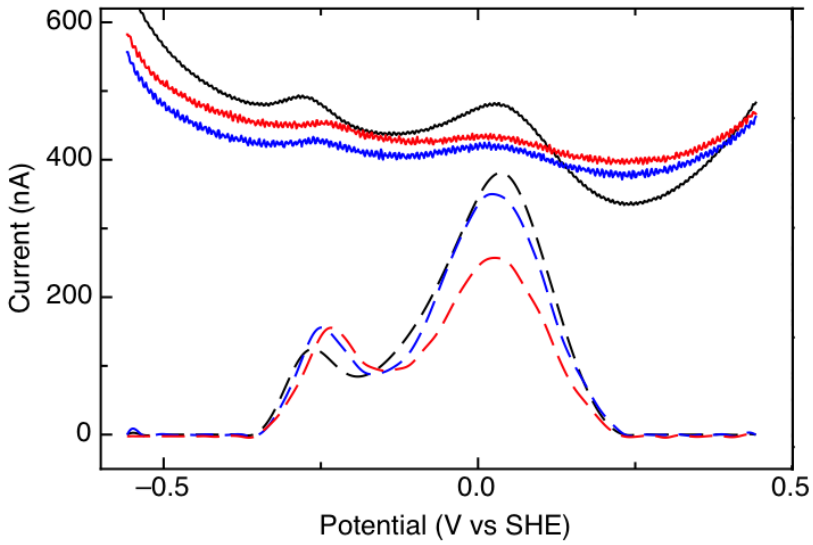

Figure 5.5: Square wave voltammetry of PFL-AE to determine the effect of the cation on reduction potentials. Top: raw data, Bottom: baseline subtracted data. PFL-AE in 200 mM NaCl (black), PFL-AE in 100 mM NaCl/100 mM choline chloride (blue), PFL-AE in 100 mM choline chloride (red). Electrochemical experiments were carried out anaerobically in an MBraun Labmaster glovebox using a PGSTAT 12 potentiostat (EcoChemie). A three-electrode configuration was used in a water-jacketed glass cell. A platinum wire was used as the counter electrode and the reference electrode was a standard calomel electrode; potentials reported are relative to the standard hydrogen electrode. Baseline measurements were collected using a pyrolytic graphite edge (PGE) electrode polished with 1 μm alumina, rinsed, and placed into a glass cell containing a 10 °C mixed buffer solution (10 mM MES, CHES, TAPS, HEPES), pH 7.5 with 200 mM NaCl, 100 mM NaCl/100 mM choline chloride, or 200 mM choline chloride. A 2 μL aliquot of protein and 2 μL aliquot of 2 mg/mL neomycin were applied directly to the polished PGE electrode surface, removed, and the electrode was placed back into the buffer cell solution. Electrochemical signals were analyzed by subtraction of baseline electrochemical response of the electrode surface from the raw data using the SOAS package.

Discussion

It was our goal for this work to understand the role of the monovalent cation on the activity of PFL-AE. Previous EPR data has shown that different monovalent cations have their own unique affect on the electronic environment of the [4Fe-4S] cluster (R. Hutchenson, unpublished data). Activity assays show that cation addition stimulates PFL-AE activity. EPR data shows that removing the cation altogether from PFL-AE also has a very dramatic effect on the electronic environment of the cluster. The choline chloride PFL-AE signal is unique and upon sodium addition, cation binding perturbs the signal, which can then be further altered by the addition of SAM. Samples prepared in 100 mM NaCl/100 mM choline chloride were virtually identical to PFL-AE prepared in 200 mM NaCl, suggesting 100 mM NaCl saturates the cation binding site. Our data shows the [4Fe-4S] cluster in PFL-AE without any contributions from monovalent cation binding.

Circular dichroism experiments were performed to determine if the cation played a structural role in PFL-AE. Using far-UV CD we were able to examine the secondary structure of PFL-AE in the presence and absence of a bound monovalent cation. Our data clearly shows that the secondary structure of PFL-AE does not change as a result of cation binding and that the enzyme is well folded in absence of the cation; this provides strong evidence that PFL-AE inactivity in choline does not appear to be caused by structural changes.

Electrochemistry has been performed on PFL-AE for the first time and provides great insight into PFL-AE activity. In the absence of a bound cation, the potentials become more positive making SAM cleavage and PFL activation less likely based on the

estimated potential required for SAM cleavage of -1.6 V (22). The reduction potential of the [4Fe-4S] cluster in PFL-AE decreases in the presence of 100 mM NaCl/100 mM choline chloride and there is a further reduction in the presence of presumably saturating concentrations of sodium. Overall the reduction potential of PFL-AE is modulated by 31 mV in the presence of the sodium cation.

The aggregate data suggests that monovalent cation binding is required for efficient PFL-AE activity. This effect appears to be caused by the cation binding in close proximity to the [4Fe-4S] cluster, which perturbs the electronic environment of the cluster and helps to modulate the reduction potential of the cluster and possibly SAM. Elegant experiments have been performed on lysine 2,3-aminomutase that show the importance of substrate binding on the reduction potentials of the [4Fe-4S] cluster and SAM and how they relate to catalytic activity (23,24). Our electrochemistry results show that monovalent cation binding lowers PFL-AE iron sulfur cluster reduction potentials and may possibly raise SAM reduction potentials thus decreasing the prohibitively large energy barrier for SAM cleavage that has been studied in lysine 2,3-aminomutase.

Footnotes

This work was supported by NIH grant 2R01GM054608.

References

1. Knappe, J., Neugebauer, F. A., Blaschkowski, H., P., and Gänzler, M. (1984) *Proc. Natl. Acad. Sci. U.S.A.* 81, 1332-1335

2. Knappe, J., and Sawers, G. (1990) *FEMS Microbiol. Rev.* 75, 383-398

3. Peng, Y., Veneziano, S. E., Gillispie, G. D., and Broderick, J. B. (2010) *J. Biol. Chem.* 285, 27224-27231

4. Vey, J. L., Yang, J., Li, M., Broderick, W. E., Broderick, J. B., and Drennan, C. L. (2008) *Proc. Natl. Acad. Sci. U.S.A.* 105, 16137-16141

5. Krebs, C., Broderick, W. E., Henshaw, T. F., Broderick, J. B., and Hanh Huynh, B. (2002) *J. Am. Chem. Soc.* 124, 912-913

6. Walsby, C. J., Ortillo, D., Broderick, W. E., Broderick, J. B., and Hoffman, B. M. (2002) *J. Am. Chem. Soc.* 124, 11270-11271

7. Henshaw, T. F., Cheek, J., and Broderick, J. B. (2000) *J. Am. Chem. Soc.* 122, 8331-8332

8. Frey, M., Rothe, M., Volker Wagner, A. F., and Knappe, J. (1994) *J. Biol. Chem.* 269, 12432-12437

9. Blaschkowski, H., P., Neuer, G., Ludwig-Festl, M., and Knappe, J. (1982) *Eur. J. Biochem.* 123, 563-569

10. Knappe, J., and Blaschkowski, H., P. (1975) *Pyruvate Formate-Lyase from Escherichia coli and its Activation System*, Academic Press Inc., New York

11. Knappe, J., Blaschkowski, H., P., Grobner, P., and Schmitt, T. (1974) *Eur. J. Biochem.* 50, 253-263

12. Knappe, J., Schacht, J., Möckel, W., Höpner, T., Vetter, H., Jr., and Edenharder, R. (1969) *European J. Biochem.* 11, 316-327

13. Vetter, H., Jr., and Knappe, J. (1971) *H-Z Physiol. Chem.* 352, 433-446

14. Maldonado, S., Irún, M., P., Campos, L., A., Rubio, J., A., Luquita, A., Lostao, A., Wang, R., Garcia-Moreno, B., E., and Sancho, J. (2002) *Protein Sci.* 11, 1260-1273

15. Nnyepi, M., R., Peng, Y., and Broderick, J., B. (2007) *Arch. Biochem. Biophys.* 459, 1-9

16. Krebs, C., Broderick, W., E., Henshaw, T., F., Broderick, J. B., and Huynh, B. H. (2002) *J. Am. Chem. Soc.* 124, 912-913

17. Broderick, J. B., Henshaw, T., F., Cheek, J., Wojtuszewski, K., Smith, S., R., Trojan, M., R., McGhan, R., M., Kopf, A., Kibbey, M., and Broderick, W., E. (2000) *Biochem. Bioph. Res. Co.* 269, 451-456

18. Bradford, M., M. (1976) *Anal. Biochem.* 72, 248-254

19. Beinert, H. (1978) *Methods Enzymol.* 54, 435-445

20. Walsby, C., J., Hong, W., Broderick, W., E., Cheek, J., Ortillo, D., Broderick, J. B., and Hoffman, B., M. (2002) *J. Am. Chem. Soc.* 124, 3143-3151

21. Greenfield, N., J. (2006) *Nat. Protoc.* 1, 2876-2890

22. Colichman, E., L., and Love, D., L. (1952) *J. Org. Chem.* 18, 40-46

23. Wang, S., C., and Frey, P., A. (2007) *Biochemistry* 46, 12889-12895

24. Hinckley, G., T., and Frey, P., A. (2006) *Biochemistry* 45, 3219-3225

CHAPTER 6

PYRUVATE:FLAVODOXIN OXIDOREDUCTASE IS THE ELECTRON DONOR FOR PYRUVATE FORMATE-LYASE ACTIVATING ENZYME

Contribution of Authors and Co-Authors

Manuscripts in Chapters 1, 3, 4, 5, 6

Author Adam V. Crain

Contributions: Conceived and implemented the study, analyzed that data, and wrote the manuscript

Co-Author: Martina D. Van Hoy

Contributions: Assisted with sequence alignments, flavodoxin activity assays with PFOR and PFL activity assays with PFOR

Co-Author: Dr. Joan B. Broderick

Contributions: Provided oversight and guidance in experimental design and interpretation. Provided all funding and resources for the projects. Advised on manuscript preparation and edited manuscript drafts.

CHAPTER 6

PYRUVATE:FLAVODOXIN OXIDOREDUCTASE IS THE ELECTRON DONOR FOR PYRUVATE FORMATE-LYASE ACTIVATING ENZYME

Adam V. Crain, Martina D. Van Hoy, and Joan B. Broderick

From the Department of Chemistry & Biochemistry and the Astrobiology Biogeocatalysis Research Center
Montana State University, Bozeman, MT 59717

To whom correspondence should be addressed: Joan B. Broderick, Department of Chemistry & Biochemistry, Montana State University, Bozeman, MT 59717, Tel: (406) 994-6160; E-mail: jbroderick@chemistry.montana.edu.

Keywords: Pyruvate:Flavodoxin Oxidoreductase, Electron Transfer, Pyruvate Formate-Lyase Activating Enzyme, Pyruvate Formate-Lyase, Flavodoxin

Abstract

Pyruvate:flavodoxin oxidoreductase (PFOR) is an iron sulfur cluster containing enzyme that catalyzes the oxidative cleavage of pyruvate to form acetyl-CoA and in the process acts as a powerful electron donor. PFOR has been shown to activate the pyruvate formate-lyase (PFL) system in *E. coli*, but has never been overexpressed or fully purified. In this work, we attempted to overexpress and purify PFOR and performed experiments to characterize PFOR that included activity assays with flavodoxin (Fld) and the PFL system. As isolated PFOR is brown in color consistent with an iron sulfur protein. Iron assays on PFOR show that the enzyme contains 1.24 ± 0.2 Fe/subunit and is inactive in Fld and PFL activity assays. However, when PFOR was reconstituted the enzyme

contained 15.9 ± 0.7 Fe/subunit and was active in Fld and PFL activity assays. PFL activity with PFOR and Fld was stimulated by the addition of $MgCl_2$ and thiamine pyrophosphate (TPP) suggesting that some of the TPP cofactor is lost during purification. $NADP^+$ dependent flavodoxin oxidoreductase (FNR) was also tested for activity with the PFL system in the presence and absence of Fld and was found to be inert as an electron donor. Neither electron donor system was capable of reducing as isolated PFL-AE in the absence of PFL, indicating that electron transfer from Fld to PFL-AE must be coupled to PFL activation.

Introduction

Inside aerobic bacteria and inside the mitochondria of eukaryotic cells, pyruvate dehydrogenase (PDH) synthesizes acetyl-CoA from pyruvate for the citric acid cycle (1). Under anaerobic conditions, pyruvate formate-lyase synthesizes acetyl-CoA by catalyzing a direct thiolytic cleavage of pyruvate resulting in an acetyl-enzyme intermediate, which then reacts with CoA to form acetyl-CoA (2-4). In archaea, bacteria and amitochondriate eukaryotes, pyruvate decarboxylation is carried out by pyruvate:flavodoxin oxidoreductase which catalyzes the reaction of pyruvate + CoA ⇆ acetyl-CoA + CO_2 + 2 e^- + 2 H^+ (5). *E. coli* contains all three systems, however, their activity is dependent on cellular conditions, with PFL and PDH both mutually exclusive (2). Although PFOR produces acetyl-CoA in *E. coli* under anaerobic conditions, the enzyme is expressed in small quantities and as a result does not significantly contribute to the citric acid cycle (2,6). The main function of PFOR is to provide extremely low potential reducing equivalents for electron acceptors such as Fld and ferredoxin (Fd)

under anaerobic conditions (7). In mesophilic bacteria, PFOR is a homodimer with a molecular weight of approximately 240 kDa (7-14). In some cases, however, PFOR has been determined to be a $\alpha_2\beta_2$ heterotetramer, a pentamer, or an octamer (15-18). PFOR can also be composed of a heterotetramer with four different subunits (19-23). The PFOR homodimer is thought to have arrived by gene rearrangement and fusion of the four different PFOR subunits (24,25).

The only available crystal structures for PFOR are from *D. Africanus* and are homodimeric with a molecular weight of 267 kDa (5,26-28). PFOR contains a thiamine pyrophosphate cofactor and anywhere from one to three [4Fe-4S] clusters per subunit (24). The reduction potential of *D. africanus* PFOR has been determined to be -390, -515, and -540 mV for each of the three iron sulfur clusters, indicating that the enzyme is a powerful electron donor for Fld and Fd (11). Electrons derived from pyruvate are transferred to the iron sulfur cluster redox centers in a stepwise manner and the clusters are thought to act as a conduit for electron transfer to Fd or Fld (26). During PFOR catalysis, in some cases a substrate based free radical carbocation is formed (9,11,29-31) and in other cases the radical is absent (13,31,32), suggesting two different mechanisms (31).

PFOR from *E. coli* is composed of a single gene known as *ydbK*, and the corresponding protein has a molecular weight of 128.7 kDa, based on the corresponding protein sequence. The molecular weight of *E. coli* PFOR has been determined to be 200 ± 15 kDa using analytical ultracentrifugation (AUC), suggesting that the enzyme is homodimer in solution with an actual molecular weight of 257.5 kDa (7). In *Escherichia*

coli, under anaerobic conditions, there are two established electron transfer systems involved in enzymatic reductions. One system composed of $NADP^+$ dependent flavodoxin reductase (FNR) and flavodoxin (Fld) or ferredoxin (Fd) delivers low potential reducing equivalents to enzymes such as methionine synthase, biotin synthase, class III anaerobic ribonucleotide reductase, and pyruvate formate-lyase activating enzyme (7,33-35). Pyruvate:flavodoxin oxidoreductase (PFOR), the second electron transfer system found in *Escherichia coli,* is an extremely powerful electron donor that delivers very low potential reducing equivalents to flavodoxin and ferredoxin (7). PFOR has been shown to be capable of activating the PFL system presumably by reducing PFL-AE in the presence of Fld (7). The reduction potentials for Fld have been determined to be -285 mV for the semiquinone and -455 mV for the hydroquinone oxidation states (36). Hydroquinone Fld has been determined to be the active species for providing reducing equivalents in PFL activity assays (7). The interaction and electron transfer between FNR and Fld has been studied and while the electron transfer event is very slow, the reaction is still thought to be physiologically relevant (35,37). Although FNR was shown to only produce a very small quantity of hydroquinone Fld, it was still capable of activating the PFL system with similar efficiency as the PFOR system (7).

In this work we overexpressed and purified PFOR to characterize the enzyme and its activity to provide greater insight into the physiological electron donor system for PFL-AE. We performed sequence alignments to determine the residues involved in cluster binding for all three [4Fe-4S] clusters and the organic cofactor TPP. UV-vis experiments were performed to show cluster reduction upon incubation with pyruvate

and CoA. We examined electron transfer from PFOR to Fld and used PFL activity assays with PFOR and Fld as electron donors to show that PFOR and Fld are the electron donors for the PFL system.

Experimental Procedures

Cloning, Expression, and Purification of PFOR

All chemicals used were of the highest commercially available quality and were used without further purification. The gene for PFOR known as *ydbK* was cloned from *E. coli* strain B genomic DNA using PCR and subsequently digested using NdeI and XbaI restriction enzymes. The pET-14b vector was digested with the same enzymes and gel purified before *ydbK* was ligated into the vector and used to transfect the NovaBlue GigaSingles cell line. The plasmid was purified using a miniprep kit from Qiagen and used to transfect the BL21(DE3)pLysS expression cell line. PFOR was expressed and purified using the same procedures used for PFL-AE (38-41). Protein concentrations for PFOR assays were determined using the Bradford assay (42). Iron numbers were determined using iron assays as previously described (43). PFOR was reconstituted according to a previously designed procedure (44).

Protein Sequence Alignments

Protein sequence alignments were preformed using Clustal Omega software. PFOR sequences from several different organisms were aligned using protein sequences from *E. coli, D. africanus, K. pneumonia, T. vaginalis, P. furiosus,* and *H. halobium.* Residues involved in TPP cofactor binding and iron sulfur cluster binding from *D.*

africanus were compared to 100 % sequence conserved residues in *E. coli* PFOR to determine the iron sulfur cluster and cofactor binding residues.

PFOR Activity Assays with Fld, PFL-AE, and PFL

UV-vis studies were performed using a Cary-50 UV-vis spectrophotometer using a 1 cm pathlength anaerobic cuvette. PFOR activity assays were performed with Fld held at a constant concentration of 40 μM and the PFOR concentration was 400 nM of the homodimer with 1mM TPP, 5 mM $MgCl_2$, 10 mM pyruvate, and 100 μM CoA in 20 mM HEPES, 10 mM NaCl, 1 mM DTT, pH 7.4. The rate of semiquinone Fld reduction was measured using a known extinction coefficient of 3820 M^{-1} cm^{-1} at 580 nm (36).

PFL activity using PFOR and Fld as electron donors was studied using an optical assay as previously described (7). In these experiments all the components required for the PFL activation system were added to a vial and incubated for 20 minutes before being added to the activity mixture to monitor PFL turnover. The activation mixture contained 5 μM PFL, 10 mM pyruvate, 10 mM oxamate, 100 μM CoA, 1 μM PFL-AE, 100 μM SAM, 3 μM Fld, 1 μM PFOR dimer, 1 mM TPP, 5 mM $MgCl_2$, 10 mM DTT in 20 mM HEPES, 10 mM NaCl, pH 7.4. A small amount of this mixture (45 μL) was then added to the PFL activity mixture (895 μL) containing 2 U/mL citrate synthase and 30 U/mL malic dehydrogenase with 10 mM malate, 10 mM pyruvate, 55 μM CoA, 0.1 mg/mL BSA, 3 mM NAD^+, 10 mM DTT, in 100 mM Tris, pH 8.1. The rate of PFL turnover was monitored optically as was performed previously (3,39). One unit of PFL activity is defined as 1 μmol/min of pyruvate consumption (45). UV-vis assays were also performed to determine if PFOR and Fld or FNR and Fld were capable of reducing the [4Fe-4S]

cluster in PFL-AE. In these experiments a sample was prepared containing 40 μM PFL-AE, 200 nM PFOR, 3 μM Fld, 1 mM TPP, 5 mM $MgCl_2$, 10 mM pyruvate, 100 μM CoA and absorbance changes were monitored by taking scans every 15 minutes over a one hour period. Experiments utilizing FNR as the Fld electron donor contained 3 μM FNR, 3 μM Fld, and 500 μM NADPH along with 40 μM PFL-AE, 10 mM pyruvate, and 55 μM CoA. These experiments were carried out at 25 °C in 20 mM HEPES, 10 mM NaCl, 1 mM DTT, pH 7.4.

PFL Activation Monitored by Glycyl Radical Formation

EPR spectra were measured on a Bruker ER-200D-SRC spectrometer at 60 K for PFL activation experiments with a frequency of 9.37 GHz. The EPR microwave power for glycyl radicals was set to 0.06 mW with a modulation frequency of 100 kHz and a 5 G modulation amplitude for all samples; all spectra were the sum of four scans. PFL activation reactions were carried out under anaerobic conditions in an mBraun box with <1 ppm O_2. All components required for PFL activation were added to a vial and incubated at 25 °C for either 5 minutes or 60 minutes including 60 μM PFL dimer, 3 μM PFL-AE, 3 μM Fld, 3 μM FNR, 50 μM SAM, 2 mM pyruvate, 100 μM CoA, and 500 μM NADPH, samples were prepared in 100 mM Tris, 100 mM KCl, 2 mM DTT, pH 7.4

Results

Overexpression, Purification, Reconstitution, and Initial Characterization of PFOR

When pyruvate:flavodoxin oxidoreductase (PFOR) from *E. coli* was first studied by Blaschkowski et al, they determined that the enzyme was capable of reducing Fld in

addition to activating the PFL system (7). They did not however overexpress PFOR, and were able to only partially purify it. We have therefore pursued the overexpression and purification of PFOR from *E. coli*. The *ydbK* gene from *E. coli,* which is annotated as a probable pyruvate:flavodoxin oxidoreductase was amplified from strain B genomic DNA and inserted into the pET-14b plasmid which was then used to over produce the *E. coli* PFOR in the BL21(DE3)pLysS cell line. PFOR was produced and purified according to a protocol designed for PFL-AE (38,39,41,46) with the exception that PFOR precipitated out in the 30 – 60 % ammonium sulfate fraction. Following ammonium sulfate fractionation and gel filtration, the protein had a distinct brown color consistent with an iron sulfur cluster containing enzyme.

When as isolated PFOR (400 nM homodimer) was added to 40 μM Fld in the presence of 1 mM TPP, 5 mM $MgCl_2$, 10 mM pyruvate, 10 mM oxamate, and 100 μM CoA, no Fld reduction or PFL activation was observed, indicating that PFOR was inactive. The iron number for as isolated PFOR was 1.24 ± 0.2 per subunit, which is clearly substoichiometric considering PFOR should have an iron number of 12 per subunit under ideal conditions. In *D. africanus,* PFOR has three [4Fe-4S] clusters that connect that surface of the enzyme to the TPP cofactor and are thought to be involved in electron transfer to electron acceptor proteins like flavodoxin or ferredoxin (26). For this reason we decided to reconstitute the enzyme with iron and sulfide to see if PFOR would be active if it contained a full compliment of iron sulfur clusters. The iron number for the reconstituted PFOR was 15.9 ± 0.7 per subunit, and the UV-visible spectrum displayed a large increase in absorbance when compared to the isolated enzyme (Figure 6.1).

Although the protein was not very pure, this data suggests that the clusters should now be intact and functional. When the PFOR substrates pyruvate and CoA were added to PFOR, a reduction in absorbance was seen, indicating that the iron sulfur clusters in PFOR were reduced.

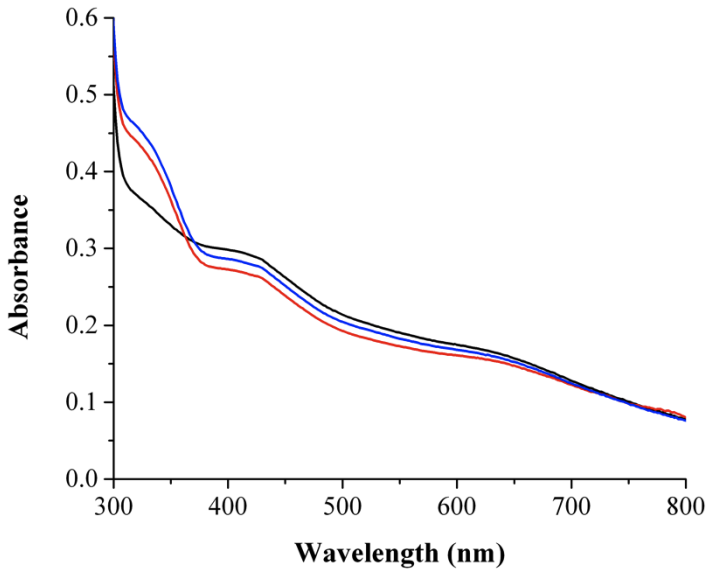

Figure 6.1: UV-vis data for the reconstituted PFOR and its reduction using pyruvate and CoA. Magenta: As isolated PFOR, Black: Reconstituted PFOR, Blue: Reconstituted PFOR plus 10 mM pyruvate, Red: Reconstituted PFOR plus 10 mM pyruvate and 100 µM CoA. The PFOR concentration was 1 µM homodimer in all assays. The enzyme was incubated for 20 minutes after the addition of pyruvate or CoA before the absorbance was measured. The buffer used was 20 mM HEPES, 10 mM NaCl, 1 mM TPP, 5 mM $MgCl_2$, 1 mM DTT, pH 7.4 and scans were taken from 300 - 800 nm.

PFOR Sequence Alignments

When PFOR protein sequences were aligned from various organisms containing homodimeric PFOR, there was a high degree of sequence conservation. Amino acid residues that bind each of three [4Fe-4S] clusters were examined and in all cases these

residues were 100 % sequence conserved. The TPP cofactor binding motif composed of G961, D962, G963 was also found to be 100 % conserved among the various organisms compared. The corresponding [4Fe-4S] cluster binding residues and cofactor binding residues were examined in *E. coli* PFOR to determine which residues were involved in iron sulfur cluster binding and cofactor binding. PFOR from *D. africanus* contains two $CX_2CX_2CX_3C$ ferredoxin like motifs and an abnormal $CX_2CX_{25}CX_{231}C$ cluster ligation motif that are all involved in iron sulfur cluster binding. *E. coli* PFOR has a $CX_2CX_{24}CX_{223}C$ motif corresponding to the proximal (near the TPP cofactor) cluster binding motif, comprising residues C818, C821, C846, and C1070. The central ferredoxin like cluster in *E. coli* PFOR corresponds to residues C744, C747, C750, and C754 and the distal ferredoxin like cluster contains residues C688, C691, C694, and C698. The TPP cofactor binding motif corresponds to *E. coli* residues G961, D962, and G963.

PFOR Activity Assays with Fld

Reconstituted PFOR was determined to be active using flavodoxin as an electron acceptor. The rate of Fld reduction could be conveniently monitored by following changes in absorbance at 580 nm and using a known extinction coefficient to solve for the concentration of semiquinone Fld. Unlike FNR, PFOR is powerful electron donor and can easily reduce Fld to the hydroquinone oxidation state in minutes (Figure 6.2). The rate of Fld reduction was determined to be 37.1 nmol/min/mg PFOR.

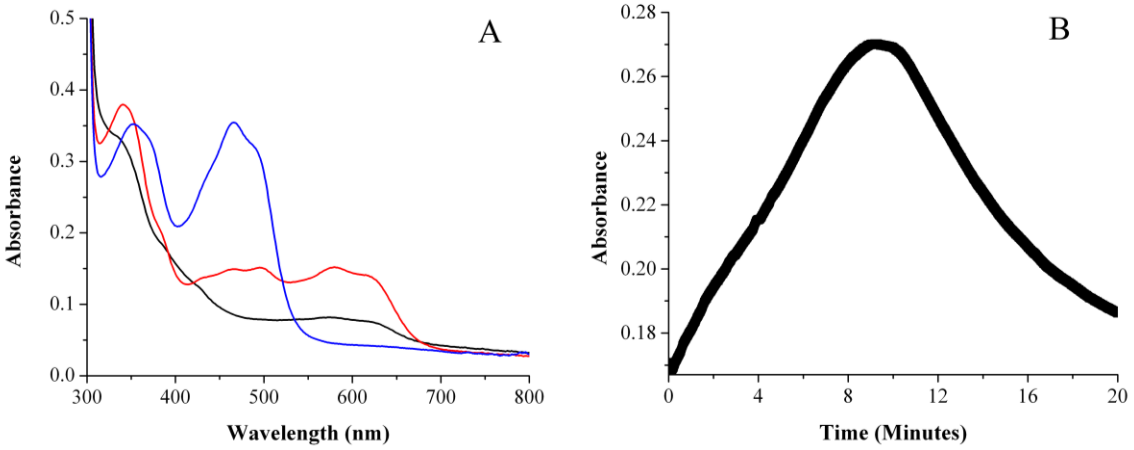

Figure 6.2: PFOR activity assays using Fld as an electron acceptor. A) UV-vis scans of Fld to monitor reduction. Blue: Fld before the start of the reduction showing the fully oxidized protein. Red: 10 minutes into the Fld reduction showing the semiquinone oxidation state. Black: 20 minutes into the Fld reduction showing hydroquinone fully reduced Fld. B) Kinetics of Fld reduction monitored at 580 nm showing formation of the semiquinone Fld which is subsequently converted to the hydroquinone oxidation state. Fld concentration was 40 µM with PFOR at 400 nM, supplemented with 10 mM pyruvate, 100 µM CoA, 1 mM TPP, and 5 mM $MgCl_2$ in 20 mM HEPES, 10 mM NaCl, 1 mM DTT, pH 7.4; UV-vis scans were taken from 300 – 800 nm in Figure 2A. In Figure 2B, data points were measured every 0.1 seconds at 580 nm for a total of 20 minutes.

Electron Donor Activity with PFL-AE in the Absence of PFL

We were interested in knowing if Fld was capable of reducing PFL-AE in the absence of PFL and substrates so we designed UV-vis experiments where PFL-AE was in excess and Fld and FNR or PFOR were at catalytic concentrations so they would not make a contribution to the spectrum (Figure 6.3 A). Experiments were set up in which 3 µM FNR was added to 50 µM PFL-AE with 500 µM NADPH and scans were taken to determine if PFL-AE was being reduced by FNR. Experiments were also performed using 2 µM FNR, 500 µM NADPH, and 3 µM Fld with 40 µM PFL-AE and in both cases FNR or FNR plus Fld were incapable of reducing PFL-AE. The same experiments were performed using 200 nM PFOR, 10 mM pyruvate, 100 µM CoA, 1 mM TPP, and 5 mM

$MgCl_2$, 2 µM Fld and in this case PFOR was determined to be inert as an electron donor in absence of PFL as well. EPR samples were also prepared under the same conditions as above for FNR and FNR plus Fld and these samples reveal only an isotropic signal corresponding to the $[3Fe\text{-}4S]^{1+}$ cluster, (present in all purifications), indicating that PFL-AE is not reduced by FNR or FNR plus Fld in the absence of PFL (Figure 6.3 B).

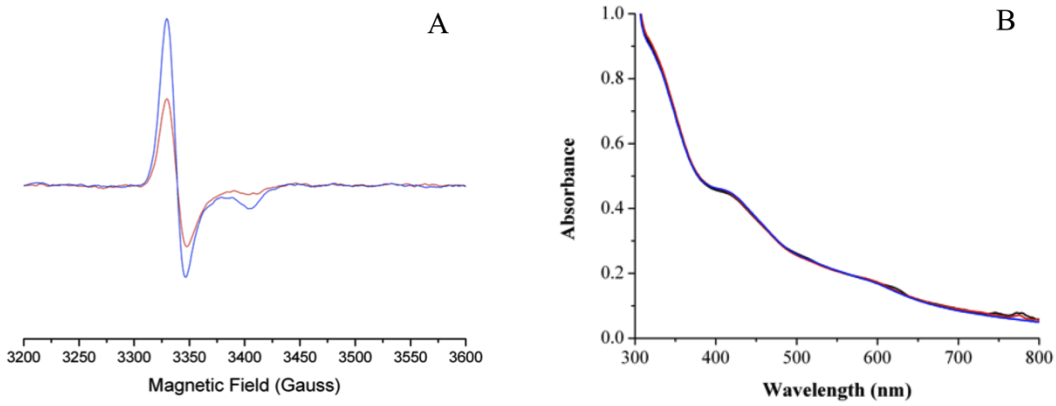

Figure 6.3: EPR and UV-vis data showing that electron donors do not reduce PFL-AE in absence of PFL. A) EPR data showing the $[3Fe\text{-}4S]^{1+}$ cluster in PFL-AE. Blue: 60 µM PFL-AE plus 3 µM FNR and 500 µM NADPH, Red: 50 µM PFL-AE plus 3 µM FNR, 3 µM Fld, and 500 µM NADPH. Both samples were incubated for 60 minutes at 25 °C in 100 mM Tris, 100 mM KCl, 10 mM DTT, pH 7.4 before EPR analysis. EPR samples were run at 12 K with a frequency of 9.37 GHz, a microwave power of 1.59 mW, a modulation frequency of 100 kHz, and a 5 G modulation amplitude; all spectra were the sum of four scans. B) UV-vis of 40 µM PFL-AE with 200 nM PFOR, 1 mM TPP, 5 mM $MgCl_2$, 10 mM pyruvate, 100 µM CoA, 3 µM Fld, 1 mM DTT, pH 7.4. UV-vis scans were taken from 300 – 800 nm. Scan taken after 10 minutes (black), 20 minutes (red), 60 minutes (blue).

PFOR Activity Assays with the PFL System

PFL activity assays were performed as previously described using a spectrophotometric study where acetyl-CoA production was coupled to NADH formation monitored by absorbance changes at 340 nm (3,39). In these experiments, 45 µL of the

activation mixture containing PFOR, Fld, PFL-AE, and PFL with substrates was added to the rim of the cuvette containing 895 µL of PFL activity mix and the cuvette was sealed so it could be removed from the anaerobic chamber and inverted immediately before starting the assay. The rate of PFL turnover was determined to be 0.78 U/mg of reconstituted PFOR in the presence of Fld. When PFOR and Fld were supplemented with 1 mM TPP and 5 mM $MgCl_2$, the rate of PFL turnover increased to 2.01 U/mg of PFOR (Figure 6.4). FNR activity in the PFL system was also studied using the same assay and it was determined that FNR in the presence or absence of Fld is inert as an electron donor for PFL activation (Figure 6.4). Reduced recombinant FNR has been shown to be unstable and unfolds at *in vivo* temperatures (47), providing a possible explanation for FNR inactivity with the PFL system.

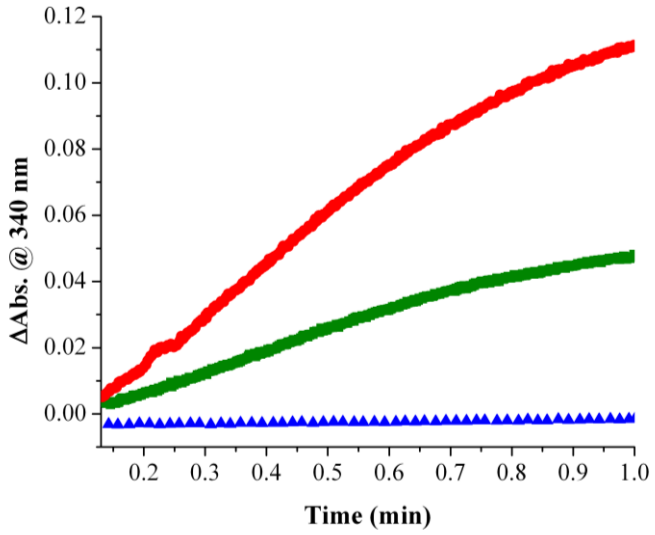

Figure 6.4: PFL Activity when activated by PFL-AE using Fld and PFOR or FNR as a source of reducing equivalents. Blue: PFL activity with 2 µM FNR and 3 µM Fld and 500 µM NADPH, Green: PFL activity with 400 nM PFOR and 2 µM Fld plus pyruvate and CoA, Red: PFL activity with 400 nM PFOR and 2 µM Fld plus 1 mM TPP, 5 mM $MgCl_2$, 10 mM pyruvate, and 100 µM CoA. NADH reduction was monitored at 340 nm for 60 seconds to determine the rate of PFL turnover. Data points were taken every 0.1 seconds for PFOR measurements and every second for FNR activity assays.

PFL Activation Studies using FNR and Fld

EPR samples were prepared using FNR and FNR plus Fld as a source of reducing equivalents for PFL activation. Samples were incubated for 5 minutes or one hour and each contained 500 µM NADPH, 3 µM FNR, 3 µM Fld, 3 µM PFL-AE, 50 µM SAM, 2 mM pyruvate, 10 mM oxamate, 100 µM CoA, and 60 µM PFL. EPR analysis shows the presence of isotropic signals corresponding to the flavin cofactors in Fld and FNR in the semiquinone oxidation states and there was a complete absence of the glycyl radical, indicating that FNR and Fld are incapable of activating the PFL system (Figure 6.5). EPR samples of the PFL system in the presence of PFOR are in the process of being set up.

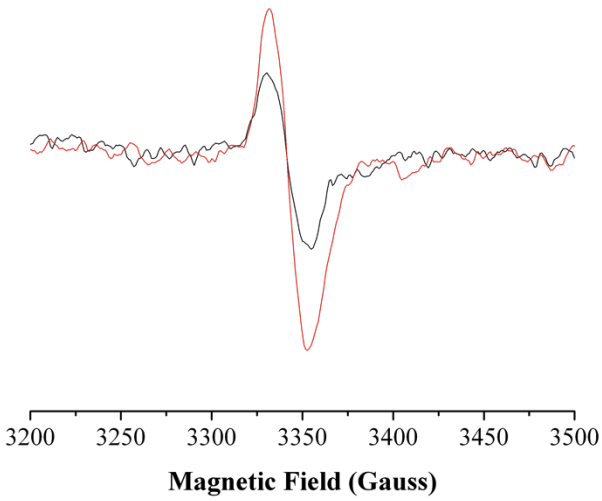

Figure 6.5: PFL activation experiments using EPR to detect the glycyl radical on active PFL. Each sample contained 60 µM PFL dimer, 3 µM PFL-AE, 3 µM Fld, 50 µM SAM, 2 mM pyruvate, 100 µM CoA, and 500 µM NADPH. Black: Sample incubated for 5 minutes, Red: Sample incubated for one hour. Samples were prepared in 100 mM Tris, 100 mM KCl, 2 mM DTT, pH 7.4. Glycyl radical signals were measured at 60 K with a microwave frequency of 9.37 GHz, microwave power of 0.06 mW, modulation amplitude of 5 G.

Discussion

PFOR is an interesting enzyme that acts as a powerful electron donor for flavodoxin and ferredoxin and likely many other electron transfer proteins *in vivo* (7). Electron transfer experiments have been performed to show that PFOR is capable of reducing Fld to the hydroquinone oxidation state. We were curious to see if PFOR and Fld could directly reduce PFL-AE in the absence of PFL, so we ran UV-vis experiments to monitor the absorbance of the iron sulfur cluster for reduction. We observed that PFOR and Fld were incapable of reducing PFL-AE under these conditions. The same experiments were performed with FNR in the presence and absence of Fld and this system was not able to directly reduce PFL-AE either. EPR experiments were carried out to examine the oxidation state of PFL-AE in the presence of FNR with or without Fld. In neither case was there a signal observed for the reduced $[4Fe\text{-}4S]^{+}$ cluster in PFL-AE (only a signal for a $[3Fe\text{-}4S]^{+}$ cluster was observed).

Previous experiments have shown that both the PFOR system with Fld and the FNR system with Fld were capable of activating the PFL system by providing reducing equivalents for PFL-AE (7). Our work clearly shows that the PFOR system is capable of activating the PFL system, however, the FNR system was found to be inert as a source of reducing equivalents for the PFL system. The hydroquinone oxidation state of Fld has been assigned as the active species in PFL activation even though only a very small amount of this species was detected in the previous work (7). In a subsequent study there was no hydroquinone Fld detected from FNR reduction (48). One possible explanation of these results is that recombinant reduced FNR unfolds at *in vivo* temperatures (47).

Electrons are easily transferred from PFOR to Fld, but not to PFL-AE from Fld, and given that PFL-AE is only reduced in the presence of PFL, this data suggests that electron transfer from Fld to PFL-AE must be coupled to PFL activation similar to that of class III anaerobic ribonucleotide reductase (48). Therefore electrons must be transferred from PFOR to Fld and then to the PFL-AE/SAM/PFL complex, resulting in PFL activation.

Our results show that PFL-AE reduction does not occur in the absence of PFL when using PFOR or FNR regardless of the presence of Fld, however, PFL was activated by PFL-AE using PFOR and Fld as electron donors. The PFL-AE crystal structure shows conformational changes upon binding SAM and the 7-*mer* peptide, which may alter the way in which Fld can interact with PFL-AE. Additional radical SAM enzymes typically undergo non-productive SAM cleavage when the cluster is reduced to the $[4Fe\text{-}4S]^{+}$ oxidation state that would be prohibited *in vivo*. Together, these results indicate that electron transfer from Fld to PFL-AE must be coupled to PFL activation. In a previous study we determined that *in vivo*, PFL-AE, SAM, PFL and PFL substrates are almost fully bound in a complex while electron transfer proteins are only partially bound, supporting the idea that Fld reduces PFL-AE when it is bound to SAM, PFL, and pyruvate (Chapter 4). It's not surprising that in our experiments electron transfer from Fld to PFL-AE only occurs under conditions that are similar to *in vivo* conditions where PFL, SAM, pyruvate, and CoA are present.

Footnotes

This work was supported by NIH grant 2R01GM054608

References

1. Wieland, O., H. (1983) *Rev. Physiol. Biochem. Pharmacol.* 96, 123-170

2. Knappe, J., and Sawers, G. (1990) *FEMS Microbiol. Rev.* 75, 383-398

3. Knappe, J., Blaschkowski, H., P., Grobner, P., and Schmitt, T. (1974) *Eur. J. Biochem.* 50, 253-263

4. Knappe, J., Schacht, J., Möckel, W., Höpner, T., Vetter, H., Jr., and Edenharder, R. (1969) *European J. Biochem.* 11, 316-327

5. Charon, M.-H., Volbeda, A., Chabriere, E., Pieulle, L., and Juan, F.-C. (1999) *Curr. Opin. Struc. Biol.* 9, 663-669

6. Henning, U. (1963) *Biochem. Z.* 337, 490-504

7. Blaschkowski, H., P., Neuer, G., Ludwig-Festl, M., and Knappe, J. (1982) *Eur. J. Biochem.* 123, 563-569

8. Brostedt, E., and Nordlund, S. (1991) *Biochem. J.* 279, 155-158

9. Docampo, R., Moreno, S., N., and Mason, R., P. (1987) *J. Biol. Chem.* 262, 12417-12420

10. Meinecke, B., Bertram, J., and Gottschalk, G. (1989) *Arch. Microbiol.* 152, 244-250

11. Pieulle, L., Guigliarelli, B., Asso, M., Dole, F., Bernadac, A., and Hatchikian, E. C. (1995) *Biochim. Biophys. acta* 1250, 49-59

12. Uyeda, K., and Rabinowitz, J., C. (1971) *J. Biol. Chem.* 246, 3111-3119

13. Wahl, R., C., and Orme-Johnson, W., H. (1987) *J. Biol. Chem.* 262, 10489-10496

14. Williams, K., Lowe, P., N., and Leadlay, P., F. (1987) *Biochem. J.* 246, 529-536

15. Garczarek, F., Dong, M., Typke, D., Witkowska, H., E., Hazen, T., C., Nogales, E., Biggin, M., D., and Glaeser, R., M. (2007) *J. Struct. Biol.* 159, 9-18

16. Ikeda, T., Ochiai, T., Morita, S., Nishiyama, A., Yamada, E., Arai, H., Ishii, M., and Igarashi, Y. (2006) *Biochem. Bioph. Res. Co.* 340, 76-82

17. Kerscher, L., and Oesterhelt, D. (1981) *Eur. J. Biochem.* 116, 587-594

18. Plaga, W., Lottspeich, F., and Oesterhelt, D. (1992) *Eur. J. Biochem.* 205, 391-397

19. Blamey, J., M., and Adams, M., W. (1994) *Biochemistry* 33, 1000-1007

20. Blamey, J., M., and Adams, M., W. (1993) *Biochim. Biophys. acta* 1161, 19-27

21. Bock, A.-K., Kunow, J., Glasemacher, J., and Schönheit, P. (1996) *Eur. J. Biochem.* 237, 35-44

22. Huges, N., J., Chalk, P., A., Clayton, C., L., and Kelly, D., J. (1995) *J. Bacteriol.* 177, 3953-3959

23. Kunow, J., Linder, D., and Thauer, R., K. (1995) *Arch. Microbiol.* 163, 21-28

24. Kletzin, A., and Adams, M., W. (1996) *J. Bacteriol.* 178, 248-257

25. Zhang, Q., Iwasaki, T., Wakagi, T., and Oshima, T. (1996) *J. Biochem.* 120, 587-599

26. Chabriere, E., Charon, M.-H., Volbeda, A., Pieulle, L., Hatchikian, E., C., and Fontecilla-Camps, J.-C. (1999) *Nat. Struct. Mol. Biol.* 6, 182-190

27. Chabrière, E., Vernède, X., Guigliarelli, B., Charon, M.-H., Hatchikian, E. C., and Fontecilla-Camps, J., C. (2001) *Science* 294, 2559-2563

28. Cavazza, C., Contreras-Martel, C., Pieula, L., Chabrière, E., Hatchikian, E. C., and Fontecilla-Camps, J., C. (2006) *Structure* 14, 217-224

29. Cammack, R., Kerscher, L., and Oesterhelt, D. (1980) *FEBS Lett.* 118, 271-273

30. Menon, S., and Ragsdale, S., W. (1997) *Biochemistry* 36, 8484-8494

31. Smith, E., T., Blamey, J., M., and Adams, M., W. (1994) *Biochemistry* 33, 1008-1016

32. Moulis, J.-M., Davasse, V., Meyer, J., and Gaillard, J. (1996) *FEBS Lett.* 380, 287-290

33. Bianchi, V., Eliasson, R., Fontecave, M., Mulliez, E., Hoover, D., M., Matthews, R., G., and Reichard, P. (1993) *Biochem. Biophys. Res. Commun.* 197, 792-797

34. Ifuku, O., Koga, N., Haze, S.-i., Kishimoto, J., and Wachi, Y. (1994) *Eur. J. Biochem.* 224, 173-178

35. Hall, D., A., Vander Kooi, C., W., Stasik, C., N., Stevens, S., Y., Zuiderweg, E., R., and Matthews, R., G. (2001) *Proc Natl Acad Sci U S A* 98, 9521-9526

36. Vetter, H., Jr., and Knappe, J. (1971) *H-Z Physiol. Chem.* 352, 433-446

37. Wan, J., T., and Jarrett, J., T. (2002) *Arch. Biochem. Biophys.* 406, 116-126

38. Henshaw, T. F., Cheek, J., and Broderick, J. B. (2000) *J. Am. Chem. Soc.* 122, 8331-8332

39. Nnyepi, M., R., Peng, Y., and Broderick, J., B. (2007) *Arch. Biochem. Biophys.* 459, 1-9

40. Krebs, C., Broderick, W. E., Henshaw, T. F., Broderick, J. B., and Hanh Huynh, B. (2002) *J. Am. Chem. Soc.* 124, 912-913

41. Broderick, J. B., Henshaw, T., F., Cheek, J., Wojtuszewski, K., Smith, S., R., Trojan, M., R., McGhan, R., M., Kopf, A., Kibbey, M., and Broderick, W., E. (2000) *Biochem. Bioph. Res. Co.* 269, 451-456

42. Bradford, M., M. (1976) *Anal. Biochem.* 72, 248-254

43. Beinert, H. (1978) *Methods Enzymol.* 54, 435-445

44. Shepard, E., M., Duffus, B., R., George, S., J., McGlynn, S., E., Challand, M., R., Swanson, K., D., Roach, P., L., Cramer, S., P., Peters, J., W., and Broderick, J. B. (2010) *J. AM. Chem. Soc.* 132, 9247-9249

45. Conradt, H., Hohmann-Berger, M., Hohmann, H.-P., Blaschkowski, H., P., and Knappe, J. (1984) *Arch. Biochem. Biophys.* 228, 133-142

46. Krebs, C., Broderick, W., E., Henshaw, T., F., Broderick, J. B., and Huynh, B. H. (2002) *J. Am. Chem. Soc.* 124, 912-913

47. Jarrett, J., T., and Wan, J., T. (2002) *FEBS Lett.* 529, 237-242

48. Mulliez, E., Padovani, D., Atta, M., Alcouffe, C., and Fontecave, M. (2001) *Biochemistry* 40, 3730-3736

CHAPTER 7

CONCLUSIONS

Fld Folding and Cofactor Binding

Flavodoxins (Fld) are small single domain proteins that are very stable and reversibly fold (1,2). Fld unfolding has been studied in several organisms and has proven to be a great model system for protein folding in the presence and absence of the flavin mononucleotide cofactor (3,4). The effect of the bound cofactor on folding has been studied and it appears that the presence of the cofactor increases the rate of folding and stabilizes an intermediate in the folding process (4).

Cofactor binding appears to change the conformation of the Fld protein so we were very interested to see the effect of cofactor binding on protein-protein interactions involving Fld. Circular dichroism is a powerful way to study changes in secondary structure that are due to small molecule binding. Thermal unfolding experiments with Fld in the presence and absence of the cofactor can provide valuable thermodynamic data that can be used to glean insight into stability and conformational changes due to cofactor binding. Far-UV CD shows that at room temperature, our Fld preparations are well folded in the presence and absence of the FMN cofactor and it appears that cofactor binding does not alter the secondary structure of the protein. At high temperatures, both apo- and holo-Fld exhibit nearly identical far-UV spectra with features at 203 nm, characteristic of unfolded proteins. Both apo and holo-Fld unfold via a three state mechanism involving an intermediate. The ΔH_1 and ΔH_2 for holo-Fld unfolding was

calculated to be 65.2 ± 0.8 kcal/mol and 39.6 ± 1.2 kcal/mol, respectively. The ΔH_1 and ΔH_2 for the apo-protein were calculated to be 45.6 ± 0.8 and 30.8 ± 2.3, respectively, indicating that holo-Fld is much more stable than apo-Fld. Thermal melting points also indicate that holo-Fld is more stable than apo-Fld with T_{m1} and T_{m2} values of 345.9 ± 0.1 K and 352.9 ± 0.2 K, respectively for holo-Fld and 323.7± 0.6 K and 326.3 ± 0.4 K, respectively for apo-Fld. The native Fld and the intermediate are stabilized in the presence of the cofactor. *Escherichia coli* apo and holo-Fld folding is very similar to folding described for *D. desulfuricans* Fld (3).

Isothermal titration calorimetry data of apo-Fld binding the flavin mononucleotide (FMN) cofactor demonstrates that the interaction between the protein and cofactor are very high affinity with an equilibrium constant of ~ 5 nM at 25 °C. This data is in reasonable agreement with previous fluorescence experiments that provided a K_D of 1 nM (5). The interaction between apo-Fld and the FMN cofactor is very favorable with a ΔG ~ -11 kcal/mol and cofactor binding is clearly driven by enthalpy with a ΔH ~ -21.6 ± 0.57 kcal/mol at 25 °C and -31.9 ± 3.3 kcal/mol at 37 °C. There is also a small unfavorable entropy contribution of binding which is most likely due to a loss of conformational freedom of the cofactor and loops involved in cofactor binding similar to what has been seen for *H. pylori* Fld (6). When apo-Fld binds FMN at 37 °C, there is a larger unfavorable entropy contribution that may be a result of apo-Fld being more dynamic at *in vivo* temperatures.

PFL-AE Interactions with Fld and FNR

The protein-protein interactions between Fld with PFL-AE and FNR were investigated to determine what effect changes in Fld conformation resulting from cofactor binding might have on protein-protein interactions. Circular dichroism studies show that when Fld interacts with FNR, the cofactors and aromatic residues are perturbed in a manner that is consistent with binding. Surface plasmon resonance under anaerobic conditions was used to determine the equilibrium constant value of 3.7 ± 1.6 μM between holo-Fld and FNR, which is in nice agreement with the previously determined value of 2.0 ± 1 μM (7). Interestingly, when the binding of apo-Fld with FNR was examined, there was no interaction detected between these two proteins, suggesting that structural changes that occur upon cofactor binding are necessary for protein-protein interactions.

The interaction between holo-Fld and PFL-AE was also investigated using surface plasmon resonance under anaerobic conditions and an equilibrium constant of 23.3 ± 3.8 μM was determined. When the interaction between apo-Fld and PFL-AE was examined under the same conditions, there was no interaction detected between these two proteins. This data is in agreement with the above data between holo-Fld and FNR and together provides very strong evidence that structural changes induced by FMN cofactor binding to apo-Fld are required for protein-protein interactions among different protein partners.

Fld Conformational Changes
Induced by Cofactor Binding

We investigated the conformational changes in Fld induced by cofactor binding that affect thermal stability and protein-protein interactions using limited proteolysis in

the presence and absence of the FMN cofactor. These samples were analyzed using LC-MS and a program called Mascot to identify the peptide fragments in each sample. These fragments were then compared between apo- and holo-Fld to look for differences in the trypsin cleavage patterns that would show the areas of the protein that were involved in conformational changes upon cofactor binding. One unique peptide was found in each sample corresponding to G112-K161 for apo-Fld and S38-R111 for holo-Fld. The peptides were mapped onto the Fld crystal structure and we used information from the literature to determine the regions involved in cofactor binding and protein-protein interactions. Not surprisingly, our limited proteolysis data showed that the regions that experienced conformational changes were also involved in cofactor binding and protein-protein interactions. This valuable data provides a more in depth understanding of the importance of Fld cofactor binding and explains why it would have such a large affect on protein-protein interactions.

PFL-AE and Fld Docking

A model for a PFL-AE/Fld complex was generated using docking studies with ZDOCK software to make a rigid-body docking model based on bioinformatic data on PFL-AE and previous studies on Fld. This structure shows that PFL-AE has two binding sites for protein-protein interactions, one for PFL binding, and the other one presumably for Fld binding. Therefore it is possible that Fld may only reduce PFL-AE after it is bound to SAM and PFL. The Fld binding site on PFL-AE has been described to be composed mainly of electrostatic and hydrophobic residues. Aromatic amino acids line the pathway between the FMN cofactor in Fld (W57) and the [4Fe-4S] cluster in PFL-AE

(W42), and may be involved in long range electron transfer between the two cofactors. The distance between the FMN cofactor in Fld and the [4Fe-4S] cluster in PFL-AE was determined to be 10.7 Å in the docking model, suggesting an outer sphere electron transfer mechanism between cofactors.

PFL-AE Interactions with
PFL and the 12-*mer* Peptide

The protein-protein interactions between PFL-AE and PFL were higher affinity than the interactions between PFL-AE with Fld or FNR, which allowed for the calculation of rates of association and dissociation. The rate of association for PFL-AE and PFL was determined to be $1028.4 \pm 33.9\ M^{-1}s^{-1}$, indicating that binding is a very slow process and that the rate is limited by large conformational changes. The dissociation rate for the interaction was $1.173 \times 10^{-3} \pm 0.165\ s^{-1}$, suggesting that the complex is reasonably stable. The equilibrium constant was determined to be 1.14 ± 0.2 μM which is in close agreement with a previously estimated K_D in the low micromolar range (~ 1-10 μM) (8).

The active site of PFL has been modeled in the crystal structure of PFL-AE using a 7-mer peptide (9). The 7-*mer* peptide and a 12-*mer* peptide were used in PFL-AE activity studies and were determined to be less active than full length PFL (10). Not surprisingly, the interaction between the 12-*mer* peptide and PFL-AE is much lower affinity than with intact PFL. The equilibrium constant was determined to be 24.6 ± 16 μM using surface plasmon resonance under anaerobic conditions. The decrease in affinity when compared to intact PFL is most likely due to important contacts between residues in PFL-AE and PFL that are absent in the truncated peptide.

SAM Binding PFL-AE and
the PFL-AE/PFL Complex

Given that PFL-AE binds PFL in the absence of SAM or other PFL substrates with a K_D of 1.14 μM, we were able to design circular dichroism experiments where the PFL binding site on PFL-AE was essentially fully occupied with PFL. We then titrated in SAM from a concentrated stock and monitored changes in the visible region of circular dichroism and determined a K_D of 5.6 ± 1.7 μM for the PFL-AE/PFL complex. When the same experiment was performed in the absence of PFL, the K_D was the same within error with a K_D of 7.6 ± 1.9 μM. Our data clearly shows that PFL binding to PFL-AE has no affect on SAM binding. Calculations of *in vivo* concentrations of PFL-AE, PFL, and SAM have been performed and given the above equilibrium constants our data suggests that PFL-AE, PFL and SAM are fully bound *in vivo* and poised for PFL activation.

The Effect of Substrates on PFL Activation

Our data demonstrates that PFL-AE binds PFL in the absence of SAM or other PFL substrates such as pyruvate, oxamate, or CoA. It stands to reason that if these two proteins interact in the absence of substrates then the active site of PFL and PFL-AE would be in proper alignment for activation of PFL by PFL-AE. Previous experiments have shown that to achieve PFL activation, pyruvate or oxamate had to be present in activity assays (11). We were interested in understanding more about the requirements for PFL activation and specifically the role of PFL substrates in activation.

EPR is a powerful technique for determining oxidation states of metal centers on proteins or protein based radicals and is perfectly suited for PFL activation experiments. The experiments were designed so that PFL-AE was photoreduced for different amounts

of time before being added to PFL in the presence of SAM with PFL and PFL-AE in a 1:1 ratio. A standard was prepared for PFL-AE and the $[4Fe\text{-}4S]^{1+}$ cluster was quantified then compared to glycyl radical formation on PFL. In experimental samples, PFL-AE was almost entirely converted to the $[4Fe\text{-}4S]^{1+}$ oxidation state after one hour of photoreduction and was completely converted to the $[4Fe\text{-}4S]^{2+}$ oxidation state after being mixed with PFL and SAM. Stoichiometric conversion of the $[4Fe\text{-}4S]^{1+}$ cluster to glycyl radical on PFL was observed in the presence of either pyruvate or oxamate. PFL activation in the presence of CoA or no substrate resulted in sub-stoichiometric conversion of reduced cluster to the PFL glycyl radical. Although PFL substrates are not required for PFL activation as once previously thought, pyruvate and oxamate do act as effector molecules that are required for efficient PFL activation. Given that in each experiment the PFL-AE is oxidized in the presence of PFL and SAM, it appears that PFL-AE activates PFL in the absence of substrates, but pyruvate and oxamate are required for efficient PFL activation.

In Vivo Concentrations for the PFL System

In vivo concentrations of the enzymes in the PFL system were calculated based on previous estimations of the number of polypeptides per cell in *E. coli*. Advances in microscopy have led to accurate measurements of cell volume and combined with the above data, this information can be used to calculate estimated *in vivo* concentrations for all the proteins in the PFL system. Under anaerobic conditions, PFL was determined to be 14.5 μM, PFL-AE was 830 nM, and Fld was determined to be 2.1 μM. FNR was calculated to be 1.7 μM and the PFOR homodimer was determined to be 470 nM *in vivo*.

SAM concentrations have been reported in the range of 50 - 400 μM in *E. coli* with pyruvate and CoA concentrations of 7.5 ± 0.5 mM and 9-100 μM, respectively. Under these conditions, PFL-AE would be essentially bound with SAM and PFL with pyruvate and possibly CoA bound to PFL. Fld has been estimated to be approximately 30 % bound to PFL-AE *in vivo*. Given that PFL-AE would be fully bound with PFL and SAM and that PFL-AE contains two binding sites, one for PFL and the other for Fld, it is possible that Fld only reduces PFL-AE when electron transfer is coupled to PFL activation.

Cation Effects on the [4Fe-4S] Cluster in PFL-AE

The crystal structure of PFL-AE clearly shows a sodium cation bound in very close proximity to the [4Fe-4S] cluster and *S*-adenosylmethionine (SAM) (9). SAM is sandwiched between the cation and the [4Fe-4S] cluster and although the significance of this cation is unknown, it is most likely an important feature in SAM cleavage and PFL activation given its location. Studies on the radical SAM enzyme LAM show that SAM and substrate binding near the [4Fe-4S] cluster significantly perturb the redox potentials of SAM and the cluster (12,13). The close proximity of the sodium cation to the [4Fe-4S] cluster in PFL-AE may modulate the reduction potential of the iron-sulfur cluster and may increase the likelihood of electron transfer from the iron-sulfur cluster to SAM.

To elucidate the importance of the cation in PFL activation we decided to examine the effect that the cation has on PFL-AE using EPR spectroscopy and activity assays. Choline chloride is a very large cation that would most likely be incapable of binding in the cation binding pocket and interacting with the iron-sulfur cluster. Experiments have been performed with Fld to interpret the effect of cation binding with

respect to structural changes using choline to maintain ionic strength (14). In our experiments we have performed UV-vis PFL activity assays in choline chloride to maintain ionic strength and to be able to determine the effect of cation binding. Samples prepared in choline chloride alone were determined to be inactive. When PFL-AE samples prepared in choline chloride were supplemented with NaCl at the same ionic strength, the enzyme was determined to be active. Our data shows that PFL-AE activity is dependent on the sodium cation concentration.

The EPR spectrum for PFL-AE in sodium chloride has been previously characterized and our samples in 200 mM NaCl are identical to what has been previously described (15). Samples that contained 100 mM choline chloride/100 mM NaCl were identical to samples prepared in sodium alone, indicating that choline does not perturb that PFL-AE EPR spectrum. When PFL-AE samples were prepared in 200 mM choline chloride, a drastically different EPR spectrum was observed, suggesting that this spectrum corresponds to the [4Fe-4S] cluster with no contribution from the monovalent cation. The large perturbation of the EPR spectrum of PFL-AE caused by sodium binding clearly demonstrates that cation binding alters the electronic properties of the [4Fe-4S] cluster. When PFL-AE was examined in the presence of SAM by EPR in 200 mM NaCl, the EPR spectrum was identical to what has been previously published for this enzyme. Samples that were prepared with PFL-AE and SAM in 100 mM choline/100 mM NaCl were identical to samples of PFL-AE plus SAM in 200 mM NaCl. However, when samples were prepared that contained PFL-AE and SAM in 200 mM choline, the signal

was drastically different than the spectrum in the presence of sodium. This signal was also different than the signal for PFL-AE in 200 mM choline.

Overall, our cation binding data suggests that sodium interacts with the [4Fe-4S] cluster and SAM, but choline chloride is too large to fit into the monovalent cation binding pocket. PFL activation assays show that sodium cation binding is important for PFL-AE activity. EPR experiments show that cation binding alters the electronic structure of the [4Fe-4S] cluster in PFL-AE as well as in the PFL-AE/SAM complex. The close proximity of the bound sodium cation to SAM and the [4Fe-4S] cluster as well as dose dependent stimulation of PFL-AE activity led to the hypothesis that cation binding may perturb the reduction potential of PFL-AE making SAM cleavage more favorable. When the reduction potential of PFL-AE was measured in 200 mM NaCl at pH 7.5, it was calculated to be -265 mV. When this study was performed in 100 mM NaCl/100 mM choline chloride, the reduction potential was determined to be -248 mV. When PFL-AE was prepared in 200 mM choline chloride, the reduction potential increased to -234 mV. This electrochemistry study clearly shows that sodium cation binding perturbs the reduction potential of the [4Fe-4S] cluster in PFL-AE making it more negative so that SAM cleavage and PFL activation are possible. Therefore, decreased PFL activity in the absence of sodium is probably the result of altered reduction potentials of the [4Fe-4S] cluster in PFL-AE and possibly SAM, making SAM cleavage less favorable.

PFOR is the Electron Donor for the PFL system

Early work into the dissimilation of pyruvate into acetyl-CoA implicated both pyruvate:flavodoxin oxidoreductase and pyruvate formate-lyase as the enzymes that were

responsible for these reactions (16). Subsequent work using a partially purified PFOR showed that this enzyme was capable of supplying the required electrons for PFL activation, presumably by using Fld to reduce PFL-AE (17). We attempted to clone *E. coli* PFOR and overexpress it and we also performed some initial characterization, however, the enzyme was impure, which limited the potential of our enzyme preparations. PFOR from *E. coli* is composed of a single gene 3.5 kb in size with a corresponding protein containing 1174 amino acids. PFOR from other similar mesophilic bacteria have been shown to be homodimers with molecular weights around 240 kDa (17-24). Previous AUC experiments calculate a molecular weight of 200 ± 15 kDa for PFOR, suggesting that the enzyme is a homodimer with a molecular weight of 257.5 kDa (17).

Sequence alignments were performed on PFOR from *E. coli* and other mesophilic bacteria such as *D. africanus, K. pneumonia, T. vaginalis, P. furiosus, H. halobium* to gain understanding of important residues involved in [4Fe-4S] cluster and TPP cofactor binding. Only residues with 100 % sequence conservation were considered in this study and they were compared to residues in the crystal structure of the enzyme from *D. africanus* to determine iron sulfur cluster and cofactor binding residues. Residues C688, C691, C694, and C698 bind the distal cluster, residues C744, C747, C750, and C754 bind the middle cluster and residues C818, C821, C846, and C1070 bind the proximal cluster. The cofactor binding region containing the TPP binding motif included residues G961, D962, and G963.

The as isolated enzyme was found to be inactive during Fld and PFL activity assays and as a result it was necessary to chemically reconstitute PFOR to achieve activity. Iron assays determined that the iron number for the as isolated enzyme was 1.24 ± 0.2 per subunit and after reconstitution PFOR exhibited iron numbers of 15.9 ± 0.7 per subunit and UV-vis studies showed a dramatic increase in absorbance around 426 nm typical of LMCT bands for bound iron sulfur clusters. Considering the iron number in as isolated PFOR, the lack of activity was not surprising since it is thought that electrons are transferred from the TPP cofactor through all three iron sulfur clusters before they can be transferred to acceptor proteins. PFOR or FNR were both inert at reducing PFL-AE regardless of the presence of Fld, indicating that Fld can only reduce PFL-AE when electron transfer is coupled to PFL activation.

References

1. Van Mierlo, C., P., Van Dongen, W., M., Vergeldt, F., Van Berkel, W., J., and Steensma, E. (1998) *Protein Sci.* 7, 2331-2344

2. Genzor, C., G., Beldarraín, A., Gómez-Moreno, C., López-Lacomba, J., L., cortijo, M., and Sancho, J. (1996) *Protein Sci.* 5, 1376-1388

3. Muralidhara, B. K., and Wittung-Stafshede, P. (2004) *Biochemistry* 43, 12855-12864

4. Apiyo, D., and Wittung-Stafshede, P. (2002) *Protein Sci.* 11, 1129-1135

5. Hoover, D., M., and Ludwig, M., L. (1997) *Protein Sci.* 6, 2525-2537

6. Credmades, N., Velazquez-Campoy, A., Freire, E., and Sancho, J. (2008) *Biochemistry* 47, 627-639

7. Wan, J., T., and Jarrett, J., T. (2002) *Arch. Biochem. Biophys.* 406, 116-126

8. Peng, Y., Veneziano, S. E., Gillispie, G. D., and Broderick, J. B. (2010) *J. Biol. Chem.* 285, 27224-27231

9. Vey, J. L., Yang, J., Li, M., Broderick, W. E., Broderick, J. B., and Drennan, C. L. (2008) *Proc. Natl. Acad. Sci. U.S.A.* 105, 16137-16141

10. Frey, M., Rothe, M., Volker Wagner, A. F., and Knappe, J. (1994) *J. Biol. Chem.* 269, 12432-12437

11. Conradt, H., Hohmann-Berger, M., Hohmann, H.-P., Blaschkowski, H., P., and Knappe, J. (1984) *Arch. Biochem. Biophys.* 228, 133-142

12. Hinckley, G., T., and Frey, P., A. (2006) *Biochemistry* 45, 3219-3225

13. Wang, S., C., and Frey, P., A. (2007) *Biochemistry* 46, 12889-12895

14. Maldonado, S., Irún, M., P., Campos, L., A., Rubio, J., A., Luquita, A., Lostao, A., Wang, R., Garcia-Moreno, B., E., and Sancho, J. (2002) *Protein Sci.* 11, 1260-1273

15. Henshaw, T. F., Cheek, J., and Broderick, J. B. (2000) *J. Am. Chem. Soc.* 122, 8331-8332

16. Knappe, J., Bohnert, E., and Brümmer, W. (1965) *Biochim. Biophys. acta* 107, 603-608

17. Blaschkowski, H., P., Neuer, G., Ludwig-Festl, M., and Knappe, J. (1982) *Eur. J. Biochem.* 123, 563-569

18. Brostedt, E., and Nordlund, S. (1991) *Biochem. J.* 279, 155-158

19. Docampo, R., Moreno, S., N., and Mason, R., P. (1987) *J. Biol. Chem.* 262, 12417-12420

20. Meinecke, B., Bertram, J., and Gottschalk, G. (1989) *Arch. Microbiol.* 152, 244-250

21. Pieulle, L., Guigliarelli, B., Asso, M., Dole, F., Bernadac, A., and Hatchikian, E. C. (1995) *Biochim. Biophys. acta* 1250, 49-59

22. Uyeda, K., and Rabinowitz, J., C. (1971) *J. Biol. Chem.* 246, 3111-3119

23. Wahl, R., C., and Orme-Johnson, W., H. (1987) *J. Biol. Chem.* 262, 10489-10496

24. Williams, K., Lowe, P., N., and Leadlay, P., F. (1987) *Biochem. J.* 246, 529-536

CHAPTER 8

FUTURE WORK

Fld as an Electron Donor for PFL-AE

The current evidence for Fld interaction with PFL-AE is based on UV-Vis activity assays and binding experiments carried out using surface plasmon resonance. Sequence alignments between different organisms that contain PFL-AE show a patch of 100% conserved residues that have been used to generate a putative complex of PFL-AE and Fld. Now that we have an idea of which residues are involved in the interaction, we can perform site directed mutagenesis in conjunction with surface plasmon resonance studies to determine the importance of each residue in complex formation. Additionally these mutants could be studied using activity assays to determine what effects these mutations have on PFL activity. Aromatic residues such as W42 in PFL-AE could be mutated to see if any of the aromatic residues at the interface between PFL-AE and Fld are involved in the electron transfer pathway.

Fld and PFL-AE Co-Crystal

PFL-AE and Fld could be co-crystallized in the presence and absence of SAM and the 7-mer peptide PFL active site analogue to get a clear picture of which residues are involved in the binding site interface and to provide insight as to how the electron is transferred from Fld to PFL-AE. This data would also show how PFL-AE undergoes conformational changes upon binding SAM and the 7-*mer* peptide (as was seen in the crystal structure) and how those changes in PFL-AE alter Fld binding and cofactor

distances between the two proteins. The structure would show the important residues that are involved in the electron transfer pathway and provide insight for the design of electron transfer studies.

Further Characterization of *E. coli* PFOR

Previous electrochemistry experiments on PFOR have measured the reduction potentials as -390 mV, -515 mV, and -540 mV, making it a very powerful electron donor (1). PFOR was capable of activating the PFL system presumably by reducing PFL-AE where FNR with Fld was found to be inert. Electrochemistry experiments have never been performed on *E. coli* PFOR and given the potential widespread use of PFOR in *E. coli* for electron donor and acceptor reactions (including for PFL-AE reduction) this enzyme is very important in anaerobic metabolism. Electrochemistry experiments could be performed using reconstituted PFOR and compare that data to as isolated PFOR to see how iron number and cluster composition effect redox chemistry in PFOR. Experiments where $MgCl_2$ is supplemented as well as separate experiments with $MgCl_2$ plus the TPP cofactor could provide insight into structural changes or cofactor influence on the oxidization potential of the enzyme.

Now that estimated *in vivo* concentrations are available for the PFL system experiments can be performed under those conditions to measure the rate of PFL activation using absorbance changes at 365 nm, corresponding to the formation of the glycyl radical. PFOR and Fld could be used as electron donors to reduce PFL-AE and activate PFL with all proteins and small molecules at estimated *in vivo* concentrations. Variables such as temperature, pH, ionic strength, crowding agents, and proteins like

BSA used to simulate *in vivo* conditions could be varied to determine conditions for the fastest PFL activation and compare them to predicted *in vivo* conditions to get a more complete understanding of PFL activation. Electron donors found in *E. coli* such as WrbA, FldB, MioC, and ferredoxin could be cloned and tested under simulated *in vivo* conditions to determine if any of these proteins are capable of supporting the PFL system.

SAM Binding and Structural Changes in PFL-AE

Preliminary work on PFL-AE has shown that the enzyme is cleaved differently and at different rates by trypsin in the presence of SAM when compared to the as isolated enzyme. As purified PFL-AE is cleaved by trypsin much more rapidly than when in the presence of SAM, indicating a structural change in the enzyme and most likely an increase in stability upon SAM binding. Several other small molecules containing an adenosine moiety have been shown to bind PFL-AE, such as ADP, AMP, MTA, and 5'-deoxyadenosine (2). Preliminary data suggest that these molecules also have an affect on PFL-AE cleavage rates and therefore likely produce a conformational change in the protein upon binding. It would be very interesting to show limited proteolysis of PFL-AE in the presence and absence of these small molecules on SDS-PAGE to demonstrate the differences in rates and stability of the enzyme with a ligand bound. This data could be followed up using LC-MS to determine which areas of PFL-AE are being digested in each case and rates could be determined for trypsin digestion in the presence of each small molecule. Additionally these cleaved peptides could be mapped back onto the PFL-AE crystal structure to elucidate these conformational changes to compare and contrast differences between small molecules.

Further Characterization of PFL Activation by PFL-AE

My work on PFL activation by PFL-AE demonstrates that for stoichiometric conversion from the reduced cluster in PFL-AE to the glycyl radical in PFL to occur, pyruvate or oxamate are required. Since it appears that these small molecule substrates play a role in the mechanism of activation, it is likely that PFL would be activated at different rates in the presence or absence of different substrates/analogues. Stopped flow experiments could be performed with photoreduced PFL-AE in a 1:1 ratio with PFL with SAM and the rate of activation could be calculated based on the absorbance changes of the iron-sulfur cluster. The rate of SAM cleavage could be calculated using LC-MS and compared with cluster oxidation rates to obtain accurate rates of PFL activation in the presence of different small molecule substrates. This data would shed new light on the mechanism of PFL activation.

Further Characterization of PFL-AE Reduction Potentials

Our preliminary work on characterizing the reduction potentials of PFL-AE in the presence of 200 mM NaCl, 100 mM NaCl/100 mM choline chloride, or 200 mM choline chloride has shown that the reduction potentials of the [4Fe-4S] cluster are perturbed by this interaction. This data needs to be repeated to obtain more accurate values for the as purified enzyme. Additional experiments should also be performed in the presence of SAM and the 7-*mer* peptide to understand the energy profile of PFL activation by PFL-AE and the affect of each of these components in the presence and absence of the bound monovalent cation. DFT studies could also be performed to determine the effects of the

cation on the [4Fe-4S] cluster and SAM-sulfonium cleavage in the presence of the 7-*mer* peptide during PFL activation by PFL-AE.

References

1. Pieulle, L., Guigliarelli, B., Asso, M., Dole, F., Bernadac, A., and Hatchikian, E. C. (1995) *Biochim. Biophys. acta* 1250, 49-59

2. Yang, J., Naik, S., G., Ortillo, D., O., Garcia-Serres, R., Li, M., Broderick, W., E., Hanh Huynh, B., and Broderick, J., B. (2009) *Biochemistry* 48, 9234-9241

CUMULATIVE REFERENCES

Aasa, R., and Vänngård, T. (1975) *J. Magn. Res.* 19, 308-315

Apiyo, D., and Wittung-Stafshede, P. (2002) *Protein Sci.* 11, 1129-1135

Ayala-Castro, C., Saini, A., and Outten, F. W. (2008) *Microbiol. Mol. Biol. Rev.* 72, 110-125

Becker, A., Fritz-Wolf, K., Kabsch, W., Knappe, J., Schultz, S., and Wagner, V., A. (1999) *Nat. Struct. Biol.* 6, 969-975

Becker, A., and Kabsch, W. (2002) *J. Biol. Chem.* 277, 40036-40042

Beinert, H. (1978) *Methods Enzymol.* 54, 435-445

Beinert, H. (2000) *J. Biol. Inorg. Chem.* 5, 2-15

Bennett, B., D., Kimball, E., H., Gao, M., Osterhout, R., Van Dien, S., J., and Rabinowitz, J., D. (2009) *Nat. Chem. Biol.* 5, 593-599

Bianchi, V., Eliasson, R., Fontecave, M., Mulliez, E., Hoover, D., M., Matthews, R., G., and Reichard, P. (1993) *Biochem. Biophys. Res. Commun.* 197, 792-797

Blamey, J., M., and Adams, M., W. (1993) *Biochim. Biophys. acta* 1161, 19-27

Blamey, J., M., and Adams, M., W. (1994) *Biochemistry* 33, 1000-1007

Blaschkowski, H., P., Neuer, G., Ludwig-Festl, M., and Knappe, J. (1982) *Eur. J. Biochem.* 123, 563-569

Bock, A.-K., Kunow, J., Glasemacher, J., and Schönheit, P. (1996) *Eur. J. Biochem.* 237, 35-44

Bogan, A., A., and Thorn, K., S. (1998) *J. Mol. Biol.* 280, 1-9

Bradford, M., M. (1976) *Anal. Biochem.* 72, 248-254

Bradley, L., H., and Swenson, R., P. (1999) *Biochemistry* 38, 12377-12386

Bradley, L., H., and Swenson, R., P. (2001) *Biochemistry* 40, 8686-8695

Broach, R., B., and Jarrett, J., T. (2006) *Biochemistry* 45, 14166-14174

Broderick, J. B., Duderstadt, R. E., Fernandez, D. C., Wojtuszewski, K., Henshaw, T. F., and Johnson, M. K. (1997) *J. AM. Chem. Soc.* 119, 7396-7397

Broderick, J., B., Henshaw, T., F., Cheek, J., Wojtuszewski, K., Smith, S., R., Trojan, M., R., McGhan, R., M., Kopf, A., Kibbey, M., and Broderick, W., E. (2000) *Biochem. Biophys. Res. Commun.* 269, 451-456

Brostedt, E., and Nordlund, S. (1991) *Biochem. J.* 279, 155-158

Burnett, R., M., Darling, G., D., Kendall, D., S., LeQuesne, M., E., Mayhew, S., G., Smith, W., W., and Ludwig, M., L. (1974) *J Biol Chem* 249, 4383-4392

Busby, R., W., Schelvis, J., P., Yu, D., S., Babcock, G., T., and Marletta, M., A. (1999) *J. AM. CHEM. SOC.* 121, 4706-4707

Cammack, R., Kerscher, L., and Oesterhelt, D. (1980) *FEBS Lett.* 118, 271-273

Campos, L., and Sancho, J. (2006) *Proteins* 63, 581-594

Cavazza, C., Contreras-Martel, C., Pieula, L., Chabrière, E., Hatchikian, E. C., and Fontecilla-Camps, J., C. (2006) *Structure* 14, 217-224
Celej, M., S., Montich, G., G., and Fidelio, G., D. (2003) *Protein Science* 12, 1496-1506

Chabriere, E., Charon, M.-H., Volbeda, A., Pieulle, L., Hatchikian, E., C., and Fontecilla-Camps, J.-C. (1999) *Nat. Struct. Mol. Biol.* 6, 182-190

Chabrière, E., Vernède, X., Guigliarelli, B., Charon, M.-H., Hatchikian, E. C., and Fontecilla-Camps, J., C. (2001) *Science* 294, 2559-2563

Chang, F., C., and Swenson, R., P. (1997) *Biochemistry* 36, 9013-9021

Chang, F., C., and Swenson, R., P. (1999) *Biochemistry* 38, 7168-7176

Charon, M.-H., Volbeda, A., Chabriere, E., Pieulle, L., and Juan, F.-C. (1999) *Curr. Opin. Struc. Biol.* 9, 663-669

Chase, T., Jr., and Rabinowitz, J., C. (1968) *J. Bacteriol.* 96, 1065-1078

Cheek, J., and Broderick, J. (2002) *J. Am. Chem. Soc.* 124, 2860-2861

Chen, L., Jiang, Z., G., Khan, A., A., Chishti, A., H., and McKnight, C. J. (2009) *Protein Sci.* 18, 629-636

Chen, R., Li, L., and Weng, Z. (2003) *Proteins* 52, 80-87
Chirpich, T. P., Zappia, V., Costilow, R. N., and Barker, H. A. (1970) *J. Biol. Chem.* 245, 1778-1789

Colichman, E., L., and Love, D., L. (1952) *J. Org. Chem.* 18, 40-46

Conradt, H., Hohmann-Berger, M., Hohmann, H.-P., Blaschkowski, H., P., and Knappe, J. (1984) *Arch. Biochem. Biophys.* 228, 133-142

Credmades, N., Velazquez-Campoy, A., Freire, E., and Sancho, J. (2008) *Biochemistry* 47, 627-639

Cremades, N., and Sancho, J. (2008) *Biophys. J.* 95, 1913-1927
Challand, M., R., Driesener, R., C. , and Roach, P. (2011) *Nat. Prod. Rep.* 28, 1696-1721

D'Anna, J., A., and Tollin, G. (1972) *Biochemistry* 11, 1073-1080

De La Cruz, E., M., and Ostap, M., E. (2009) *Method. Enzymol.* 455, 157-192

Docampo, R., Moreno, S., N., and Mason, R., P. (1987) *J. Biol. Chem.* 262, 12417-12420

Drennan, C., L., and Peters, J., W. (2003) *Curr. Opin. Struct. Biol.* 13, 220-226

Driesener, R., C., Challand, M., R., McGlynn, S., E., Shepard, E., M., Boyd, E., S., Broderick, J., B., Peters, J., W. , and Roach, P., L. (2010) *Angew. Chem., Int. Ed. Engl.* 49, 1687-1690

Eliasson, R., Fontecave, M., Jörnvall, H., Krook, M., and Pontis, E. (1990) *Proc. Natl. Acad. Sci. USA* 87, 3314-3318

Epand, R., F., Epand, R., M., and Jung, C., Y. (2001) *Protein Sci* 10, 1363-1369

Englard, S., and Seifter, S. (1990) *Method. Enzymol.* 182, 291

Frey, M., Rothe, M., Volker Wagner, A. F., and Knappe, J. (1994) *J. Biol. Chem.* 269, 12432-12437

Fukuyama, K., Matsubara, H., and Rodgers, L., J. (1992) *J. Mol. Biol.* 225, 775-789

Garczarek, F., Dong, M., Typke, D., Witkowska, H., E., Hazen, T., C., Nogales, E., Biggin, M., D., and Glaeser, R., M. (2007) *J. Struct. Biol.* 159, 9-18

Genzor, C., G., Beldarraín, A., Gómez-Moreno, C., López-Lacomba, J., L., cortijo, M., and Sancho, J. (1996) *Protein Sci.* 5, 1376-1388

Genzor, C., G., Perales-Alcón, A., Sancho, J., and Romero, A. (1996) *Nat. Struct. Biol.* 3, 329-332

Greenfield, N., J. (2006) *Nat. Protoc.* 1, 2876-2890

Hall, D., A., Jordan-Starck, T., C., Loo, R., O., Ludwig, M., L., and Matthews, R., G. (2000) *Biochemistry* 39, 10711-10719

Hall, D., A., Vander Kooi, C., W., Stasik, C., N., Stevens, S., Y., Zuiderweg, E., R., and Matthews, R., G. (2001) *Proc Natl Acad Sci U S A* 98, 9521-9526

Halliday, N. M., Hardie, K. R., Williams, P., Winzer, K., and Barrett, D. A. (2010) *Anal. Biochem.* 403, 20-29

Hänzelmann, P., and Schindelin, H. (2006) *Proc. Natl. Acad. Sci. USA* 103, 6829-6834

Henning, U. (1963) *Biochem. Z.* 337, 490-504

Henshaw, T. F., Cheek, J., and Broderick, J. B. (2000) *J. Am. Chem. Soc.* 122, 8331-8332

Hinckley, G., T., and Frey, P., A. (2006) *Biochemistry* 45, 3219-3225

Hoover, D., M., Drennan, C., L., Metzger, A., L., Osborne, C., Weber, C., H., Pattridge, K., A., and Ludwig, M., L. (1999) *J. Mol. Biol.* 294, 725-743

Hoover, D., M., Jarrett, J., T., Sands, R., H., Dunham, W., R., Ludwig, M., L., and Matthews, R., G. (1997) *Biochemisty* 36, 127-138

Hoover, D., M., and Ludwig, M., L. (1997) *Protein Sci.* 6, 2525-2537

Huges, N., J., Chalk, P., A., Clayton, C., L., and Kelly, D., J. (1995) *J. Bacteriol.* 177, 3953-3959

Ifuku, O., Koga, N., Haze, S.-i., Kishimoto, J., and Wachi, Y. (1994) *Eur. J. Biochem.* 224, 173-178

Ikeda, T., Ochiai, T., Morita, S., Nishiyama, A., Yamada, E., Arai, H., Ishii, M., and Igarashi, Y. (2006) *Biochem. Bioph. Res. Co.* 340, 76-82
Irún, M., P., Garcia-Mira, M., M., Sanchez-Ruiz, J., M., and Sanch, J. (2001) *J. Mol. Biol.* 306, 877-888
Jackowski, S., and Rock, C., O. (1981) *J. Bacteriol.* 148, 926-932

Jarrett, J., T., and Wan, J., T. (2002) *FEBS Lett.* 529, 237-242

Johnson, D., C., Dean, D., R., Smith, A., D. , and Johnson, M., K. (2005) *Annu. Rev. Biochem.* 74, 247-281

Jung, Y.-S., Roberts, V., A., Stout, D., C., and Burgess, B., K. (1999) *J. Biol. Chem.* 274, 2978-2987

Kasim, M., and Swenson, R., P. (2001) *Biochemistry* 40, 13548-13555

Kerscher, L., and Oesterhelt, D. (1981) *Eur. J. Biochem.* 116, 587-594

Kletzin, A., and Adams, M., W. (1996) *J. Bacteriol.* 178, 248-257

Knappe, J., Blaschkowski, H. P., and Edenharder, R. (1972) *Enzyme-dependent activation of pyruvate formate-lyase of Escherichia coli*, Springer, Berlin Heidelberg New York

Knappe, J., Blaschkowski, H., P., Grobner, P., and Schmitt, T. (1974) *Eur. J. Biochem.* 50, 253-263

Knappe, J., and Blaschkowski, H., P. (1975) *Methods Enzymol.* 41, 508-518

Knappe, J., and Blaschkowski, H., P. (1975) *Pyruvate Formate-Lyase from Escherichia coli and its Activation System*, Academic Press Inc., New York

Knappe, J., Bohnert, E., and Brümmer, W. (1965) *Biochim. Biophys. acta* 107, 603-608
Knappe, J., Neugebauer, F. A., Blaschkowski, H., P., and Gänzler, M. (1984) *Proc. Natl. Acad. Sci. U.S.A.* 81, 1332-1335

Knappe, J., and Sawers, G. (1990) *FEMS Microbiol. Rev.* 75, 383-398

Knappe, J., Schacht, J., Möckel, W., Höpner, T., Vetter, H., Jr., and Edenharder, R. (1969) *European J. Biochem.* 11, 316-327

Krebs, C., Broderick, W., E., Henshaw, T., F., Broderick, J. B., and Huynh, B. H. (2002) *J. Am. Chem. Soc.* 124, 912-913

Kuchenreuther, J., M., George, S., J., Grady-Smith, C., S., Cramer, S., P., and Swartz, J., R. (2011) *PLoS ONE* 6, e20346

Kuchenreuther, J., M., Stapleton, J., A., and Swartz, J., R. (2009) *PLoS ONE* 4, e7565

Kulzer, R., Pils, T., Kappl, R., Huttermann, J., and Knappe, J. (1998) *J. Biol. Chem.* 273, 4897-4903

Kunow, J., Linder, D., and Thauer, R., K. (1995) *Arch. Microbiol.* 163, 21-28

Lambeth, D., J., Seybert, D., W., and Kamin, H. (1980) *J. Biol. Chem.* 255, 4667-4672

Laudenbach, D. E., Straus, N. A., Pattridge, K. A., and Ludwig, M. L. (1987) Flavins and Flavoproteins. in *Proceedings of the Ninth International Symposium on Flavins and Flavoproteins* (Edmondson, D. E., and McCormick, D. B. eds.), W. de Gruyter, Berlin, Atlanta, Georgia, USA

Leckner, J., Wittung, P., Bonander, N., Karlsson, B. G., and Malmstrom, B., G. (1997) *J. Biol. Inorg. Chem.* 2, 368-371

Lees, N., S., Chen, D., Walsby, C., J., Behshad, E., Frey, P., A. , and Hoffman, B., M. (2006) *J. Am. Chem. Soc.* 128, 10145-10154

Loewen, P., C. (1978) *Can. J. Biochem.* 56, 753-759

López-Llano, J., Maldonado, S., Bueno, M., Lostao, A., Ángeles-Jiménez, M., Lillo, M. P., and Sancho, J. (2004) *Journal of Biological Chemistry* 279, 47177-47183

Lostao, A., Gomez-Moreno, C., Mayhew, S., G., and Sancho, J. (1997) *Biochemistry* 36, 14334-14344

Ludwig, M., L., Pattridge, K., A., Metzger, A., L., and Dixon, M., M. (1997) *Biochemistry* 36, 1259-1280

Luo, Y., Kay, M., S., and Baldwin, R., L. (1997) *Nature Struct. Biol.* 4, 925-930

Luschinsky, C. L., Dunham, W. R., Osborne, C., Pattridge, K. A., and Ludwig, M. L. (July 15-20, 1990) Flavins and flavoproteins. in *Proceedings of the Tenth International Symposium* (Curti, B., Ronchi, S., and Zanetti, G. eds.), W. de Gruyter, Berlin, New York, Como, Italy

Magnusson, O., T., Reed, G., H. , and Frey, P., A. (1999) *J. Am. Chem. Soc.* 121, 9764-9765

Maldonado, S., Irún, M., P., Campos, L., A., Rubio, J., A., Luquita, A., Lostao, A., Wang, R., Garcia-Moreno, B., E., and Sancho, J. (2002) *Protein Sci.* 11, 1260-1273

Maldonado, S., Jimènez, M., Á., Langdon, G., M., and Sancho, J. (1998) *Biochemistry* 37, 10589-10696

Mayhew, S., G., and Massey, V. (1969) *J. Biol. Chem.* 244, 794-802

McGlynn, S., E., Ruebush, S., S., Naumov, A., Nagy, L., E., Dubini, A., King, P., W., Broderick, J., B., Posewitz, M., C. , and Peters, J., W. (2007) *J. Biol. Inorg. Chem.* 12, 443-447

Medina, M., Peleato, L., M., Mendez, E., and Gomez-Moreno, C. (1992) *Eur. J. Biochem.* 203, 373-379

Meinecke, B., Bertram, J., and Gottschalk, G. (1989) *Arch. Microbiol.* 152, 244-250

Menon, S., and Ragsdale, S., W. (1997) *Biochemistry* 36, 8484-8494

Michnik, A., and Drzazga, Z. (2010) *J. Therm. Calorim.* 101, 513-518

Morrison, J. F. (1969) *Biochim. Biophys. Acta* 185, 269-286

Moss, M., L., and Frey, P., A. . (1990) *J. Biol. Chem.* 265, 18112-18115

Moulis, J.-M., Davasse, V., Meyer, J., and Gaillard, J. (1996) *FEBS Lett.* 380, 287-290

Mulder, D., W., Boyd, E., S., Sarma, R., Lange, R., K., Endrizzi, J., A., Broderick, J., B. , and Peters, J., W. (2010) *nature* 465, 248-251

Mulliez, E., Fontecave, M., Gaillard, J., and Reichard, P. (1993) *J. Biol. Chem.* 268, 2296-2299

Mulliez, E., Padovani, D., Atta, M., Alcouffe, C., and Fontecave, M. (2001) *Biochemistry* 40, 3730-3736

Muralidhara, B. K., and Wittung-Stafshede, P. (2004) *Biochemistry* 43, 12855-12864

Murib, H., J., and Ritter, D., M. (1952) *J. AM. Chem. Soc.* 74, 3394-3398

Myers, J., K., Pace, C. N., and Scholtz, J. M. (1995) *Protein Sci.* 4, 2138-2148

Nicolet, Y., De Lacey, A., L., Vernède, X., Fernandez, V., M., Hatchikian, E. C., and Fontecilla-Camps, J., C. (2001) *J. Am. Chem. Soc.* 123, 1596-1601

Nicolet, Y., Piras, C., Legrand, P., Hatchikian, C., E. , and Fontecilla-Camps, J., C. (1999) *Structure* 7, 13-23

Nicolet, Y., Rubach, J., K., Posewitz, M., C., Amara, P., Mathevon, C., Atta, M., Fontecave, M., and Fontecilla-Camps, J., C. (2008) *J. Biol. Chem.* 283, 18861-18872

Nnyepi, M., R., Peng, Y., and Broderick, J., B. (2007) *Arch. Biochem. Biophys.* 459, 1-9

Nogués, I., Martinez-Júlvez, M., Navarro, J., A., Hervás, M., Armenteros, L., Angel de la Rosa, M., Brodie, T., B., Hurley, J., K., Tollin, G., Gómez-Moreno, C., and Medina, M. (2003) *Biochemistry* 42, 2036-2045

O'Farrell, P., A., Walsh, M., A., McCarthy, A., A., Higgins, T., M., Voordouw, G., and Mayhew, S., G. (1998) *Biochemistry* 37, 8405-8416

Olteanu, H., and Banerjee, R. (2001) *J. Biol. Chem.* 276, 35558-35563

Paine, M., J.I., Garner, A., P., Powell, D., Sibbald, J., Sales, M., Pratt, N., Smith, T., tew, D., G., and Wolf, R., C. (2000) *J. Biol. Chem.* 275, 1471-1478

Pearlstone, J., R., McCubbin, W., D., Kay, C., M., Sykes, B., D., and Smillie, L., B. (1992) *Biochemistry* 31, 9703-9708

Pecher, A., Blaschkowski, H., P., Knappe, K., and Böck, A. (1982) *Arch. Microbiol.* 132, 365-371

Peleato, M., L., Ayora, S., Inda, L., A., and Gomez-Moreno, C. (1994) *Biochem. J.* 302, 807-811

Peng, Y., Veneziano, S., E., Gillispie, G., D. , and Broderick, J. (2010) *J. Biol. Chem.* 285, 27224-27231

Peters, J., W., Lanzilotta, W., N., Lemon, B., J., and Seefeldt, L., C. (1998) *Science* 282, 1853-1858

Petrovich, R., M., Ruzicka, F., J., Reed, G., H. , and Frey, P., A. (1991) *J. Biol. Chem.* 266, 7656-7660

Pieulle, L., Guigliarelli, B., Asso, M., Dole, F., Bernadac, A., and Hatchikian, E. C. (1995) *Biochim. Biophys. acta* 1250, 49-59

Pilet, E., Nicolet, Y., Mathevon, C., Douki, T., Fontecilla-Camps, J., C. , and Fontecave, M. (2009) *FEBS Lett.* 583, 506-511

Plaga, W., Frank, R., and Knappe, J. (1988) *Eur. J. Biochem.* 178, 445-450

Plaga, W., Lottspeich, F., and Oesterhelt, D. (1992) *Eur. J. Biochem.* 205, 391-397

Posewitz, M., C., King, P., W., Smolinski, S., L., Zhang, L., Seibert, M., and Ghirardi, M., L. (2004) *J. Biol. Chem.* 279, 25711-25720
Privalov, P., L., and Potekhin, S., A. (1986) *Methods Enzymol.* 131, 4-51

Privalov, P., L. (1997) *J. Chem. Thermodyn.* 29, 447-474

Sancho, J. (2006) *Cell. Mol. Life Sci.* 63, 855-864

Sanyal, I., Cohen, G., and Flint, D., H. (1994) *Biochemistry* 33, 3625-3631

Sanyal, I., Gibson, K., J., and Flint, D., H. (1996) *Arch. Biochem. Biophys.* 326, 48-56

Schreiber, G., Haran, G., and Zhou, H. X. (2009) *Chem. Rev.* 109, 839-860

Sekowska, A., Kung, H.-F., and Danchin, A. (2000) *J. Mol. Mircobiol. Biotechnol.* 2, 145-177

Silakov, A., Wenk, B., Reijerse, E., and Lubitz, W. (2009) *Phys. Chem. Chem. Phys.* 11, 6592-6599

Shih, C., Museth, A., K., Abrahamsson, M., Blanco-Rodriguez, A., M., Di Bilio, A., J., Sudhamsu, J., Crane, B., R., Ronayne, K., L., Towrie, M., Vlček, A., Jr., Richards, J., H., Winkler, J., R., and Gray, H., B. (2008) *Science* 320, 1760-1762

Shepard, E., M., and Broderick, J., B. . (2010) S-adenosylmethionine and iron-sulfur clusters in biological radical reactions: the radical SAM superfamily. in *Comprehensive natural products II chemistry and biology* (Mander, L., Lui, H.-W. ed.), Elsevier, Oxford. pp

Shepard, E., M., Duffus, B., R., George, S., J., McGlynn, S., E., Challand, M., R., Swanson, K., D., Roach, P., L., Cramer, S., P., Peters, J., W., and Broderick, J. B. (2010) *J. AM. Chem. Soc.* 132, 9247-9249

Shepard, E., M., McGlynn, S., E., Bueling, A., L., Grady-Smith, C., S., George, S., J., Winslow, M., A., Cramer, S., P., Peters, J., W. , and Broderick, J., B. (2010) *Proc. Natl. Acad. Sci. USA* 107, 10448-10453

Smith, E., T., Blamey, J., M., and Adams, M., W. (1994) *Biochemistry* 33, 1008-1016
Smith, W., W., Burnett, R., M., Darling, G., D., and Ludwig, M., L. (1977) *J. Mol. Biol.* 117, 195-225

Sofia, H., J., Chen, G., Hetzler, B., G., Reyes-Spindola, J., F., and Miller, N., E. (2001) *Nucleic Acids Res.* 29, 1097-1106

Spolar, R., S., and Record, T., M., (1994) *Science* 263, 777-784

Sreerama, N., and Woody, R., W. (2004) *Methods Enzymol.* 383, 318-351

Subramanian, P., Rodrigues, A., V., Ghimire-Rijal, S., and Stemmler, T., L. (2011) *Curr. Opin. Chem. Biol.* 15, 312-318

Swenson, R., P., and Krey, G., D. (1994) *Biochemistry* 33, 8505-8514

Taylor, A., M., Farrar, C., E. , and Jarrett, J., T. (2008) *Biochemistry* 47, 9309-9317
Tilak Chandra, S. C. S., Egidijus Zilinskas, Eric M. Shepard, William E. Broderick, and Joan B. Broderick. (2009) *J. Am. Chem. Soc.* 131, 2420-2421

Tse Sum Bui, B., Benda, R., Schünemann, V., Florentin, D., Trautwein, A., X. , and Marquet, A. (2003) *Biochemistry* 42, 8791-8798

Unkrig, V., Neugebauer, F. A., and Knappe, J. (1989) *Eur. J. Biochem.* 184, 723-728

Uyeda, K., and Rabinowitz, J., C. (1971) *J. Biol. Chem.* 246, 3111-3119

Val, D., L., and Cronan, J., E. Jr. (1998) *J. Bacteriol* 180, 2644-2651

Van de Bogart, M., and Beinert, H. (1978) *Methods Enzymol.* 54, 435-445

Van Mierlo, C., P., Van Dongen, W., M., Vergeldt, F., Van Berkel, W., J., and Steensma, E. (1998) *Protein Sci.* 7, 2331-2344
Vetter, H., Jr., and Knappe, J. (1971) *H-Z Physiol. Chem.* 352, 433-446

Vey, J. L., Yang, J., Li, M., Broderick, W. E., Broderick, J. B., and Drennan, C. L. (2008) *Proc. Natl. Acad. Sci. U.S.A.* 105, 16137-16141

Vey, J., L., and Drennan, C., L. (2011) *Chem. Rev.* 111, 2487-2506

Vignais, P., M., and Billoud, B. (2007) *Chem. Rev.* 107, 4206-4272

Volker Wagner, A. F., Frey, M., Meugebauer, F., A., Schäfer, W., and Knappe, J. (1992) *Proc. Natl. Acad. Sci.* 89, 996-1000

Volkmer, B., and Heinemann, M. (2011) *PLoS ONE* 6, e23126
Wahl, R., C., and Orme-Johnson, W., H. (1987) *J. Biol. Chem.* 262, 10489-10496

Walsby, C., J., Hong, W., Broderick, W., E., Cheek, J., Ortillo, D., Broderick, J. B., and Hoffman, B., M. (2002) *J. Am. Chem. Soc.* 124, 3143-3151

Walsby, C. J., Ortillo, D., Broderick, W. E., Broderick, J. B., and Hoffman, B. M. (2002) *J. Am. Chem. Soc.* 124, 11270-11271
Wan, J., T., and Jarrett, J., T. (2002) *Arch. Biochem. Biophys.* 406, 116-126

Wang, S., C., and Frey, P., A. (2007) *Biochemistry* 46, 12889-12895

Watenpaugh, K. D., Sieker, L. C., and Jensen, L. H. (1976) *Flavins and Flavoproteins: Proceedings*, Elsevier Scientific, Amsterdam, New York

Watt, W., Tulinsky, A., Swenson, R., P., and Watenpaugh, K., D. (1991) *J. Mol. Biol.* 218, 195-208

Wieland, O., H. (1983) *Rev. Physiol. Biochem. Pharmacol.* 96, 123-170
Williams, K., Lowe, P., N., and Leadlay, P., F. (1987) *Biochem. J.* 246, 529-536

Wittung-Stafshede, P., Lee, J., C., Winkler, J., R., and Gray, H., B. (1999) *Proc. Natl. Acad. Sci. U S A* 96, 6587-6590

Wittung-Stafshede, P., Malmstrom, B., G., Sanders, D., Fee, J., A., Winkler, J., R., and Gray, H., B. (1998) *Biochemistry* 37, 3172-3177

Wittung-Stafshede, P., Malmstrom, B., G., Winkler, J., R., and Gray, H., B. (1998) *J. Phys. Chem. A* 102, 5599-5601

Wong, K., K., Murray, B., W., Lewisch, S., A., Baxter, M., K., Ridky, T., W., Ulissi-DeMario, L., and Kozarich, J., W. (1993) *Biochemistry* 32, 14102-14110

Wuebbens, M., M., Liu, M., T., Rajagopalan, K., V. , and Schindelin, H. (2000) *Structure* 8, 709-718

Yang, J., Naik, S., G., Ortillo, D., O., Garcia-Serres, R., Li, M., Broderick, W., E., Hanh Huynh, B., and Broderick, J., B. (2009) *Biochemistry* 48, 9234-9241

Yacoby, I., Pochekailov, S., Toporik, H., Ghirardi, M., L., King, P., W. , and Zhang, S. (2011) *Proc. Natl. Acad. Sci. USA* 108, 9396-9401

Yang, Y.-T., Bennett, G., N., and San, K.-Y. (2001) *Metab. Eng.* 3, 115-123
Zhang, Q., Iwasaki, T., Wakagi, T., and Oshima, T. (1996) *J. Biochem.* 120, 587-599

Zhao, Q., Modi, S., Smith, G., Paine, M., McDonage, P., D., Wolf, R., C., Tew, D., Lian, L.-y., Roberts, G., C.K., and Driessen, H., P.C. (1999) *Protein Sci.* 8, 298-306

Zhou, Z., and Swenson, R., P. (1995) *Biochemistry* 34, 3183-3192

Zhou, Z., and Swenson, R., P. (1996) *Biochemistry* 35, 15980-15988

Zu, Y., Couture, M., M.-J., Kolling, D., R. J., Crofts, A., R., Eltis, L., D., Fee, J., A., and Hirst, J. (2003) *Biochemistry* 42, 12400-12408